25647

National Library of Canada | Bibliothèque nationale du Canada | CANADIAN THESES ON MICROFICHE | THÈSES CANADIENNES SUR MICROFICHE

NAME OF AUTHOR/*NOM DE L'AUTEUR* Mr. Raymond M. Hoff

TITLE OF THESIS/*TITRE DE LA THÈSE* Raman Scattering in GaSe

UNIVERSITY/*UNIVERSITÉ* Simon Fraser University

DEGREE FOR WHICH THESIS WAS PRESENTED/ *GRADE POUR LEQUEL CETTE THÈSE FUT PRÉSENTÉE* Ph.D.

YEAR THIS DEGREE CONFERRED/*ANNÉE D'OBTENTION DE CE DEGRÉ* 1975

NAME OF SUPERVISOR/*NOM DU DIRECTEUR DE THÈSE* Dr. J. C. Irwin

Permission is hereby granted to the NATIONAL LIBRARY OF CANADA to microfilm this thesis and to lend or sell copies of the film.

The author reserves other publication rights, and neither the thesis nor extensive extracts from it may be printed or otherwise reproduced without the author's written permission.

L'autorisation est, par la présente, accordée à la BIBLIOTHÈQUE NATIONALE DU CANADA de microfilmer cette thèse et de prêter ou de vendre des exemplaires du film.

L'auteur se réserve les autres droits de publication; ni la thèse ni de longs extraits de celle-ci ne doivent être imprimés ou autrement reproduits sans l'autorisation écrite de l'auteur.

DATED/*DATÉ* 19 Feb 1975 SIGNED/*SIGNÉ*

PERMANENT ADDRESS/*RÉSIDENCE FIXE* [redacted]

NL-91 (11-73)

RAMAN SCATTERING IN GaSe

by

RAYMOND MEYER HOFF

A.B. University of California, 1970

A DISSERTATION SUBMITTED IN PARTIAL FULFILMENT

OF THE REQUIREMENTS FOR THE DEGREE OF

DOCTOR OF PHILOSOPHY

in the Department

of

Physics

SIMON FRASER UNIVERSITY

JANUARY 1975

APPROVAL

Name: Raymond Meyer Hoff

Degree: Doctor of Philosophy

Title of Thesis: Raman Scattering in GaSe

Examining Committee:

Chairman: A. E. Curzon

J. C. Irwin
Senior Supervisor

K. E. Rieckhoff
Examining Committee

R. H. Enns
Examining Committee

B. P. Clayman
Examining Committee

T. J. Wieting
External Examiner
Research Physicist
Naval Research Laboratory
Washington, D. C., U.S.A.

Date Approved: Jan 24/75

PARTIAL COPYRIGHT LICENSE

I hereby grant to Simon Fraser University the right to lend my thesis or dissertation (the title of which is shown below) to users of the Simon Fraser University Library, and to make partial or single copies only for such users or in response to a request from the library of any other university, or other educational institution, on its own behalf or for one of its users. I further agree that permission for multiple copying of this thesis for scholarly purposes may be granted by me or the Dean of Graduate Studies. It is understood that copying or publication of this thesis for financial gain shall not be allowed without my written permission.

Title of Thesis/Dissertation:

Raman Scattering in GaSe

Author: Raymond M. HOFF

(signature)

(name)

19 Feb 1975

(date)

ABSTRACT

The resonant Raman spectrum of GaSe has been investigated using a cw tunable dye laser. In order to fully comprehend this spectrum it was necessary to study the non-resonant Raman spectrum of GaSe and its sister compound GaS. The frequencies of vibration of the phonon modes at the zone centre have been measured at room and at liquid nitrogen temperatures for both compounds. The results from the Raman experiments have made possible a determination of the polytype content of these compounds. In particular it has been found that GaS crystallizes in the β-polytype (D_{6h}^4). GaSe, however, is found to be predominantly of the ε-polytype (D_{3h}^1) when obtained in platelets or flakes and of the γ-polytype (C_{3v}^5) when obtained in needles. All of the modes have been assigned, on the basis of their observed polarization dependence, to the irreducible representations of the appropriate point group. Excellent agreement has also been obtained between the observed and predicted anisotropic behaviour of the polar modes in GaSe.

In the resonant Raman experiments, a detailed investigation of the energy dependence of the scattering efficiency has been carried out in the region just below the energy gap, which for GaSe falls in the middle of the spectral range of the dye laser. The scattering efficiency was observed to undergo a maximum when the laser energy was equal to the energy of the free exciton. The general energy dependence

was found to be in good agreement with that predicted by Martin for q-dependent scattering. The observed angular independence of the scattering is, however, in apparent discord with this theory, and for one mode, A_2'' (LO), crystal momentum conservation is observed to be broken. The non-polar modes have been observed to exhibit a strong anti-resonant behaviour similar to that observed in CdS; but the present results cannot be interpreted in terms of the previous empirical models.

ACKNOWLEDGEMENTS

I would like to thank the National Research Council of Canada, the Department of Physics and Dr. J.C. Irwin for financial support. While this support was substantial, I would also like to acknowledge the financial (and, oh yes, moral) support of Ms B.L. Hoff who made these five years more enjoyable.

I would like to thank Dr. John Brebner of the Université de Montreal and Dr. R.M.A. Lieth of Eindhoven University, The Netherlands, for the loan of the GaSe samples used in this work. My thanks go to Dr. R.M. Martin for his permission to use his results for the Resonant Raman cross-section in the parameterized form.

I would like to thank Dr. J.C. Irwin, my supervisor, for his continued, although at times somewhat sarcastic, support, and to the rest of our group for their help. My thanks go to Ms M.G. Jacques for her help in typing the manuscript. And finally,

I'll thank all the guys in the shops
For all the successes and flops
As the man once said
With hammer on head
"It feels so damn good when it stops".

TABLE OF CONTENTS

LIST OF TABLES

LIST OF FIGURES

CHAPTER 1

INTRODUCTION

The study of the lattice dynamics of crystals by the use of the vibrational Raman effect has become quite extensive in recent years. The reader will recall that the Raman effect is the inelastic scattering of light with the shift in energy of the final photon being due to the creation or annihilation of a phonon. The technique is most effective in those crystals which are transparent at the incident light frequency and thus the use of Raman scattering has become widespread in studying the lattice dynamics of wide band semiconductors and insulators.

In studying the lattice dynamical properties of a crystal, then, one usually chooses an excitation source whose frequency lies deep in the energy gap. With the availability of common gas lasers, such as the Helium-Neon, Argon ion, Krypton ion and Helium-Cadmium lasers, it is usually quite easy to obtain a suitable line to perform Raman measurements. The theory of the first-order Raman effect in crystals developed by Loudon (1963, 1964), however, revealed another important consideration concerning the frequency of the incident light. It was predicted that as the incident frequency approaches a real electronic transition of the crystal, the cross-section for Raman scattering should increase dramatically. This effect became known as the Resonance Raman effect (RRE).

The RRE in crystals was first experimentally observed by

Leite and Porto (1966) in CdS. Within a relatively short time several compounds had been investigated with the available lines of the existing gas lasers. Several interesting results appeared including the observation of multiple LO phonon peaks indicating the creation of more than one LO phonon and the breakdown of normal selection rules for Raman scattering.

The explanation of these effects seemed to centre on two crucial questions. What was required was an understanding of first, the nature of the intermediate electronic state in the scattering process and second , the behaviour of the Raman cross-section as resonance is approached (and thus the form of the interaction). As one can imagine, the coincidence of a real electronic transition in a crystal with one of the existing gas laser lines would be truly fortuitous. As a result much of the early work left the answers to these questions either hazy or completely unresolved. An adequate examination of these questions required an intense light source with energy resolution capable of discriminating between the various electronic transitions in a semiconducting crystal. At the same time the source must be able to cover a large frequency region about the band gap energy (since this was the region where the earlier work had indicated the RRE was largest).

With the advent of the tunable dye laser such a study became possible. When this work was initiated there had been

no quantitative results for the RRE obtained with a tunable dye laser. GaSe was an obvious choice for such a study, however, since its band gap at 77°K is 2.10 eV (Mercier et al., 1973) and this lies midway in the tuning range of Rhodamine 6G tunable dye lasers (range 5400Å to 6400Å or 2.3 eV to 1.94 eV). GaSe is one of only a few compounds in which the RRE can be studied with such a laser.

This study followed a chronological course of first studying the lattice dynamics of GaSe and its sister compound GaS when the light was far from the intrinsic band edge, making assignments of the one-phonon lines in the Raman spectra, and later with the use of a tunable dye laser observing the Raman scattering efficiency as the band edge is approached from the low energy (long wavelength) side. This thesis is thus divided along these lines.

Chapter II will begin by presenting a qualitative and then a quantitative introduction to the Raman effect. This will involve the inclusion of the theory of Raman scattering in ionic crystals developed by Loudon (1963, 1964), which is of particular interest for anisotropic gallium compounds. The crystal structure and group theoretical predictions for the number and symmetry of the phonon modes at the Brillouin zone centre in the gallium chalcogenides will then be presented. The layered symmetry of these crystals gives rise to what has been termed "conjugate modes" and an estimate of the frequencies of these modes and their probability of occurrence will be discussed. Chapter III will present the

experimental work on the first-order Raman spectrum of these compounds.

The results obtained for the Resonant Raman Effect in GaSe will be presented in Chapters IV and V. Chapter IV will present the theoretical description of the RRE as developed by Martin (1971b, 1973). Included will be applications of his formalism to some simple intermediate states. Chapter V contains the result of the Resonant Raman experimental work on GaSe. The results are compared quantitatively to the theoretical predictions. Finally Chapter VI will present suggestions for future work and the conclusions to be drawn from this study.

CHAPTER II

THE RAMAN EFFECT IN THE GALLIUM CHALCOGENIDES GaS AND GaSe - THEORY

2.1 Introduction

There are several experimental methods by which the frequencies of the long wavelength vibrational modes in a crystal may be obtained. One of the most direct methods is by thermal neutron scattering whereby the phonon frequencies can be mapped throughout the Brillouin zone. This technique, however, has disadvantages in that it requires quite large samples (> 1 cm^3) and generally needs quite large neutron fluxes. In order to obtain frequencies of phonons near the zone centre, small angle neutron scattering is required and thus zone centre phonon frequencies obtained by this method lack precision.

Optical methods for obtaining these frequencies include far infrared absorption, phonon-assisted absorption and emission, Raman scattering and Brillouin scattering. It is possible in far infrared absorption to see first-order phonon peaks if the phonon has the symmetry characteristic of a translation of the crystal, since the dipole moment transforms as a uniform translation. This is usually a limitation since not all phonon branches will be infrared active, but it is for this reason as well that identification of phonon modes can be made.

Absorption of light near the band edge can also give information on the phonon frequencies when this absorption is phonon-assisted. This, however, takes place primarily in compounds which have an indirect energy gap. The phonons manifest themselves in absorption steps below the gap and are indicative only of phonons which conserve both energy and momentum in the absorption process. This requires the phonon involved to be from the same point in the Brillouin zone as the indirect energy gap. Since indirect energy gaps are by definition not at the zone centre and tend to be at or near the zone boundary, the energy of the phonons involved will be that of zone boundary optical or acoustic phonons. Because of phonon dispersion within the Brillouin zone, one usually does not obtain information on the zone centre phonon frequencies by this method.

Brillouin scattering gives information on acoustic phonon frequencies for phonons with wavevector near that of the incident light. Thus, the effect is useful in obtaining the velocities of sound and the elastic constants of the crystal.

Raman scattering, on the other hand, gives information on the optical phonons near the zone centre (in the first-order effect). The phonons observed to be Raman active, as will be explained in the following section, are those whose symmetry of vibration transforms as the polarizability tensor of the material (Loudon, 1964). This can be a completely different set of phonon modes than those obtained in far infrared

absorption and in fact for centrosymmetric crystals, the two effects are complementary. In these crystals, all infrared active modes are odd with respect to inversion and all modes which are Raman active are even with respect to inversion.

The above techniques are all complementary to a certain extent and all should be considered in obtaining the frequencies of the long wavelength phonons in the crystal. To date neutron scattering on the Gallium chalcogenides has been performed on GaSe only in the direction of the $\hat{c}$-axis (Brebner et al., 1973). Far infrared measurements have been done by Leung et al. (1966), Wieting and Verble (1972), Kuroda et al. (1968, 1970) and Irwin et al. (1973). Kamimura (1969) observed absorption steps in the edge spectrum. Brillouin scattering has not been performed on these compounds to date. Raman measurements have been extensive yet contradictory. Wright and Mooradian (1966) performed the first measurements of the phonon frequencies on unoriented samples and made no assignments of the symmetries of the phonons. Wieting and Verble (1972) made assignments of the phonon frequencies on the basis that GaSe crystallized in the β-polytype. Van der Ziel et al. (1973) performed experiments on GaS and obtained assignments for the observed spectral features. Irwin et al. (1973) analyzed the spectrum of both GaS and GaSe and made assignments in GaSe with the conclusion that GaSe crystallized in the ε-polytype. Hayek et al. (1973) and Yoshida et al. (1973) studied mixed crystals of GaS_x and $GaSe_{1-x}$ $(0 \leq x \leq 1)$

and assignments were made which indicated the existence of "conjugate" modes. Mercier et al. (1974) also studied mixed crystals of these types and obtained a somewhat different interpretation than the previous two papers. Finally, the results of the present Resonant Raman experiments (Hoff and Irwin, 1974) confirmed the existence of resonance effects which manifested themselves in Hayek's work and confirmed the polar nature of GaSe.

2.2 The First Order Raman Effect in Crystals

Raman scattering of light in crystals involves the inelastic scattering of light of frequency ω_i ($= \frac{c}{n} k_i$) to a frequency ω_s ($= \frac{c}{n} k_s$) with the simultaneous creation (destruction) of a phonon of frequency ω_o ($= v_p q$). The scattering event conserves both momentum and energy:

$$\hbar\omega_s = \hbar\omega_i \pm \hbar\omega_o \tag{2.1}$$

$$\vec{k}_s = \vec{k}_i \pm \vec{q} \tag{2.2}$$

In a classical sense, the polarizability of the medium is modulated at the phonon frequency if the lattice is distorted by some mechanism:

$$\alpha = \alpha_o + \frac{\partial \alpha}{\partial q_m} q_m = \alpha_o + \alpha_1 \cos \omega_m t \tag{2.3}$$

and thus the polarization of the medium will be modulated by:

$$P = \alpha E = \alpha_o E_o \cos \omega_i t + \alpha_1 E_o \cos \omega_m t \cos \omega_i t$$

$$= \alpha_o E_o \cos \omega_i t + \alpha_1 E_o \left[\cos(\omega_i+\omega_m)t + \cos(\omega_i-\omega_m)t\right] \tag{2.4}$$

Thus, classically, the polarization field will reradiate energy at $\omega_s = \omega_i \pm \omega_m$ (+=anti-Stokes scattering, -=Stokes scattering).

It is possible to treat this first order event semiclassically by response theory techniques. To do this one would look at the various contributions to the dielectric susceptibility which give rise to Raman Scattering (Burstein

and Pinczuk, 1971). It has proved to be more useful and possibly more transparent, to treat the scattering event quantum mechanically. By this approach each type of interaction is introduced by an interaction potential (and thus through its contribution to the Hamiltonian). The quantum mechanical approach to the Raman effect in crystals has been done by Loudon (1963, 1964), and his notation will be modified somewhat here. The lowest type of interaction which gives rise to one phonon scattering requires use of third order perturbation theory. The Raman scattering probability per unit time is (Loudon, 1964):

$$W_o = \frac{2\pi}{\hbar 6} \sum_{q,k_s} \sum_{a,b} \Big| \langle n_i - 1, 1;\ n_o + 1,\ 0 | H_I | a \rangle \langle a | H_I | b \rangle \times \langle b | H_I | n_i,\ 0,\ n_o,\ 0 \rangle \times (\omega_a - \omega_i)^{-1} (\omega_b - \omega_i)^{-1} \Big|^2 \times \delta(\omega_i - \omega_o - \omega_s) \qquad (2.5)$$

where

n_i = the number of photons in field of state i

n_o = the number of phonons in the initial state

a,b = the possible electronic intermediate states

ω_a, ω_b = the energies of these states

H_I = the interaction Hamiltonian

The interaction Hamiltonian will consist of an electron-photon term, H_{eR}, and an electron-phonon term, H_{eL}:

$$H_I = H_{eR} + H_{eL} \qquad (2.6)$$

The electron-photon part comes from the $\vec{A}\cdot\vec{p}$ interaction and is:

$$H_{eR} = \left(\frac{-e}{m}\right)\sum_{\mu} \frac{2\pi\hbar^2}{n^2 V\omega_\mu} \vec{\epsilon}_\mu \cdot \vec{p}_\mu \, e^{i\vec{k}_\mu \cdot \vec{r}} a_\mu + \text{c.c.} \qquad (2.7)$$

where

n = index of refraction $\quad \vec{\epsilon}_\mu$ = photon polarization

V = volume of the crystal $\quad \vec{k}_\mu$ = photon momentum

μ = photon state

a_μ = destruction operator in state μ.

The electron-phonon part may best be written in a form where the electron-phonon coupling potential is left unspecified for the moment:

$$H_{eL} = \frac{1}{V^{\frac{1}{2}}} \sum_{\nu} \theta^{\nu}(\vec{r}) e^{i\vec{q}_\nu \cdot \vec{r}} b_\nu + \text{c.c.} \qquad (2.8)$$

where

$\theta^{\nu}(r)$ = electron-phonon interaction potential

b_ν = phonon destruction operator in the state ν

ν = phonon state index (includes polarization).

The form of eq. 2.8 is taken from Martin (1971b) and is applicable to any form of electron-phonon interaction of which two, the deformation potential and the Fröhlich interaction, will be of interest in this work.

Equation 2.5 can be rewritten after inserting H_I into each matrix element. In two of the matrix elements the electron-photon interaction will be operative and in the other the electron-phonon interaction will be the operator. This gives rise to six possible time orderings of the

scattering shown schematically by the Feynman diagrams of Figure 2.1. Substituting 2.6, 2.7 and 2.8 into 2.5 one obtains:

$$W_o = \frac{4\pi^3 e^4}{\hbar^3 m^4 n^4} \sum_{\vec{q},\vec{k}_s} \frac{n_i(n_o+1)}{\omega_i \omega_s} \left| \hat{\xi}_q^j R_{12}{}^j(-\omega_i,\omega_s,\omega_o) \right|^2 \quad (2.9)$$

where

$\hat{\xi}_q^j$ = the jth component of the phonon polarization vector (j = x,y,z)

and the summation of repeated indices is assumed. The Raman tensor $R_{12}{}^j$ in 2.9 is given by six terms corresponding to the ordering of the diagrams of Figure 2.1 (Loudon, 1964):

$$R_{12}{}^j(-\omega_i,\omega_s,\omega_o) = \frac{1}{V}\sum_{\alpha\beta}\left\{\frac{P_{o\beta}{}^2 P_{\beta\alpha}{}^1 \Theta_{\alpha o}{}^j}{(\omega_\beta+\omega_o-\omega_i)(\omega_\alpha+\omega_o)} + \frac{P_{o\beta}{}^1 P_{\beta\alpha}{}^2 \Theta_{\alpha o}{}^j}{(\omega_\beta+\omega_o+\omega_s)(\omega_\alpha+\omega_o)}\right.$$

$$+ \frac{P_{o\beta}{}^2 \Theta_{\beta\alpha}{}^j P_{\alpha o}{}^1}{(\omega_\beta+\omega_o-\omega_i)(\omega_\alpha-\omega_i)} + \frac{P_{o\beta}{}^1 \Theta_{\beta\alpha}{}^j P_{\alpha o}{}^2}{(\omega_\beta+\omega_o+\omega_s)(\omega_\alpha+\omega_s)}$$

$$\left. + \frac{\Theta_{o\beta}{}^j P_{\beta\alpha}{}^2 P_{\alpha o}{}^1}{(\omega_\beta+\omega_s-\omega_i)(\omega_\alpha-\omega_i)} + \frac{\Theta_{o\beta}{}^j P_{\beta\alpha}{}^1 P_{\alpha o}{}^2}{(\omega_\beta+\omega_s-\omega_i)(\omega_\alpha+\omega_s)}\right\} \quad (2.10)$$

Here 1,2 indicate the polarizations of the incoming and scattered light, respectively, α and β are the intermediate electronic states, and the symbol $\Theta_{\nu\mu} = \langle\nu|\Theta|\mu\rangle$.

The notation $R_{12}^j(-\omega_i,\omega_s,\omega_o)$ is read as the Raman tensor for the creation of a scattered photon ω_s (polarization represented by index 2) and phonon ω_o with the annihilation (minus sign) of an initial photon ω_i (polarization represented by the index 1). This notation is somewhat over-specific

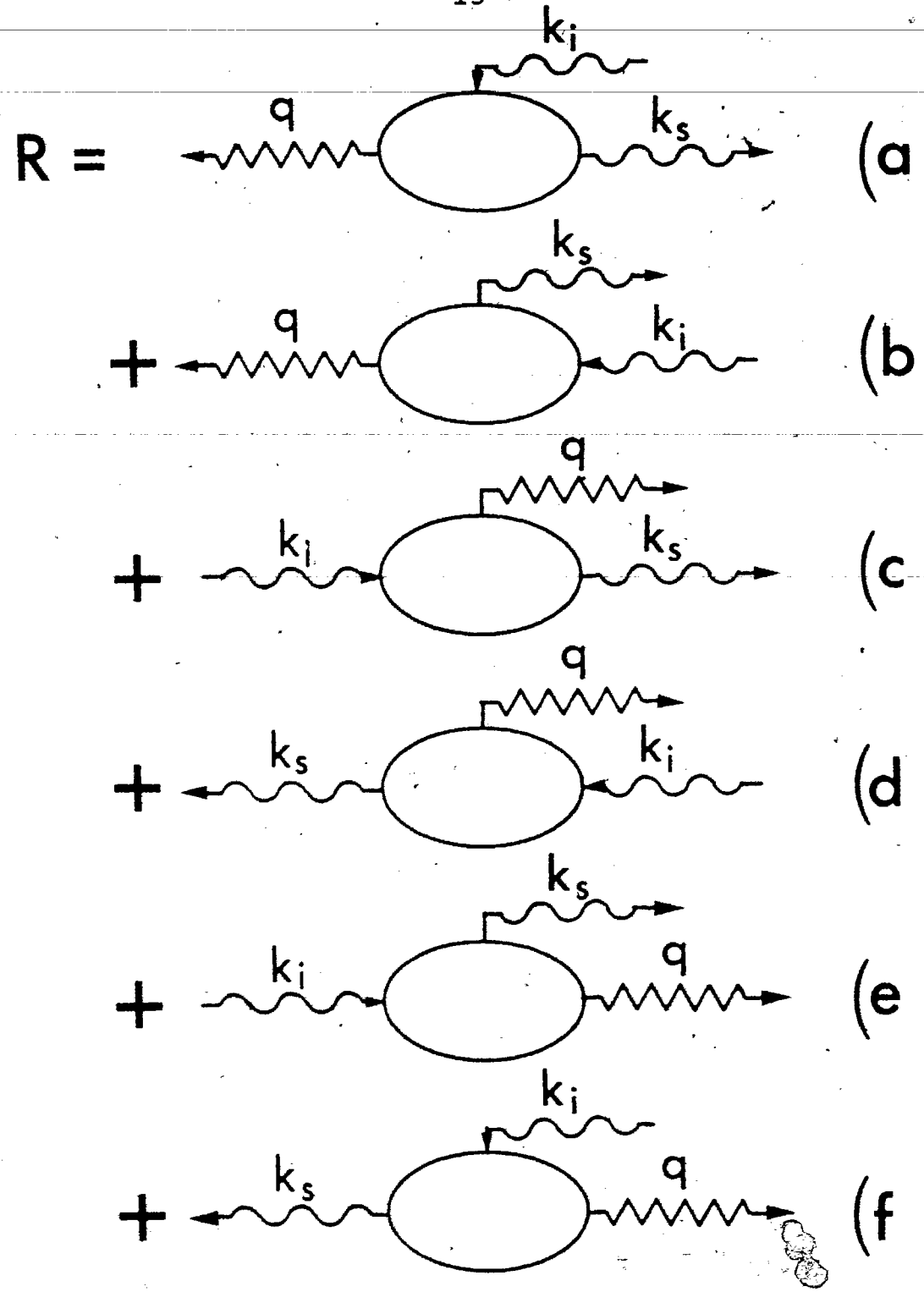

Figure 2.1. The six possible time orderings of the first-order Raman scattering event. k represents the incident and scattered photons and q is the phonon created in the Stokes process.

in this form and will be modified in a later section when it is necessary to calculate the selection rules for Raman scattering in these compounds. In the form of 2.9 and 2.10, however, several things should be noticed. Three of these terms have energy denominators which can give divergences in the optical regime. The third term in 2.10 is a second order singularity and the first and fifth are first order singularities in the visible frequency region. In the other three terms, the denominators do not go to zero in this region and the terms are non-resonant. It is precisely the third term (c) which is treated in the Resonant Raman effect of Chapter 4. It must be noted that when the photon frequencies lie within the energy gap (as in the non-resonant spectra), the Raman scattering efficiency can only be found by summing over the complete set of the possible electronic levels, α and β. This is a horrendous problem and has yet to be attempted. It is fortunately not necessary to do this sum to determine the symmetry properties of the scattering and thus in first order Raman scattering absolute efficiencies are rarely determined from the experiment. Instead it is usually sufficient to present the results in terms of the relative scattered intensities and deduce the symmetry properties from this relative behaviour.

When the frequency of the incident light is near resonance with a real electronic transition, however, the resonant terms in equation 2.10 single out the terms in the sum where α

and/or β is the electronic state being excited. This is a much more manageable problem and is treated in the next chapter.

The symmetry properties of the Raman tensor can be derived from equation 2.10 and it will suffice here to reproduce them from Loudon's paper (1963):

$$R^j_{12}(-\omega_i,\omega_s,\omega_o) = R^j_{21}(\omega_s,-\omega_i,\omega_o) \tag{2.11}$$

$$\vec{P}_{\alpha\beta} = -\vec{P}_{\beta\alpha} \tag{2.12}$$

$$\Theta^j_{\alpha\beta} = \Theta^j_{\beta\alpha} \tag{2.13}$$

and for Stoke's scattering ($\omega_i=\omega_s+\omega_o$):

$$R^j_{12}(-\omega_i,\omega_s,\omega_o) = R^j_{12}(\omega_i,-\omega_s,-\omega_o) \tag{2.14}$$

Combining 2.11 and 2.14, one obtains:

$$R^j_{12}(-\omega_i,\omega_s,\omega_o) = R^j_{21}(-\omega_i+\omega_o,\omega_s+\omega_o,-\omega_o) \tag{2.15}$$

Thus in general the Raman tensor is not symmetric. However, if $\omega_o \ll \omega_\alpha - \omega_{i,s}$ for all α, the dominant terms in the tensor will be symmetric under exchange of 1 and 2 (the polarization indices). Loudon gives $\frac{\omega_o}{\omega_{\alpha,\beta}-\omega_{i,s}} < 10^{-2}$ as a criterion for the Raman tensor to be symmetric. For GaS and GaSe the lowest energy optical phonons have energy of about 2 meV and thus if one were within 200 meV of the band edge with the incident photon energy, one would not expect the scattering to be symmetric. In GaSe all of the data taken was within this

range. For the larger energy phonons (≳25 meV) the above criterion requires the incident light to be farther away from the band edge than the width of the gap itself ($E_g \cong 2.1$ eV in GaSe, 2.5 eV in GaS). If Loudon's criterion is used, then, one would not expect the Raman spectrum to be symmetric with respect to interchange of the polarization indices. One finds, however, that the Raman spectrum in these compounds appears to be predominantly symmetric and leads one to question the strictness of the above rule. In particular, it appears to be not necessary to have such a large displacement of the light from the electronic states ($\omega_{\alpha,\beta}-\omega_{i,s}$) in order that the Raman tensor be nearly constant between the frequency ω_i and $\omega_i-\omega_o$. From the Resonant Raman work, it is possible to conclude that for GaSe the region where the tensor may be asymmetric will be related to the region where resonance effects are important, that is within 150 meV of the exciton energy.

2.3 Crystal Structure

The two gallium chalcogenide semiconductors GaS and GaSe are layered crystals. While there are several polytypes which describe the stacking sequences between these layers, the unit layer is similar in both compounds. In the following subsections the unit layer will be described and the various material parameters and stacking sequences for GaS and GaSe will be given.

2.3.1 The Unit Layer

The unit layer is composed of a hexagonal array of atoms four atoms thick. There are two gallium atoms and two chalcogenide atoms, X, per layer in the unit cell. The layer is shown in Figure 2.2. These compounds are III-VI compounds and, thus, there is not a specific GaX molecule as such. The compound could more properly be described as a Ga_2X_2 compound since the valence charges of a chalcogenide atom are shared both with the gallium atom and the other chalcogenide atom (Sapre and Mande, 1973, Mercier et al., 1973). The unit layer shown in Figure 2.2 has a space group symmetry D_{3h}^1 ($P\bar{6}m2$) (Schubert et al., 1955).

2.3.2. Gallium Sulphide

Gallium sulphide has a unit cell spanning two layers and containing eight atoms. It has been found to crystallize in only one polytype, called β (Basinski et al., 1961). In this polytype, the unit layer is repeated with the layers adjoining having both a rotation of 180° about the c-axis drawn through any two adjacent gallium atoms and a uniform

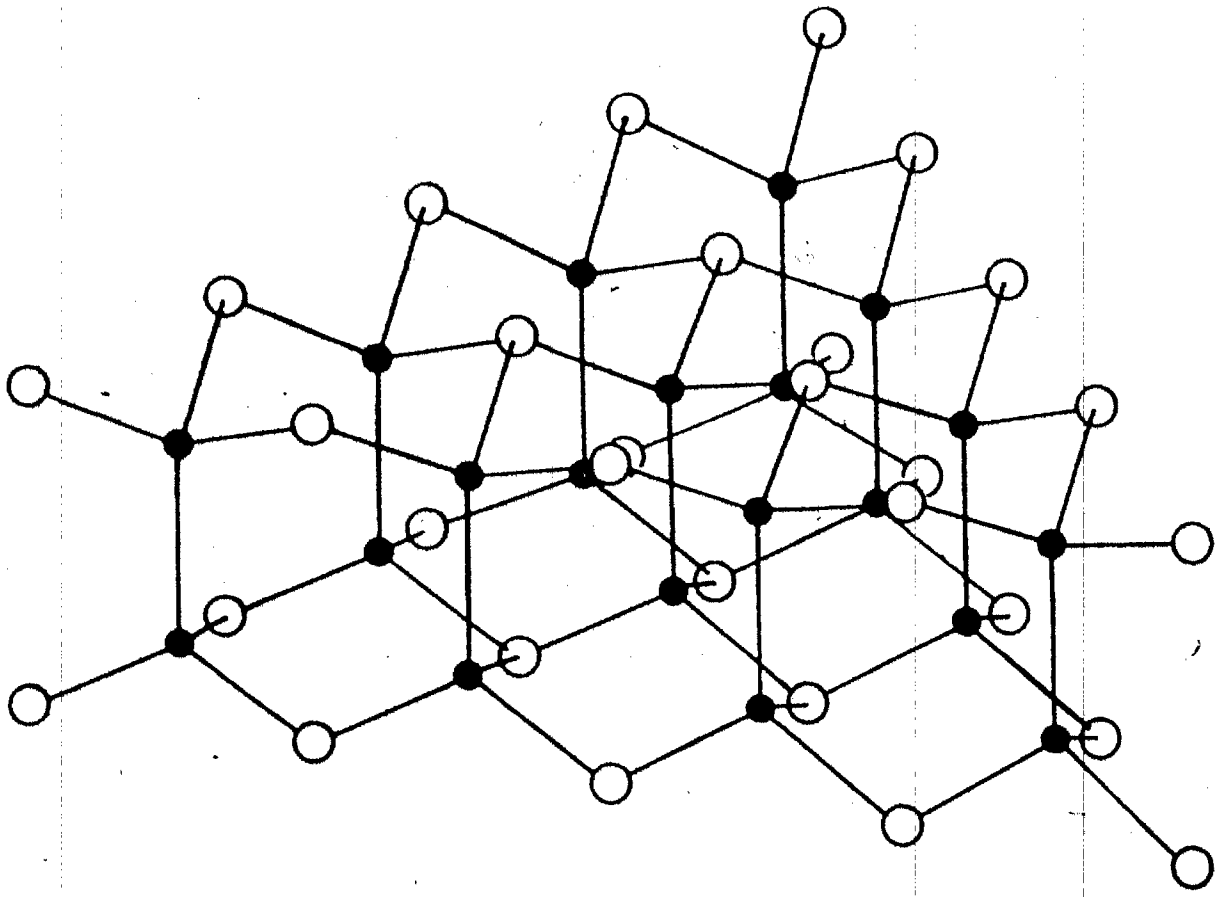

Figure 2.2. The unit layer of GaS and GaSe. The gallium atom is represented by the dark circles and the sulphur or selenium atoms by the light.

translation. The β-stacking sequence is shown in Figure 2.3. This type of stacking of the layers is equivalent to the introduction of an inversion centre between the layers and thus the point group of the β-polytype is $D_{3h} \otimes i = D_{6h}$. The space group is D_{6h}^4 (P6/mmm) (Schubert et al., 1955). The lattice parameters of β-GaS are summarized in Table 2.1.

2.3.3. Gallium Selenide

Gallium selenide has been reported to crystallize in three polytypes, two hexagonal and one rhombehedral. The first two, β and ε contain two layers per unit cell, and the rhombehedral form, γ, is three layers thick.

The actual structure of GaSe has been the subject of some controversy. Wieting and Verble (1972) concluded that GaSe crystallizes in the β-polytype as does GaS. They based this conclusion on X-ray powder patterns as did Jellinek and Hahn (1961) who reached the same conclusion. Other workers, however, by taking X-ray photographs from single crystal platelets determined that the crystal form of the largest plate crystals is of a mixed ε-γ character (Schubert et al., 1955; Terhell et al., 1971, 1972; Basinski et al., 1961). It was an objective of the analysis of the Raman spectrum of GaSe to determine the exact polytype nature of the compound.

The ε-polytype is shown in Figure 2.3. The layers while identical to the β-polytype are stacked somewhat differently. In the ε-polytype, each adjacent layer differs from the preceding layer by only a uniform translation with the 180° rotation of the GaS β-polytype lacking. Thus, the

TABLE 2.1
LATTICE PARAMETERS OF THE GALLIUM CHALCOGENIDES

β - GaS

a_o = 3.585 Å [a] c_o = 15.50 Å [a]

Ga-Ga Bond Length = 2.52 Å [a]; 2.46 Å [b]

S-Ga Bond Length = 2.30 Å [a]; 2.43 Å [b]

S-S Minimum Distance = 3.75 Å [b]

Layer Separation = 3.09 Å [b]

ε - GaSe

a_o = 3.74 Å [c] c_o = 15.89 Å [c]

Ga-Ga Bond Length = 2.39 Å [b]

Ga-Se Bond Length = 2.37 Å [b]

Se-Se Minimum Distance = 3.84 Å [b]

Layer Separation = 3.18 Å [b]

γ - GaSe

a_o = 3.74 Å [c] c_o = 23.86 Å [c]

---

a) Wykoff (1965); b) Fischer (1963); c) Schubert et al. (1955)

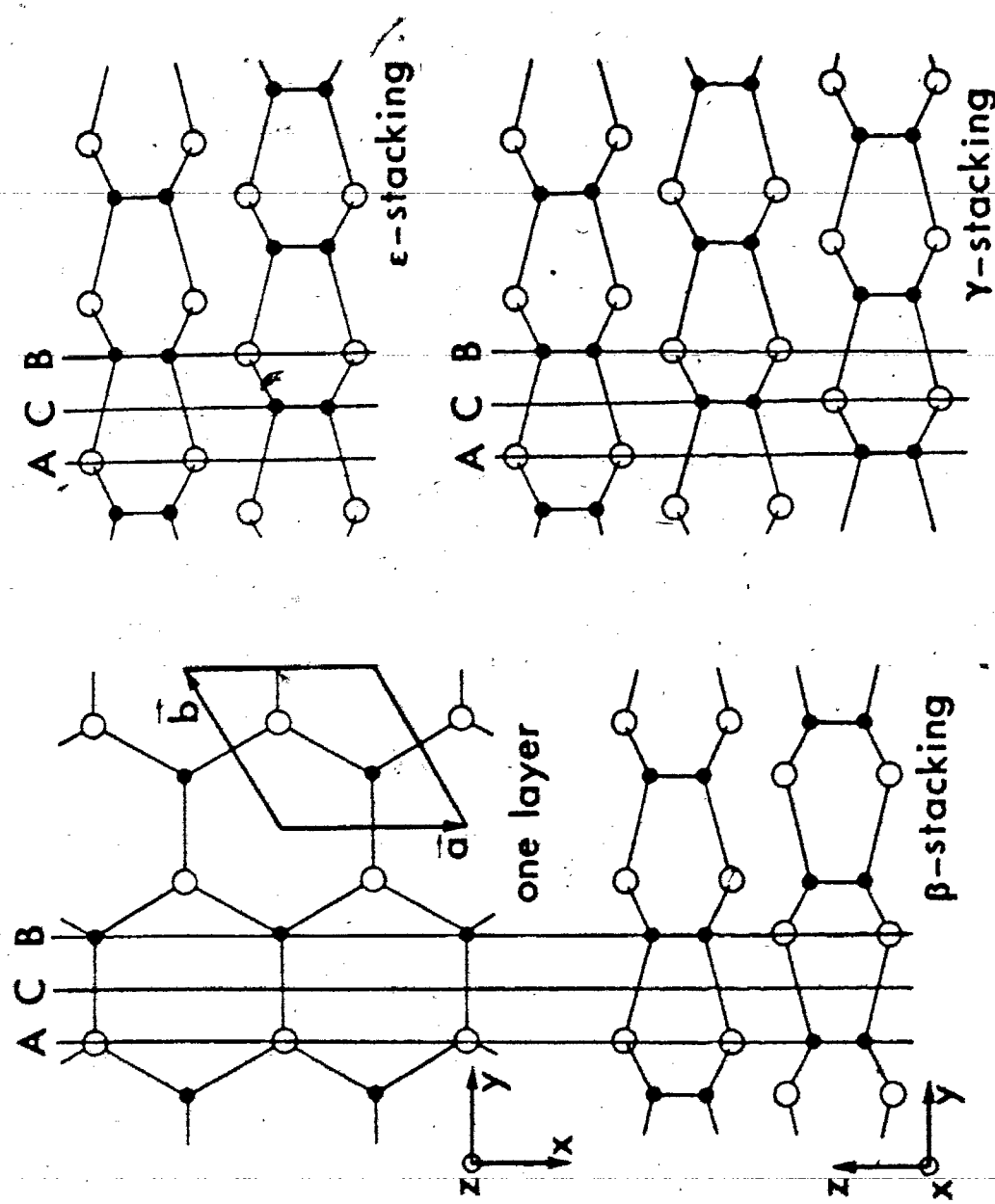

Figure 2.3. Stacking sequences for the β-, ε-, and γ-polytypes.

overall symmetry of the crystal is merely that of the layer giving the space group D_{3h}^{1} ($P\bar{6}m2$) (Basinski et al., 1961).

The γ-polytype has a stacking sequence which includes three layers in the unit cell. The relative position of any two adjacent layers is the same as for the ε-polytype and thus, there are two translations before the initial layer is repeated (Figure 2.3) . The space group for this polytype is C_{3v}^{5} (R3m) (Brebner et al., 1973; Schubert et al., 1955).

2.4 Group Theory and Selection Rules

Knowledge of the point and space group symmetry of the crystal makes it possible to predict the number and symmetry of the modes throughout the Brillouin zone. Since most of the work in this thesis is concerned with scattering around the zone centre, it is sufficient to know the phonon symmetries at this point, Γ. The point group at Γ is just the point group of the space group: D_{3h} for the ε-polytype, D_{6h} for the β-polytype and C_{3v} for the γ-polytype. The normal modes of vibration can be obtained from the correlation method of group theory (Fateley et al., 1971). This calculation is carried out in Appendix A, and the results will merely be stated here.

The β-polytype contains 8 atoms per unit cell and thus there are 3n or 24 normal modes of vibration in the crystal. These modes have symmetry given by the irreducible representations of the D_{6h} point group (eq. A.11):

$$\Gamma = 2A_{1g} \oplus 2A_{2u} \oplus 2B_{1u} \oplus 2B_{2g} \oplus 2E_{1g} \oplus 2E_{1u} \oplus 2E_{2g} \oplus 2E_{2u} \qquad (2.16)$$

of which one A_{2u} mode and one doubly degenerate E_{1u} mode are acoustic.

The ε-polytype also has 24 normal modes of vibration given by the irreducible representations of the D_{3h} point group (eq. A.17):

$$\Gamma = 4\ A_1' \oplus 4\ A_2'' \oplus 4\ E' \oplus 4\ E'' \qquad (2.17)$$

of which one A_2'' and one E' are acoustic.

The γ-polytype has 12 atoms per unit cell and thus thirty-six normal modes of vibration given by the C_{3v} point group (eq. A.23):

$$\Gamma = 12\ A_1 \oplus 12\ E \qquad (2.18)$$

of which one A_1 and one E mode are acoustic.

From the symmetry of the crystal it is also possible to derive the selection rules for Raman scattering and infrared absorption. Many of the techniques used to do this are based on the theory of the polarizability derivative as was suggested by equation 2.3 (Born and Bradburn, 1947). These results are summarized neatly, however, by Loudon (1964) who presents representations for each Raman active vibration in each crystal class. The crucial aspect of this approach is that a phonon can participate in a first-order Raman scattering event if and only if its irreducible representation is the same as one of the irreducible representations of the reduction of the polarizability tensor. The reduction of the polarizability tensor has been done for each crystal class and can be found by inspection of the basis functions for each point group (Tinkham, 1964). The various bilinear combinations of coordinates represented by the basis functions transform as do the irreducible representations of the polarizability tensor.

Similarly, the selection rules for infrared absorption can be found as the dipole moment transforms as the translational symmetry of the crystal. Thus, phonons with irreducible representations which are represented by linear basis functions of each point group will be infrared active.

These general rules as are found in common texts (Tinkham, 1964; Wilson, Decius and Cross, 1955) are valid as long as the Raman active vibrations concerned are not also infrared active. This dual activity can occur only in piezoelectric crystals, that is crystals that do not possess a centre of inversion. Thus, GaS should obey the selection rules as derived by the common technique. For those phonons which are infrared active in piezoelectric crystals, the macroscopic electric field carried by the long wavelength optic vibration produces a splitting between the transverse phonon and the longitudinal optical phonon. It will be necessary to treat these modes in some detail to understand their behaviour and thus complete the calculation of the selection rules.

It has been shown (Born and Huang, 1954) that for an optic vibration of frequency ω of polar diatomic cubic lattice (which we will treat first for simplicity) the relative motion of the positive and negative sublattices are related by the macroscopic equations:

$$(\omega_o - \omega^2)\vec{r} = \left(\frac{V}{4\pi M}\right)^{\frac{1}{2}} (\epsilon_o - \epsilon_\infty)^{\frac{1}{2}} \omega_o \vec{E} \qquad (2.19)$$

and

$$\vec{P} = \left(\frac{M}{4\pi V}\right)^{\frac{1}{2}} (\epsilon_o - \epsilon_\infty)^{\frac{1}{2}} \omega_o \vec{r} + (\epsilon - 1) \frac{\vec{E}}{4\pi} \qquad (2.20)$$

where $\vec{r}$ is the relative displacement of the two sublattices, $\vec{E}$ the electric field of the vibration, ω the vibrational frequency, ω_o the lattice dispersion frequency (which at k-vectors much greater than ω_i/c is equal to the TO phonon frequency), $\vec{P}$ is the polarization field, V the crystal volume and M the reduced mass of the two sublattices.

From Maxwell's equations in a non-conducting medium it is easy to show that there is the additional constraint:

$$\vec{E} = \frac{-4\pi(\vec{k}(\vec{k}\cdot\vec{P}) - \omega^2\vec{P}/c^2)}{k^2 - \omega^2/c^2} \qquad (2.21)$$

where $\vec{k}$ is the wavevector of the vibration. From 2.19, 2.20 and 2.21, one gets the transverse solutions ($\vec{k}\cdot\vec{P} = 0$):

$$\frac{k^2c^2}{\omega^2} = \frac{\omega_o^2\epsilon_o - \omega^2\epsilon_\infty}{\omega_o^2 - \omega^2} \qquad (2.22)$$

and for the longitudinal solution ($\vec{k}\cdot\vec{P} = kP$):

$$\omega = \omega_o \left(\frac{\epsilon_o}{\epsilon_\infty}\right)^{\frac{1}{2}} \equiv \omega^{\ell} \qquad (2.23)$$

Equation 2.23 is recognizable as the Lyddane-Sachs-Teller equation for the splitting between the longitudinal and transverse optic phonons. Equation 2.22 also describes the polariton dispersion for the transverse optical phonon in a cubic piezoelectric material.

This must, however, be extended to uniaxial crystals to

apply for GaSe, the piezoelectric crystal of interest here. In a uniaxial crystal atoms displaced along the crystallographic c-axis during a vibration will have a frequency $\omega_{\parallel}$ in general different from the same vibration in the ab-plane, given by frequency $\omega_{\perp}$. There are now two high frequency and two static dielectric constants, parallel to and perpendicular to the c-axis. Equation 2.21 will continue to be valid and can be divided into components parallel to and perpendicular to the c-axis. Carrying through a procedure similar to that used for cubic symmetry one obtains the frequencies for $\omega/c << k << \frac{\pi}{a}$ of (Loudon, 1964):

$$\omega = \omega_{\perp} \qquad \text{(ordinary phonon)} \qquad (2.24)$$

and

$$\left(\frac{\omega_{\parallel}^{2}\epsilon_{\parallel}^{o} - \omega^{2}\epsilon_{\parallel}^{\infty}}{\omega_{\parallel}^{2} - \omega^{2}}\right)\cos^{2}\theta + \left(\frac{\omega_{\perp}^{2}\epsilon_{\perp}^{o} - \omega^{2}\epsilon_{\perp}^{\infty}}{\omega_{\perp}^{2} - \omega^{2}}\right)\sin^{2}\theta = 0$$

(extraordinary phonons) (2.25)

where θ is the angle between the phonon k-vector and the c-axis and where one <u>defines</u> analogous quantities to equation 2.23:

$$\omega_{\parallel}^{\ell} = \omega_{\parallel}\left(\frac{\epsilon_{\parallel}^{o}}{\epsilon_{\parallel}^{\infty}}\right)^{\frac{1}{2}} \qquad (2.26)$$

$$\omega_{\perp}^{\ell} = \omega_{\perp}\left(\frac{\epsilon_{\perp}^{o}}{\epsilon_{\perp}^{\infty}}\right)^{\frac{1}{2}} \qquad (2.27)$$

Several words of explanation are necessary at this point. An "ordinary" phonon is a phonon whose k-vector and polarization are both perpendicular to the c-axis. Equation 2.25 thus has two solutions for each value of θ corresponding in general to a "quasi"-longitudinal optical phonon and to an orthogonal

"quasi"-transverse optical phonon. The longitudinal optical frequencies $\omega_{\parallel}^{\ell}$ and $\omega_{\perp}^{\ell}$ defined by 2.26 and 2.27 are not necessarily those measured in the crystal, then, since the longitudinal phonon frequency (as does the TO phonon frequency) near (but not at) the zone centre varies between these two frequencies as the angle θ varies. This facet will be probed in detail below.

If ω_1 and ω_2 are the two roots of 2.25, one obtains a modified LST relation:

$$\frac{\omega_1^2\omega_2^2}{\omega_{\perp}^2\omega_{\parallel}^2} = \frac{\epsilon_{\parallel}^{o}\cos^2\theta + \epsilon_{\perp}^{o}\sin^2\theta}{\epsilon_{\parallel}^{\infty}\cos^2\theta + \epsilon_{\perp}^{\infty}\sin^2\theta} \qquad (2.28)$$

For $k \parallel c$, for example, one has roots of 2.25 of $\omega = \omega_{\parallel}^{\ell}$ and $\omega = \omega_{\perp}$, thus 2.28 becomes

$$\frac{\omega_{\parallel}^{\ell 2}}{\omega_{\parallel}^2} = \frac{\epsilon_{\parallel}^{o}}{\epsilon_{\parallel}^{\infty}}$$ which satisfies 2.26.

It is also necessary to point out at this time that this calculation is based on assumption that only one optical phonon branch is infrared active. When more than one branch is infrared active, one would expect Reststrahlen effects in each branch and thus the splitting between the optical and static dielectric constants should be displayed in some combination of the LO-TO phonon frequency splittings of the various branches, j. Cochran and Cowley (1962) have generalized the LST relation for more than one infrared active branch in a cubic (or isotropic) crystal to the form

$$\prod_{j=1}^{N} \left(\frac{\omega_L(j)}{\omega_T(j)}\right)^2 = \frac{\epsilon^o}{\epsilon^\infty} \qquad (2.29)$$

For a uniaxial crystal one may expect two product relations for the splitting perpendicular and parallel to the c-axis.

Loudon (1964) treats two limits for equation 2.25 which are instructive. The first case (I) is the electrostatic limit where the splitting between the TO phonon frequencies caused by the anisotropy of the crystal is small compared to the LO-TO splittings (i.e. $|\omega_{\parallel}-\omega_{\perp}| << \omega_{\parallel}^{\ell}-\omega_{\parallel}$, $\omega_{\perp}^{\ell}-\omega_{\perp}$). For the other limit (II) called the anisotropic limit, the splitting between the TO phonons is predominant. Curves for the phonon dispersion as a function of propagation direction for the two cases are reproduced in Figures 2.4 and 2.5. In these figures L stands for the longitudinal optical phonons and T is for the transverse optical phonons. Note that the momentum scale only extends to approximately twice the momentum of the photon ($k \approx \frac{n}{c}\omega$) at the energy of the LO phonons and thus is extremely close to $\vec{k} \approx 0$. The lowest branches are not to be confused with acoustic phonons. The lowest branch displays the dispersion of transverse optical phonons in the "polariton" regime, that is, where the "phonon" is more properly described as a mixture of electromagnetic and mechanical vibrations. In first order Raman scattering the momentum of the phonons sampled is $\vec{q}=\vec{k}_i-\vec{k}_s$ or of magnitude $|q| = (k_i^2+k_s^2-2k_ik_s\cos\theta)^{\frac{1}{2}}$, where θ is the angle between the incident and scattered light. This gives approximately

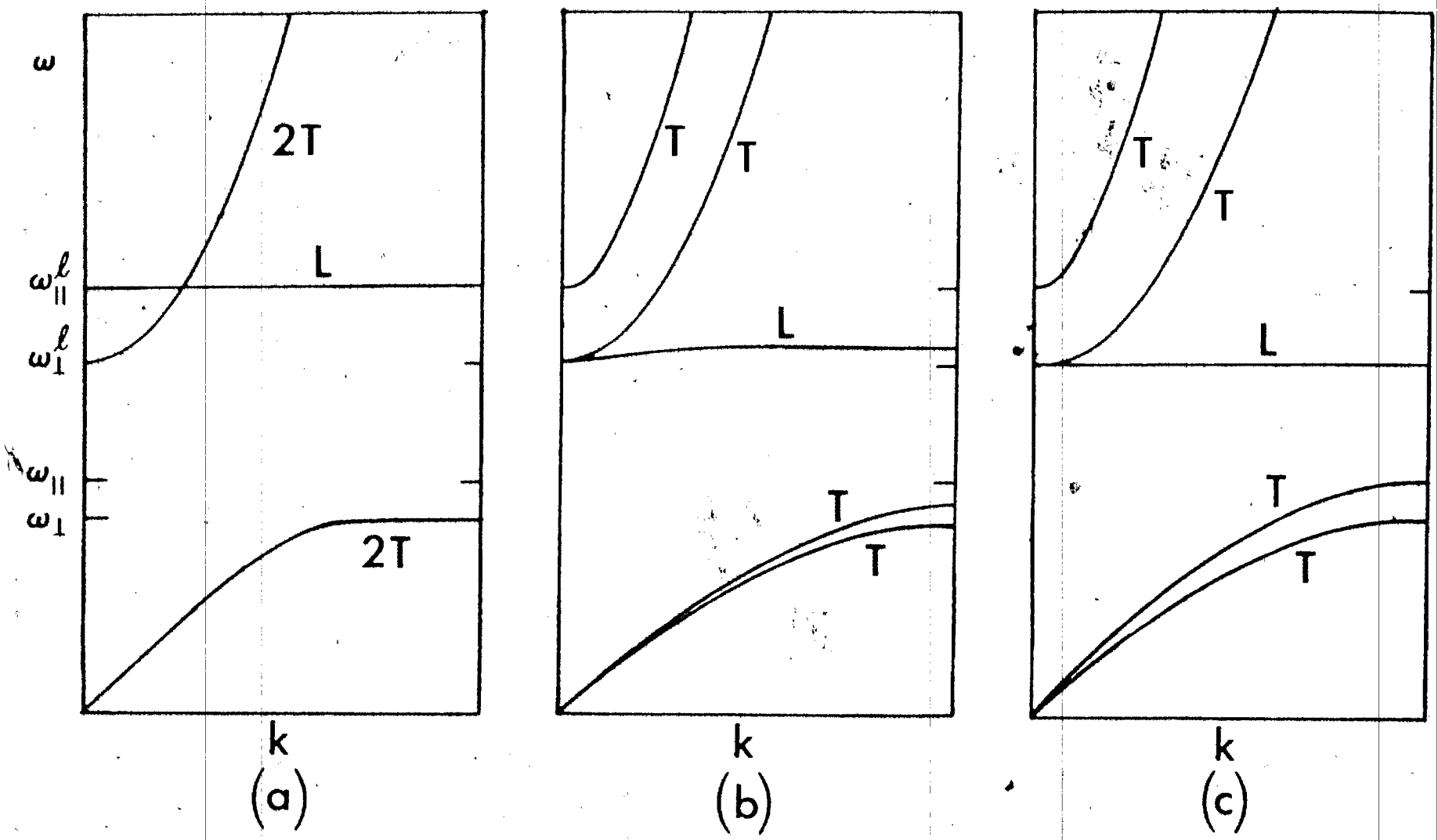

Figure 2.4. CASE I (Electrostatic Limit): Phonon dispersion curves at small wavevector in a uniaxial crystal for which electrostatic forces predominate over anisotropy. Phonon wavevector (a) parallel to c-axis, (b) in intermediate direction, and (c) lying in the ab-plane (After Loudon, 1964).

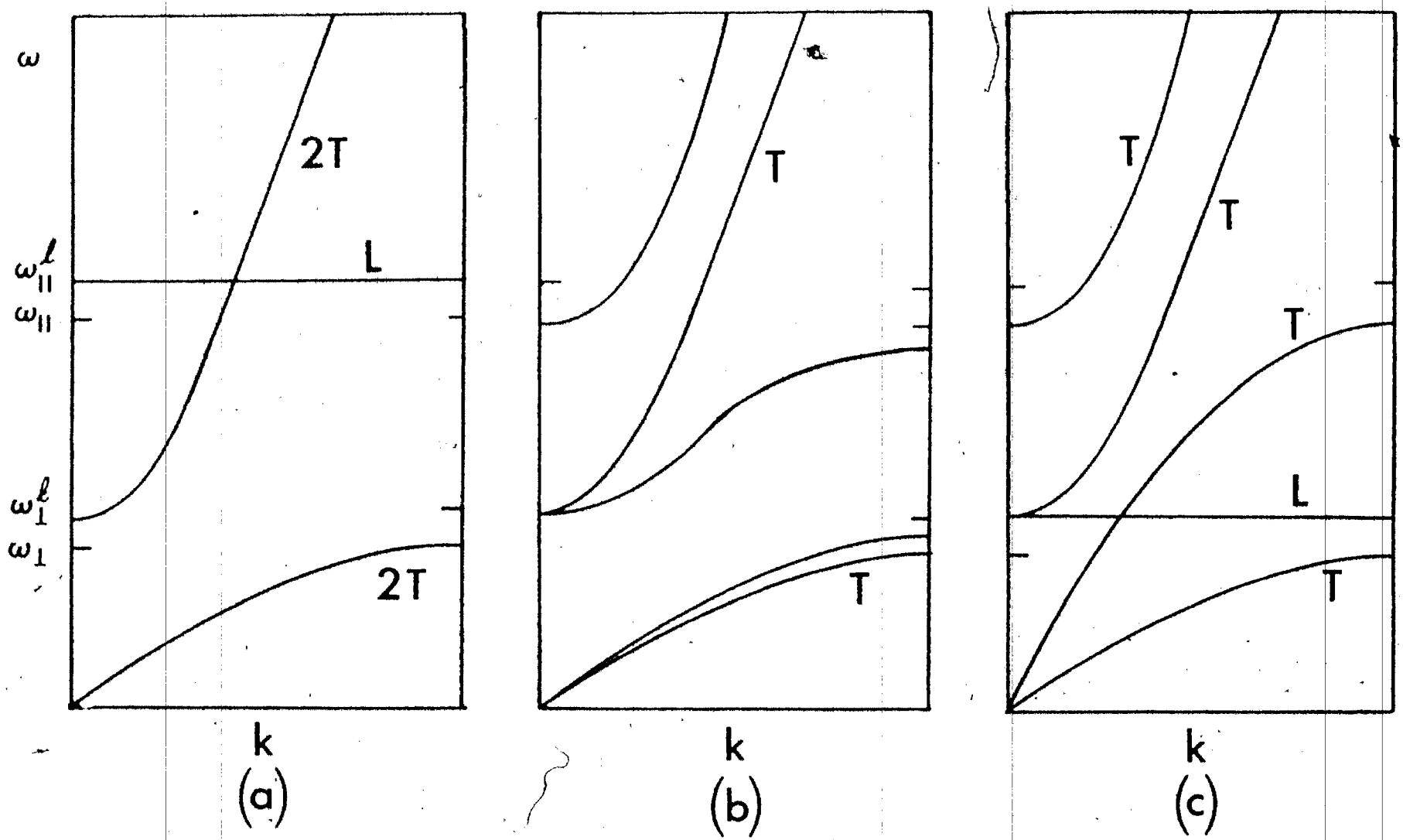

Figure 2.5. CASE II (Anisotropic Limit): Phonon dispersion curves at small wavevector in a uniaxial crystal for which anisotropy in the interatomic forces predominates over electrostatic forces. Phonon wavevector (a) parallel to c-axis, (b) in intermediate direction, and (c) lying in the ab-plane (After Loudon, 1964).

$|q| \approx \sqrt{2}\ \frac{\omega_i}{c/n}\ (1-\cos\theta)$. Since ω_i, the frequency of the light, is much greater than ω_{LO} or ω_{TO}, the frequencies of the phonons, the momentum of the phonon sampled in general will be much further out in the Brillouin zone than the region drawn. The exception to this would be scattering in the very forward direction ($\theta \approx 0°$) and then polariton effects would become important. In viewing the diagrams then one should recognize the frequencies seen in the first order effect as those on the very right hand edge of each drawing. In both cases, for phonon propagation along the c-axis the LO frequency is $\omega_{\parallel}^{\ell}$ and the TO phonons are both ordinary at frequency $\omega_{\perp}$. For phonon propagation in the ab-plane (drawing (c) of each figure), the LO phonon is of frequency $\omega_{\perp}^{\ell}$ and the TO branch splits into an ordinary and an extraordinary phonon of frequencies $\omega_{\perp}$ and $\omega_{\parallel}$, respectively. For intermediate directions the frequency and symmetry of the phonons is of mixed character and must be found by equation 2.25. In a later section it will be seen that GaSe does not quite meet the criteria for either limit (although the phonon curves are qualitatively like case I) and the most general form of equation 2.25 is needed to calculate the phonon dispersion with propagation angle.

To reiterate, before continuing with a discussion of the selection rules, in a uniaxial piezoelectric crystal Raman active phonons which are also infrared active do not

simply obey the normal selection rules discussed in common texts since they carry with them a macroscopic electric field. Besides changing the group theoretical selection rules, this field is responsible for enhancing the frequency of the longitudinal optical phonon and gives rise to the Lyddane-Sachs-Teller splitting. In a uniaxial crystal the transverse optical phonon(s) which is (are) infrared active displays an angularly dispersive frequency dependence due to the anisotropy of the crystal. Depending on the strength of this macroscopic electric field relative to this anisotropy, the longitudinal optical phonons will show a more complicated dispersive behaviour than for the cubic case.

As was shown in equation 2.9, the strength of the scattering and thus the selection rules were given by a dot product between the unit vector of the phonon mechanical polarization and the Raman tensor for that phonon. The selection rules can then be obtained by writing the scattering efficiency in the form:

$$S = A\left[\sum_{\substack{\rho\sigma\tau= \\ x,y,z}} e_i{}^{\sigma} R_{\sigma\rho}^{\tau} \xi^{\tau} e_s{}^{\rho}\right]^2 \qquad (2.30)$$

where e_i, e_s are the incident and scattered polarizations and $R_{\sigma\rho}^{\tau}$ is the symmetric tensor (since the selection rules to be derived are for the non-resonant spectrum) and ξ^{τ} is the τth component of the phonon polarization. This equation is valid, then, primarily far from resonance and where the phonons concerned are not both IR and Raman active. Thus,

in centrosymmetric crystals, such as GaS, and for the non-polar phonons in GaSe the above form is adequate to determine the selection rules. The result obtained will be identical to that of merely inspecting the basis functions of the point group of the crystal.

For a uniaxial piezoelectric crystal several modifications must be made. There are two types of electron-lattice interaction of interest here: the deformation potential where the lattice displacement $\vec{r}$ is parallel to $\vec{\xi}$, the polarization of the phonon, and the polar scattering mechanism (Fröhlich coupling) in which the $\vec{E}$ vector of the macroscopic field is parallel to $\vec{k}$, the phonon wavevector. Thus, equation 2.30 must be generalized to (Loudon, 1964):

$$S = \left[\sum_{\substack{\rho\sigma\tau= \\ x,y,z}} e_i^{\sigma} R_{\sigma\rho}^{\tau} (\alpha \xi^{\tau} + \beta k^{\tau}) e_s^{\rho} \right]^2 \qquad (2.31)$$

where β is proportional to the electric field strength $|\vec{E}|$. It should be noted that $\beta = 0$ for exactly transverse optical phonons.

The selection rules calculated by equations 2.30 and 2.31 for β-GaS and for ε- and γ-GaSe are given in Appendix B. The results are summarized in Table 2.2.

TABLE 2.2
SELECTION RULES FOR β, ε, AND γ POLYTYPES*

β - Polytype - D_{6h}^4 - centrosymmetric (no polar phonons)

Phonon Symmetry	Polarizability Tensor
A_{1g}	$\alpha_{xx} + \alpha_{yy}$, α_{zz}
E_{1g}	α_{yz} , α_{zx}
E_{2g}	$\alpha_{xx} - \alpha_{yy}$, α_{xy}

ε - Polytype - D_{3h}^1 - piezoelectric (E´ modes polar)

Phonon Symmetry	Polarizability Tensor
non-polar modes:	
A_1'	$\alpha_{xx} + \alpha_{yy}$, α_{zz}
E''	α_{xz} , α_{yz}
polar modes:	
E´(LO)	$Y(XX)\bar{Y}$, $X(YX)Y$, $Y(XY)X$ $Y(XX)Z$, $X(YX)Z$, $Z(XX)Y$ $Z(XY)X$
E´(TO) extraordinary	$Y(XX)Z$, $X(YX)Z$, $Z(XX)Y$ $Z(XY)X$
E´(TO) ordinary	$X(YY)\bar{X}$, $Z(YY)\bar{Z}$, $X(YX)Y$ $Y(XY)X$, $Y(XY)Z$, $X(YY)Z$ $Z(YX)Y$, $Z(YY)X$

γ - Polytype - C_{3v}^5 - piezoelectric (All modes polar)

Phonon Symmetry	Allowed Geometries
LO Phonons:	
A_1(LO)	$Z(XX)\bar{Z}$, $Z(YY)\bar{Z}$
E(LO)	$Y(XX)\bar{Y}$, $X(YX)Y$, $X(ZX)Y$ $X(YZ)Y$, $Y(XY)X$, $Y(ZY)X$ $Y(XZ)X$

Table 2.2 (continued)

Phonon Symmetry	Allowed Geometries
LO Phonons (cont.):	
A_1 + E(LO)	Y(ZY)Z, Y(XX)Z, X(YX)Z, X(ZX)Z, X(YY)Z, Z(YZ)Y, Z(XX)Y, Z(XZ)X, Z(XY)X, Z(YY)X
Extraordinary TO:	
A_1(TO)	X(ZZ)$\bar{X}$, X(YY)$\bar{X}$, Y(ZZ)$\bar{Y}$, Y(XX)$\bar{Y}$, X(ZZ)Y, Y(ZZ)X
A_1 + E(TO)	Y(ZY)Z, Y(XX)Z, X(YX)Z, X(ZX)Z, X(YY)Z, Z(YZ)Y, Z(XX)Y, Z(XZ)Y, Z(XY)X, Z(YY)X
Ordinary TO:	
E(TO)	X(YZ)$\bar{X}$, X(YY)$\bar{X}$, X(ZY)$\bar{X}$, Y(XZ)$\bar{Y}$, Y(ZX)$\bar{Y}$, Z(XX)$\bar{Z}$, Z(XY)$\bar{Z}$, Z(YY)$\bar{Z}$, Z(YX)$\bar{Z}$, X(YX)Y, X(ZX)Y, X(YZ)Y, Y(ZZ)X, Y(XY)Z, Y(ZX)Z, X(YY)Z, X(ZY)Z, Z(XZ)Y, Z(YZ)Y, Z(YZ)X, Z(YY)X

* Unless specifically noted polarizability tensor elements give the Raman selection rules for all geometries.

2.5 Normal Modes of Vibration

The normal modes of vibration for GaS and GaSe have been drawn for the various polytypes in Figures 2.6, 2.7 and 2.8. The description of the modes for the β-polytype is due to Wieting and Verble (1972) and the ε-polytype to Brebner et al. (1973) and Yoshida et al. (1973). The γ-polytype displacements have been identified generally by Mercier and Voitchovsky (1974) but the phasing of the modes has not been published to date.

The diagrams are drawn so that the eight columns are each grouped by the eight distinct intralayer vibrations. Since the bonding between the layers is very weak, the layers vibrate nearly independently and thus rigid-layer mode vibrations develop. These rigid-layer modes, B_{2g}^2 and E_{2g}^2 in the β-polytype, $A_2''(1)$ and $E'(1)$ of the ε-polytype and $A_1(1)$ and $E(1)$ of the γ-polytype, are low frequency modes with the weak interlayer coupling as the only force constant involved in the vibration. While always occurring in the β-polytype, the term "rigid-layer" is really only applicable (and thus the diagrams correct as drawn) in the ε- and γ-polytypes if the interlayer force constant is so small as to leave the intralayer vibrations unperturbed. This has been found to be a very good approximation in these compounds (Wieting, 1973).

The eight distinct intralayer vibrations (four of which are two dimensional) are doubled by this interlayer coupling in the β and ε-polytypes and trebled in the γ-polytype to give the 24 and 36 normal modes, respectively. The two modes

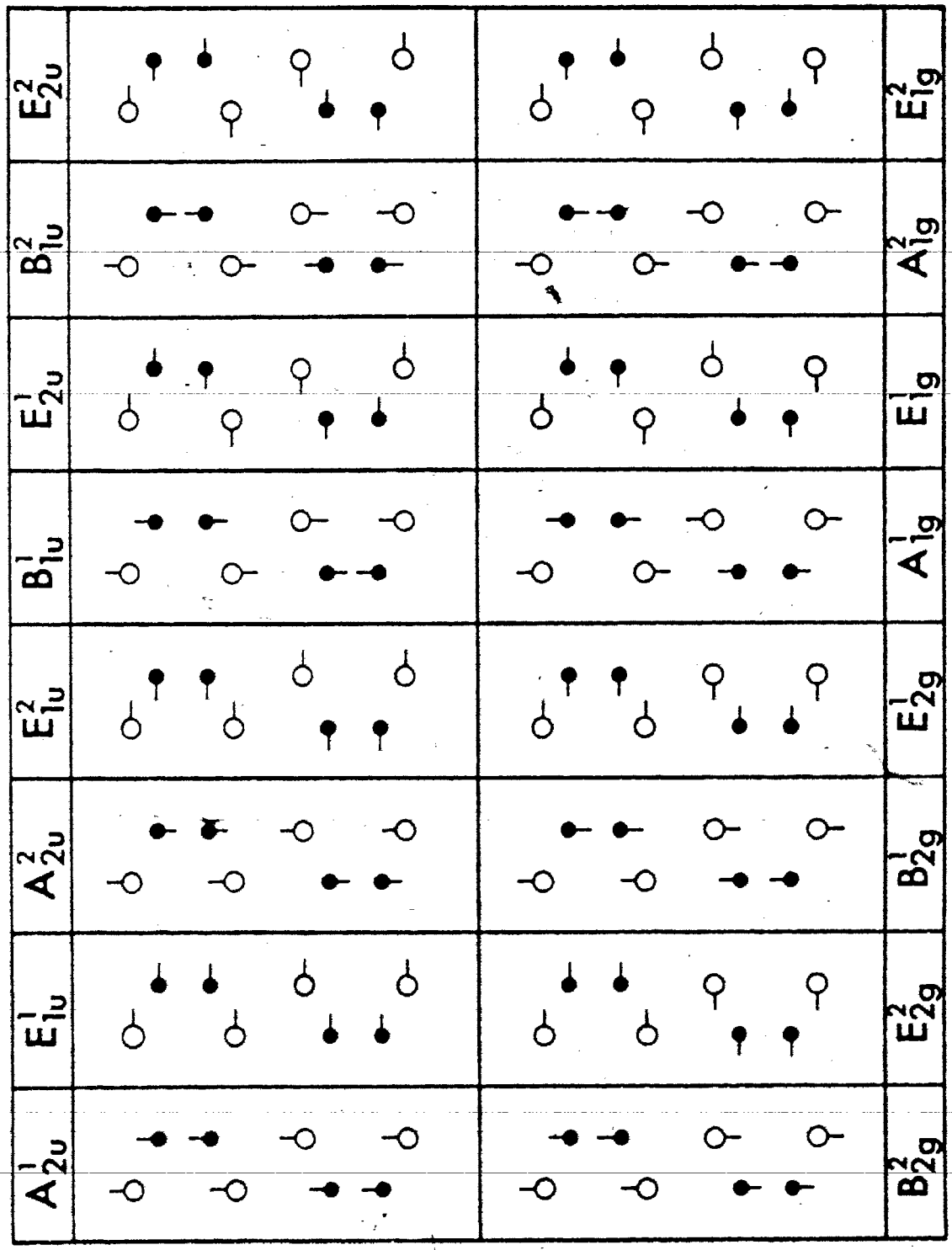

Figure 2.6. Normal modes of vibration of the β-polytype.

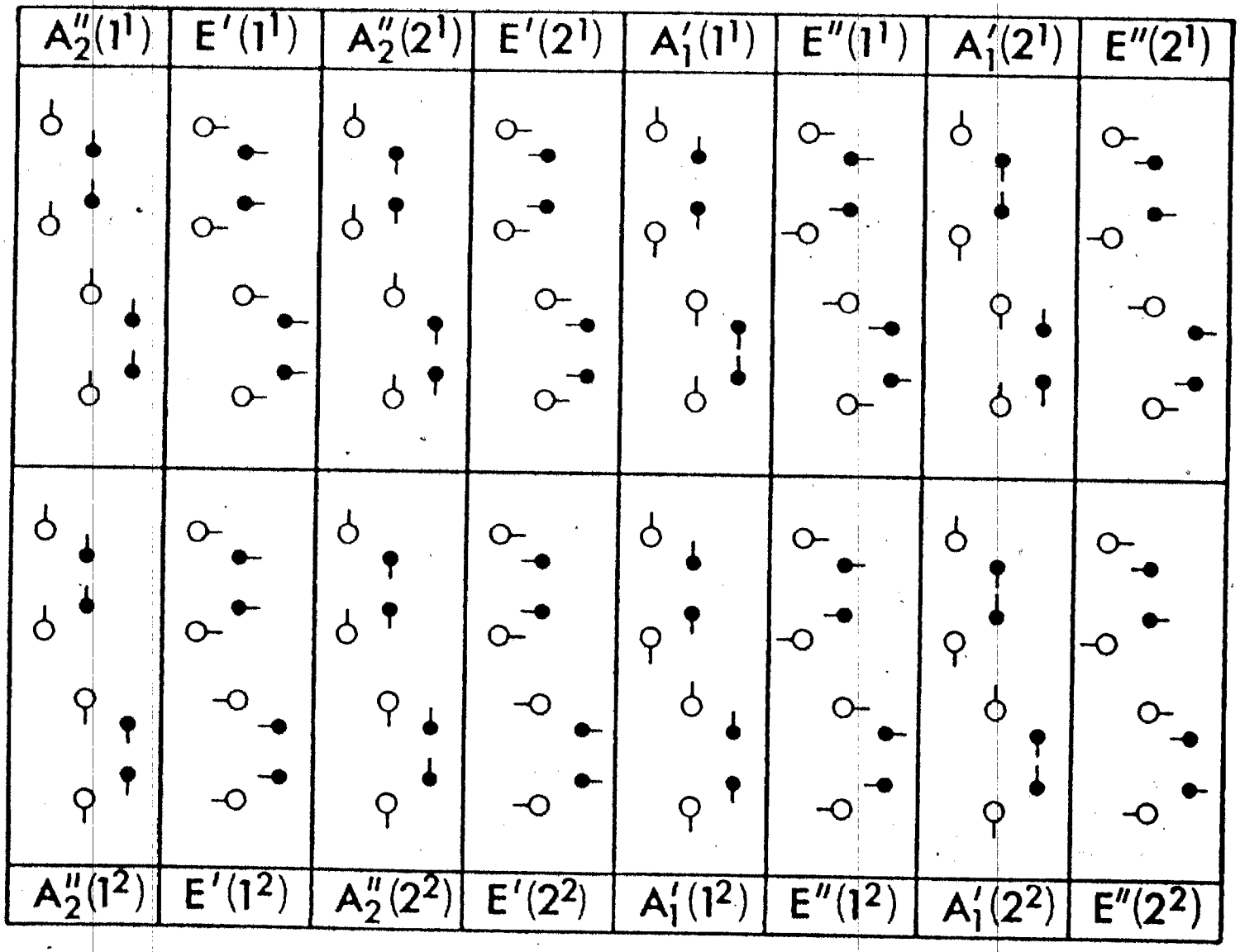

Figure 2.7. Normal modes of vibration of the ε-polytype.

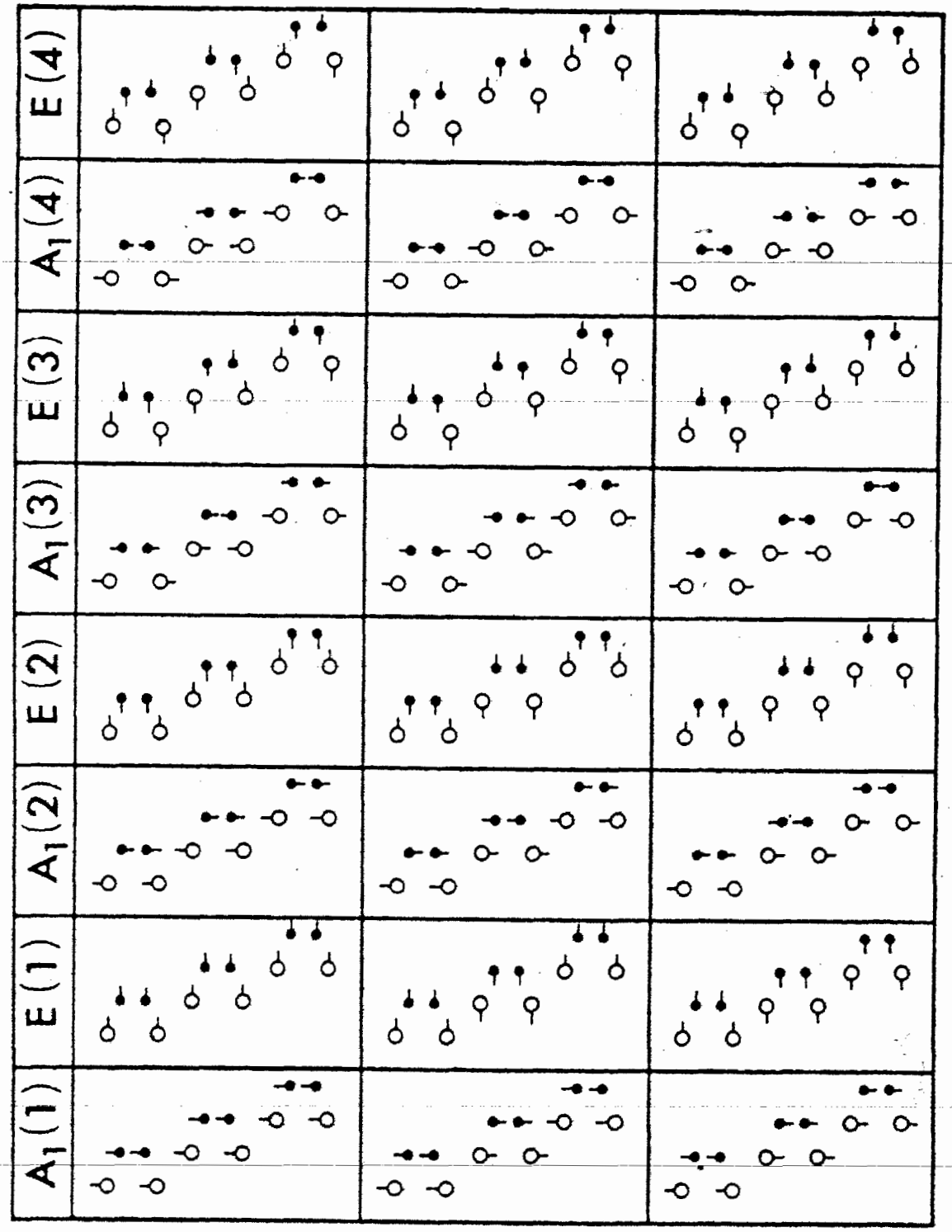

Figure 2.8. Normal modes of vibration of the γ-polytype.

in each column in the β and ε cases and the three in each column in the γ-polytype should be nearly degenerate in energy if the interlayer coupling is indeed small and this gives rise to the terminology "conjugate modes" (Wieting and Verble, 1972; Hayek et al., 1973). The rows of the three figures are grouped so that the top row of vibrations has the interlayer selenium atoms moving in phase, the second row has them moving out of phase. The rationale for such a grouping is that in the two layer polytypes, the top row of vibrations will have each layer in phase with respect to a mirror plane parallel to the layers. In the β-polytype, where there is a centre of inversion, this makes all the vibrations of the top row odd with respect to inversion while the bottom row is even with respect to inversion. In the ε-polytype such a grouping is again retained, and the author will refer to these vibrations (for the lack of a better system) as "odd-type" and "even-type" vibrations, although they are strictly neither odd nor even. In the γ-polytype there is an additional degree of freedom given by the third layer of the unit cell and the other possibility is that the layers alternate between being in phase and then out of phase.

There has been considerable controversy concerning possible observation of these conjugate modes in the Raman spectrum of GaSe. The difficulty arises in distinguishing nearly degenerate but distinct interlayer vibrations from the

predicted conjugate pairs (or triplets). Hayek et al. (1973) based many of their assignments of the phonon frequencies of GaSe on the conclusion that these conjugate pairs are visible in the spectrum. This work finds itself in disagreement with that conclusion and only the symmetry characteristics of the observed phonons are used to assign the spectral peaks.

It is possible to estimate the degree of splitting between the conjugate pairs (Wieting and Verble, 1972; Wieting, 1973). The intralayer force constant is easily determined since the rigid layer modes differ from the zero frequency acoustic vibration by the frequency involving only the vibration between the layers. Thus, for the two layer polytypes β and ε: $\omega_i^2 = \frac{C_i}{M}$ where M is the reduced mass of a gallium-chalcogenide pair. There are two frequencies ω_A and ω_E corresponding to vibrations parallel to and perpendicular to the c-axis, giving one compressional and one shear interlayer force constant.

From a simple concept, then, of two coupled harmonic oscillators of frequency ω_o, one has the two vibrational frequencies with coupling constant C_i of:

$$\omega^2 = \omega_o^2, \omega_o^2 + \omega_i^2 \qquad (2.32)$$

This is, however, only an approximation of the splitting valid for very small interlayer force constants. Wieting (1973) has calculated the frequencies of splittings on the basis of a linear chain of eight atoms with two masses and three spring

constants. His result is also a crude approximation to the actual crystal, but the two above approaches should give the order of magnitude of the conjugate pair splittings. These results will be used in the discussion of the assignments made for GaSe.

CHAPTER III

THE FIRST ORDER RAMAN SPECTRA OF GaS AND GaSe-EXPERIMENTAL

3.1.1 Crystals

The crystals used in this study were grown by the modified Bridgeman technique of Beck and Mooser (1961) by iodine vapour transport and by sublimation (Terhell and Lieth, 1972). These techniques yield quite different results. The Bridgeman technique, which involves the drawing of the crystal from the melt, yields large plate crystals which in some cases can give the very thick (1-2 mm) samples which were used in this work. These thick crystals are rare, however, and we were very fortunate to obtain thick samples of GaS and GaSe from Dr. John Brebner of the Université de Montreal. Crystals grown by this technique always yield the β-polytype for GaS, but as was mentioned previously there is some dispute about GaSe. While Wieting and Verble (1972) and Jellinek and Hahn (1961) interpreted the GaSe samples grown from this technique as also of the β-polytype, the more common interpretation at present is that they are a mixture of ε and γ stackings. The degree of admixing, however, has never been determined and this work sheds some light on that question.

GaSe crystals grown by sublimation usually yield thin flakes, ribbons or needles (Terhell and Lieth, 1972). It has been found that the needles can be purely of the γ-polytype and several of these needles were obtained from Dr. R.M.A. Lieth of Eindhoven University, The Netherlands. Thus, by

analyzing the Raman spectra of the needles in comparison to the thick crystals, one can obtain considerable information on the stacking of these compounds.

It should be noted in this regard that Laue X-ray photographs are only of limited usefulness in differentiating between the polytypes. Laue pictures on the large cyrstals can be easily taken only along the c-axis and in this orientation the Laue reflections from $D_{6h}^{4}(\beta)$ and $D_{3h}^{1}(\varepsilon)$ polytypes are identical. While the $C_{3v}^{5}(\gamma)$ polytype does have systematic absences when viewed along this axis, this is of no use in determining the composition of mixed ε-γ crystals because of the superposition of the spots. From rotating crystal techniques, however, X-ray studies of the large single crystals shows a high degree of stacking faults (Terhell and Lieth, 1972) and this has been tentatively attributed to polytype mixing (Mercier et al., 1973).

The gallium sulphide samples studied consisted of an oriented thick layer crystal approximately 0.8×1.0×0.2 cm in size and several flakes which were less than 0.5mm in thickness. The crystals were all bright yellow and as grown (from the melt) are expected to be p-type (Fischer, 1963).

The gallium selenide samples consisted of a thick sample which was X-ray oriented and cut on a wire saw along the x and y crystals axes (as defined by Nye (1957)), and of several large thin flakes. The large oriented crystal, which was also used in the Resonant Raman experiments, was

approximately 2mm thick in the c-direction and trapezoidal in shape as viewed from the c-axis. The y-face is approximately 2mm × 3mm and the x-face is approximately 2mm × 7mm. Attempts at polishing or otherwise improving the quality of the faces obtained from the wire saw cut proved unsuccessful as the process of mechanical polishing deformed these very soft crystals, and the author knows of no proven etch. The z-faces of these crystals could be greatly improved by cleaving new surfaces in this direction. This process is easily accomplished with a minimum of strain since the layers separate quite easily with the use of cellophane tape.

The γ-polytype needles of GaSe used are equilateral triangles in cross section and are tapered. The faces of the needle are thus not along pure symmetry directions but are (1 $\bar{1}$ 0 1) faces (Terhell and Lieth, 1972). However, since the c-axis cell dimension is so large with respect to the ab cell dimensions, the angle these faces make with the orthogonal y-crystalline axis is about 83° and thus near right angle scattering can be done. Refraction at these surfaces, which initially seems to be problematic, proves to be quite useful in the study of these needles and of the γ-polytype.

3.1.2. Apparatus

All spectra obtained in this work were excited by laser excitation. Three lasers were used in this work. The highest energy excitation was obtained with the various lines of a Spectra Physics Model 165 Argon Ion laser. It was found that

in order to obtain spectra in GaS far below the band gap at room temperature, the 5145 Å line of this laser was the most advantageous. With the Ar^+ laser running in a single longitudinal mode with the use of the Spectra Physics Model 589 intracavity etalon, it was possible to employ a molecular iodine filter (Devlin et al., 1971) in order to remove the unshifted component of the scattered light. The molecular iodine cell was five centimeters in length and its attenuation, construction and description of operation may be found in the thesis of C.G. Hodgins of this department who calibrated the cell (Hodgins, 1974).

Also used in this study was a 50mW Spectra Physics Model 125He-Ne laser at 6328 Å and a Spectra Physics Model 370 tunable dye laser. The dye laser contained Rhodamine 6G as its lasing element and provided a tunable output from 5470 Å to 6420 Å. The maximum output of the dye laser is between 5700 and 5900 Å and was 300mW at its peak. Typical power levels used in this study were less than 150mW.

The crystals were placed on a goniometer mount for room temperature work and in a cold finger dewar for the low temperature work. Because of the number of windows in the optical dewar, the sample temperature was somewhat higher than 77°K when liquid nitrogen was used. The ambient temperature measured with a gold-chromel thermocouple was typically 81 ± 1°K.

Spectra were taken in a variety of geometries where

the scattering angle between the incident and scattered beam ranged from 0° to 180°. The most common geometry, however, was the 90° configuration. In all cases, the geometry of the scattering event is given by the notation A(BC)D where A and D are the k-vectors of the incident and scattered photons, respectively, and B and C their respective polarizations.

Light from the sample in all but the backscattering spectra was collected by an f/1.2 Canon 50 mm focal length lens and imaged on the input slit of a Spex 1400 3/4 meter Czerny double monochrometer. An ITT FW-130 (S20 response) photomultiplier monitored the output of the spectrometer and the signal was fed through standard photon counting electronics and displayed on a strip chart recorder.

In the backscattering geometry, a combination of two simple lenses replaced the Canon lens in the collecting optics. In both cases, the scattered light was analyzed with sheet polaroid and then depolarized by a quartz wedge before entering the slit of the spectrometer to eliminate polarization effects of the gratings.

When the dye laser was employed as a source, the frequency of the line was calibrated before and after each series of runs at the wavelength being studied versus the known lines of a Neon discharge tube. The linewidth of the dye laser can become somewhat broad at the ends of the tuning range of the laser if the resonator controls of the dye laser

are not set carefully. In order to monitor this linewidth, the dye laser beam was checked periodically by passing the light through a Fabry-Perot interferometer with a 2mm spacer ($\Delta\tilde{\nu} = 1/2d = 2.5\ cm^{-1}$, free spectral range). By inspection of the thickness of the fringes, the laser linewidth was constrained to be less than 1 cm^{-1} sometimes with a consequent loss of intensity in the dye laser output.

3.2 Results

The first order Raman spectra of GaS and GaSe were studied chronologically by looking at β-GaS, then ε-γ crystals of GaSe and finally needles of γ-GaSe. There is an advantage in presenting the results in this chronological form since the structures in the Raman spectrum build on the knowledge of the identification of the modes in the simplest spectrum, GaS.

3.2.1 GaS

The Raman spectrum of GaS is shown for two orientations in Figure 3.1. The notation has been previously described. The spectra shown here were taken at room temperature with the 5145 Å line of the Argon ion laser with the use of a molecular iodine filter to discriminate against the unshifted component of the scattering. There are six features in the first order Raman spectrum and the two orientations shown here clearly display the differences in diagonal polarizations and off-diagonal elements of the scattering. The measured frequencies of the phonons are given in Table 3.1 where they are compared to the results of Van der Ziel et al. (1973). These assignments were made on the basis of the symmetry properties of the scattering and are consistant with the results obtained by Van der Ziel. In Table 2.2 it was shown that six first-order Raman active modes have been predicted from group theory and these six modes have been observed.

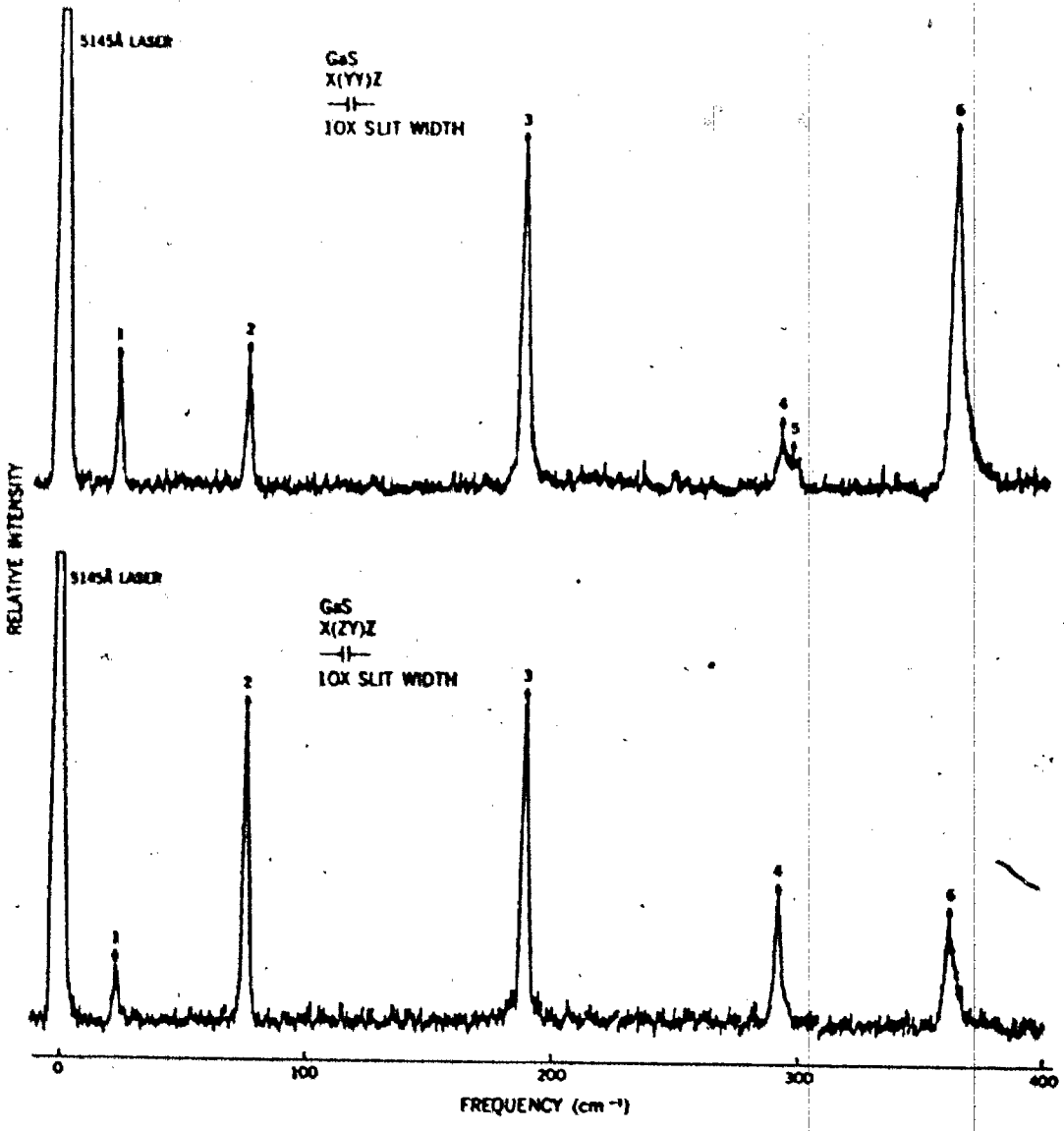

Figure 3.1. Raman Spectrum of GaS. The spectra shown represent the (a) X(YY)Z and (b) X(ZY)Z geometries. Spectra were taken at room temperature with the 5145 Å line of the Ar^{++} laser using an iodine filter.

TABLE 3.1 - Assignments and Frequencies of Vibration for β - GaS. All values obtained are ± 1.0 cm^{-1}.

Feature	Irred. Rep.	Polarizability Tensor	Raman Frequencies (cm^{-1}) 293 °K $\tilde{\nu}$ a	293 °K $\tilde{\nu}$ b	81 °K $\tilde{\nu}$ a
1	E_{2g}^2	$\alpha_{xx} - \alpha_{yy}, \alpha_{xy}$	22.0	22.0	23.0
2	E_{1g}^1	α_{yz}, α_{zx}	75.2	74.2	75.7
3	A_{1g}^1	$\alpha_{xx} + \alpha_{yy}, \alpha_{zz}$	187.9	188.0	189.7
4	E_{1g}^2	α_{yz}, α_{zx}	290.5	291.4	294.3
5	E_{2g}^1	$\alpha_{xx} - \alpha_{yy}, \alpha_{xy}$	295.0	295.2	298.4
6	A_{1g}^2	$\alpha_{xx} + \alpha_{yy}, \alpha_{zz}$	360.7	359.9	364.5

a) This work , b) Van der Ziel et al. (1973)

3.2.2 ε-γ GaSe

The Raman spectrum of the large crystals of GaSe is shown in Figures 3.2 through 3.5. These four figures display all the symmetry components which should be distinct by the group theoretical selection rules. The spectra shown here were obtained at liquid nitrogen temperature with the He-Ne laser and thus are far from resonance. The frequencies, polarization properties and assignments of these features are given in Table 3.2. It should be noted that while the assignments shown here are in some disagreement with previous authors (Wieting and Verble, 1972; Hayek et al., 1973), they are in substantial agreement with other recent results (Mercier and Voitchovsky, 1974; Yoshida et al., 1973).

The first spectrum (Figure 3.2) is the diagonal Y(ZZ)X geometry. In this ZZ orientation the only phonons which are Raman allowed are the A_1' (135 cm^{-1}) and the A_1' (308 cm^{-1}) phonons. These modes can be clearly seen to be the dominant features in the spectrum. The appearance of the other modes in the spectrum is due to sample depolarization (most of which probably occurs at the surfaces of these crystals). The relative strength of these features is much stronger in this spectrum than in off-diagonal scattering and thus identification of these modes is easily accomplished.

Figure 3.3 shows the off-diagonal Y(ZY)X geometry. In this geometry the 60 cm^{-1} E"(1) and the 212 cm^{-1} E"(2) phonons are quite strong as would be expected by group theory

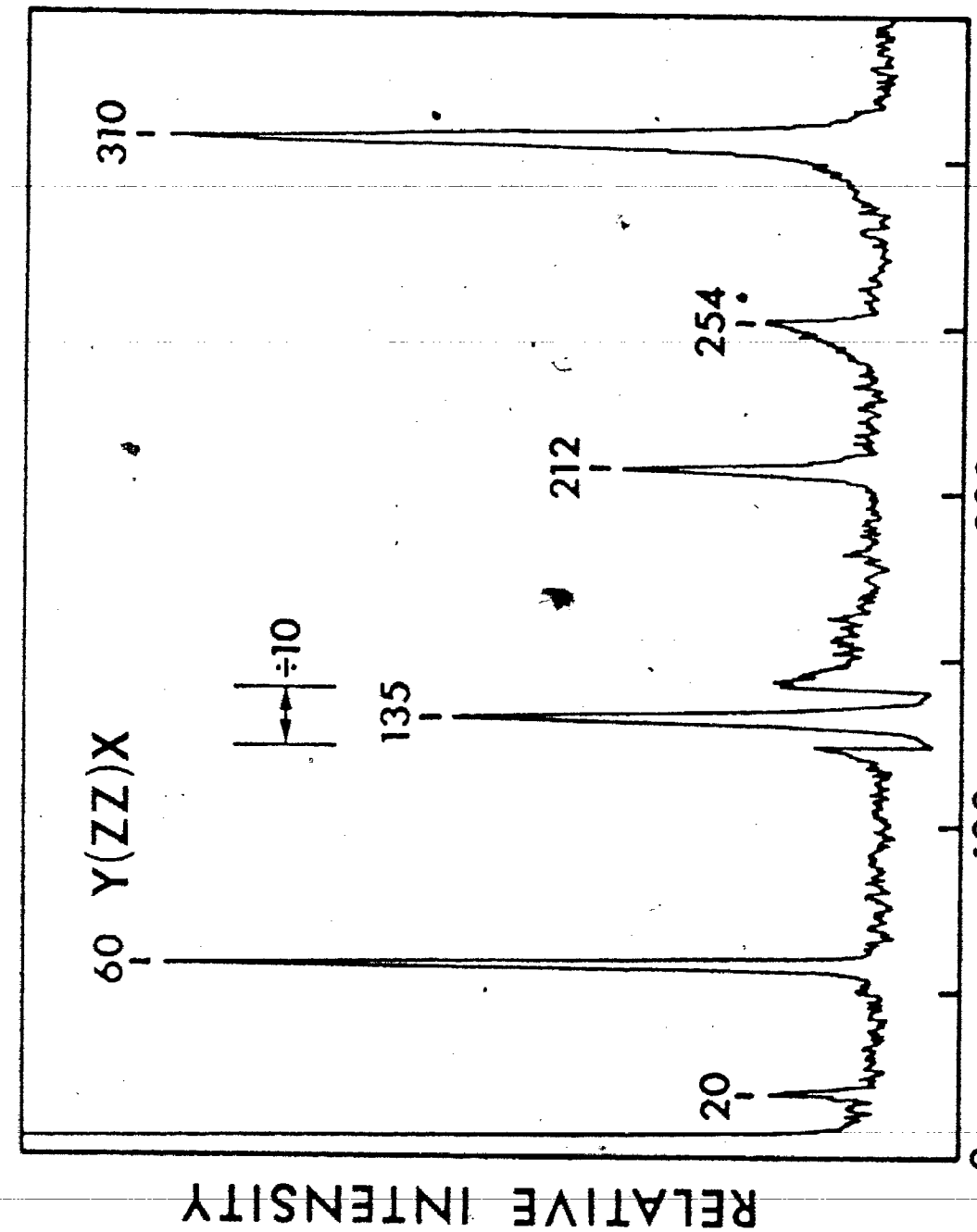

Figure 3.2. Raman spectrum of ε-Y GaSe: Y(ZZ)X geometry. Spectrum taken at 6328 A at 81 °K.

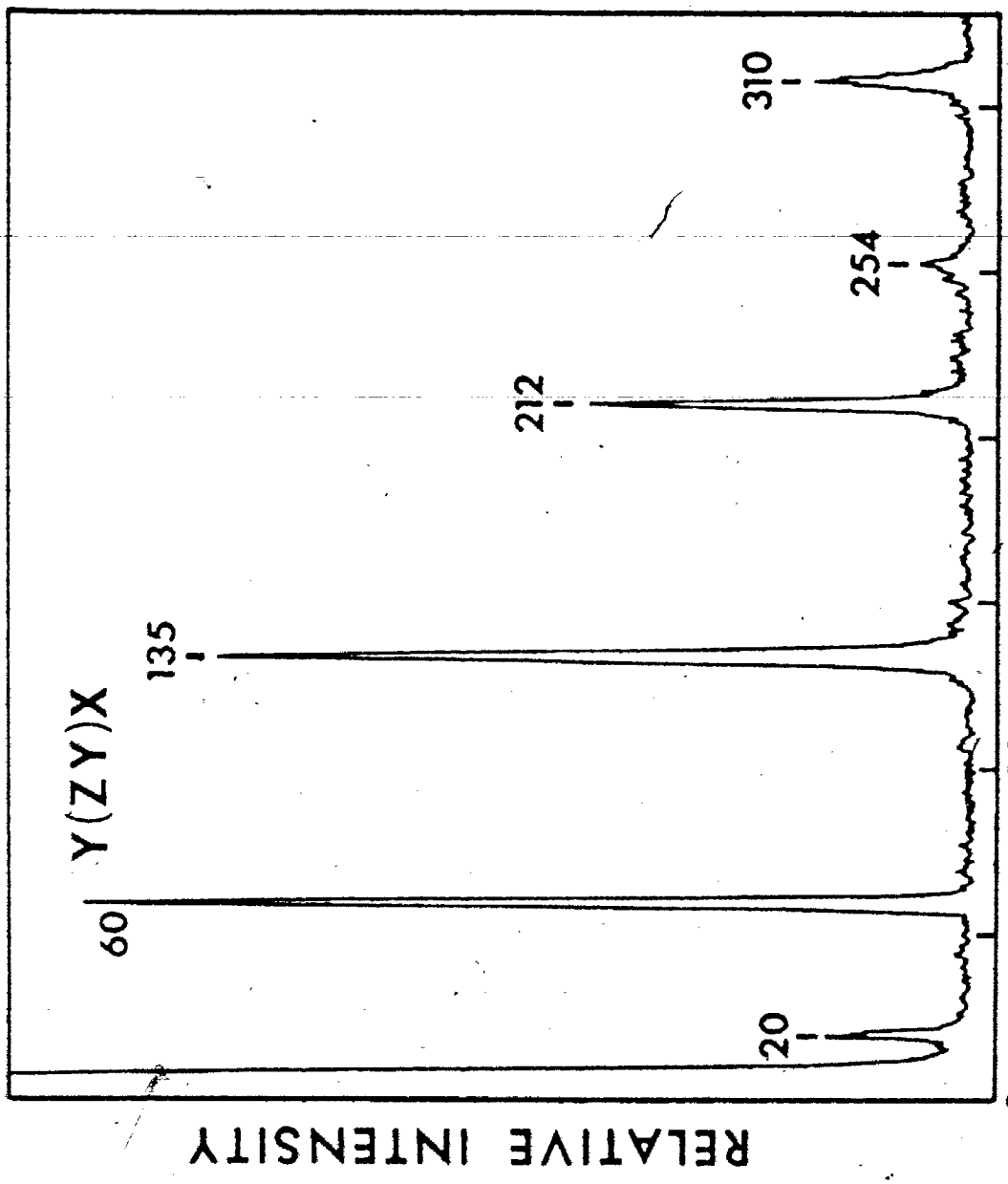

Figure 3.3. Raman spectrum of ε-γ GaSe: Y(ZY)X geometry. Spectrum taken at 6328 A at 81 °K.

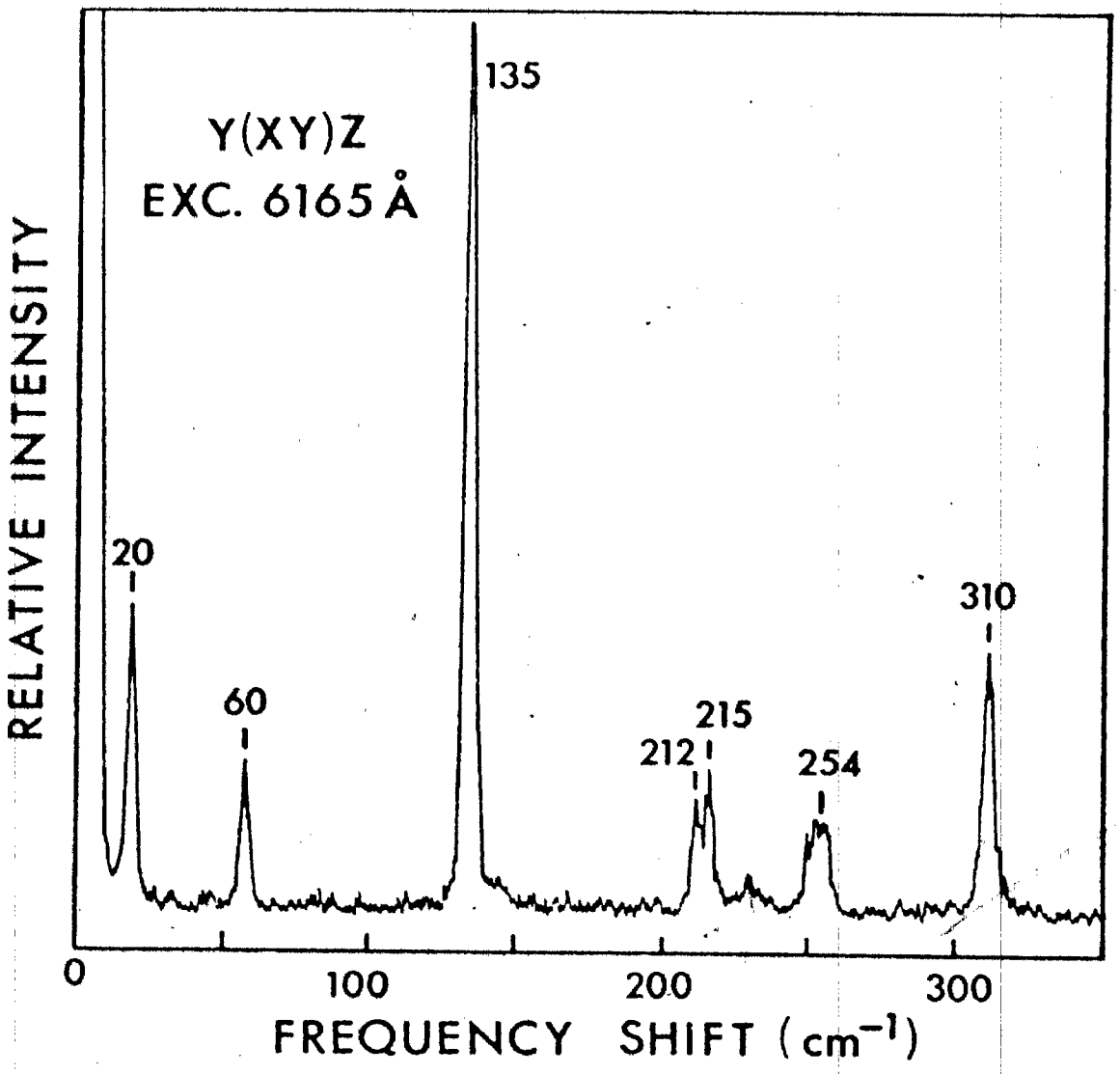

Figure 3.4. Raman spectrum of ε-γ GaSe: Y(XY)Z geometry. Spectrum taken at 6165 A at 81 °K.

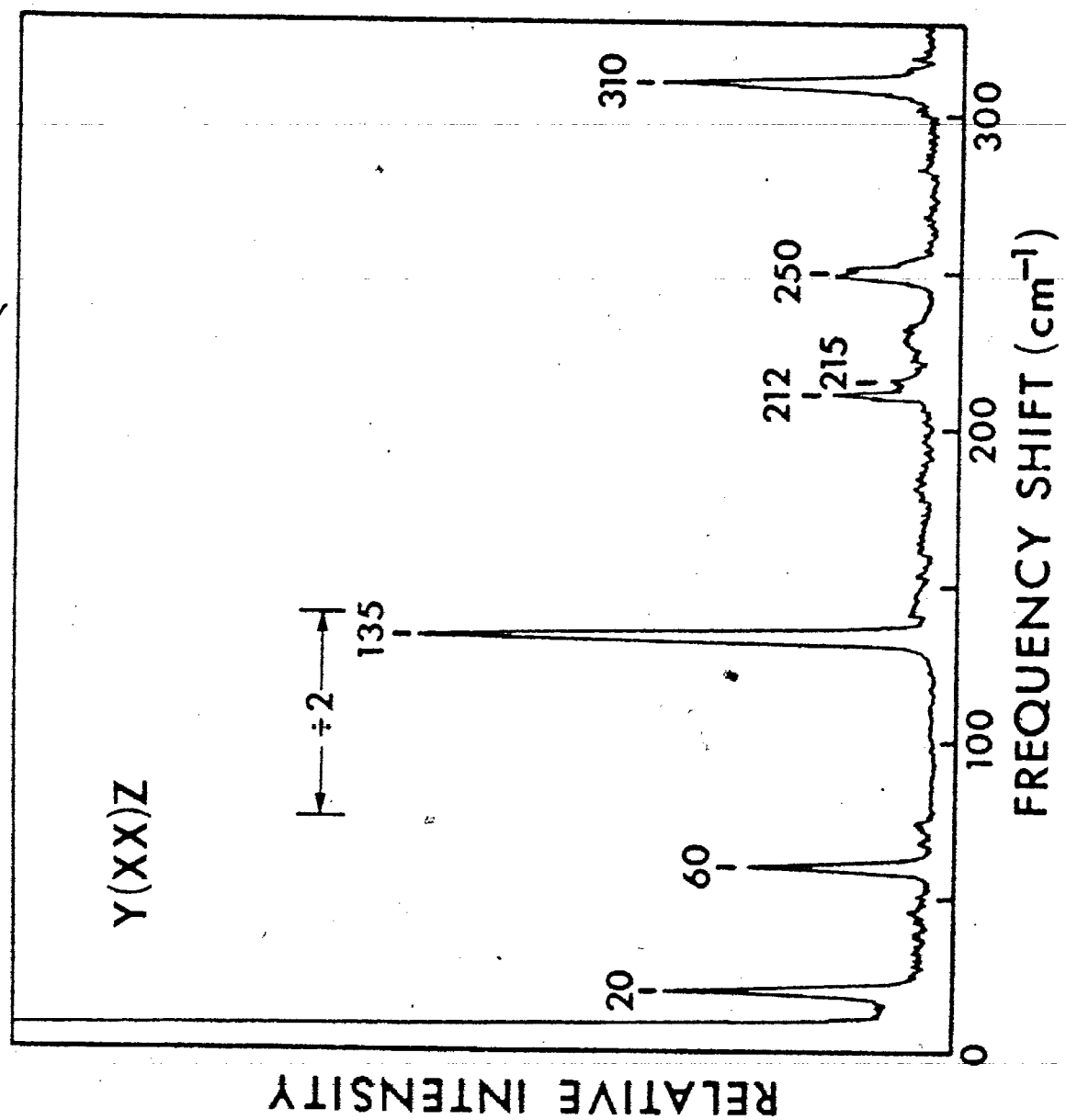

Figure 3.5. Raman spectrum of ε-γ GaSe: Y(XX)Z geometry. Spectrum taken at 6328 A at 81 °K.

TABLE 3.2 - Assignments and Frequencies of Vibration for (ε - γ) crystals of GaSe. Assignments are based on the ε-polytype, D_{3h}. All frequencies are ± 1.0 cm^{-1} unless otherwise noted.

Irreducible Represent.	Polarizability Tensor	Raman Frequencies (cm^{-1}) $\tilde{\nu}$ (293 °K)	$\tilde{\nu}$ (80 °K)
$E'(1^2)$	$\alpha_{xx} - \alpha_{yy}$, α_{xy}	19.5	19.8
$E''(1)$	α_{yz}, α_{zx}	60.1	60.0
$A_1'(1)$	$\alpha_{xx} + \alpha_{yy}$, α_{zz}	134.3	135.7
$E''(2)$	α_{yz}, α_{zx}	211.9	212.3
$E'(TO)$ (2)	*	214.0 ± 2.0	215.6
$E'(LO)$ (2)	*	252.1†	254.5
$A_1'(2)$	$\alpha_{xx} + \alpha_{yy}$, α_{zz}	308.0	310.8

* See selection rules (Table 2.2)

† This frequency possibly contains some A_2'' phonon involvement at room temperature.

(Table 2.2). Figure 3.4 shows the other off-diagonal component Y(XY)Z and the other E symmetry phonons E'(1^2) at 20 cm^{-1} and E'(TO)(2) at 215 cm^{-1} become relatively strong. Finally another diagonal spectrum Y(XX)Z is shown in Figure 3.5. In this spectrum all the phonons are relatively weak, but the E" modes at 60 and 212 cm^{-1} have almost disappeared, which is in agreement with the lack of an XX symmetry element for these vibrations.

3.2.3 γ-GaSe

The most conclusive evidence of the above assignments of the modes comes by examining the γ-polytype of GaSe. In the γ-polytype all modes become Raman active and thus the modes which were previously obscured by their inactivity may be deduced. Furthermore, it is possible to study the behaviour of the polar phonons as a function of the angle of propagation of the phonons, as was discussed in Section 2.4.

Before presenting these results, however, it is necessary to describe the geometry of the scattering events as a function of angle. As was mentioned in Section 3.1.1, the γ-polytype samples were triangular needles of equilateral cross section. The needle faces as grown in this fashion are (1 $\bar{1}$ 0 1) or permutations of the first three indices. The end face of the needle is a (0 0 0 1) face. In the convention of Nye (1957), the group theoretical orthogonal coordinates x, y, and z (or Nye's x_1, x_2, and x_3) are defined

relative to the hexagonal coordinates (x, y, u, z) by z = z and x = x_1. For the γ-GaSe needles, then, each face is crystallographically equivalent, with the x axis parallel to the face of the needle, the y-axis (the orthogonal y-axis) not quite normal to the face of the needle and the z-axis along the axis of the needle. The position of the gallium and selenium atoms on the lattice sites and the relevant directions are shown in Figure 3.6. A diagram of the needle itself is shown in Figure 3.7. From the notation of the long faces, it is an easy matter to show that the faces make an angle with the c-axis $\phi = \tan^{-1}\left(\frac{\sqrt{3}}{2}\frac{a}{c}\right) = 7.4°$, where c and a are the unit cell dimensions from Table 2.1.

Spectra were taken on the γ-needle both at room temperature and at 81°K. Various orientations are shown in Figures 3.8 through 3.11. All the spectra are at 81°K unless otherwise noted in the diagrams. Three new features are seen in the γ-polytype spectrum. First is the observation of a weak phonon near 40 cm^{-1} (Figures 3.8(a), 3.10(a), and 3.11) which has been tentatively identified as the $A_1(1)$ rigid layer compressional mode previously seen at 37 cm^{-1} in far infrared spectra in ε-γ crystals (Irwin et al., 1973). The other two features are the TO-LO phonon pair of the previously inactive $A_1(2)$ phonon. The frequency of these modes shows a strong angularly dispersive character which will be discussed more fully below.

Figure 3.8 shows the diagonal Z(XX)Y and off-diagonal

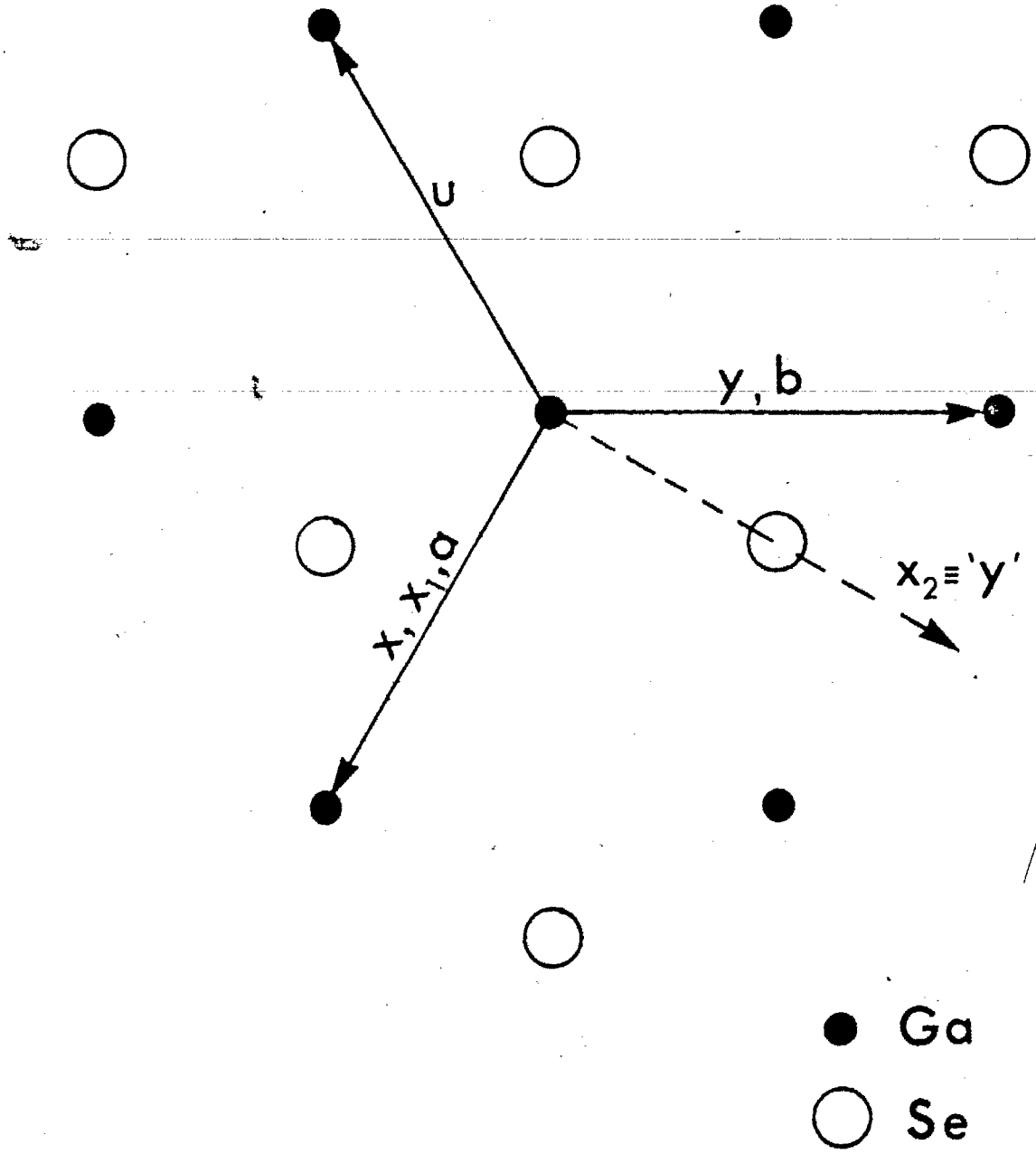

Figure 3.6. The spatial coordination of atoms in the ab-plane of the γ-polytype. The orthogonal directions (x_1,x_2, and x_3) and the hexagonal directions (x,y,u,z) for this C_{3v} symmetry crystal are also identified. The crystal faces cut the ab-plane along the directions x, y, and u of the hexagonal notation.

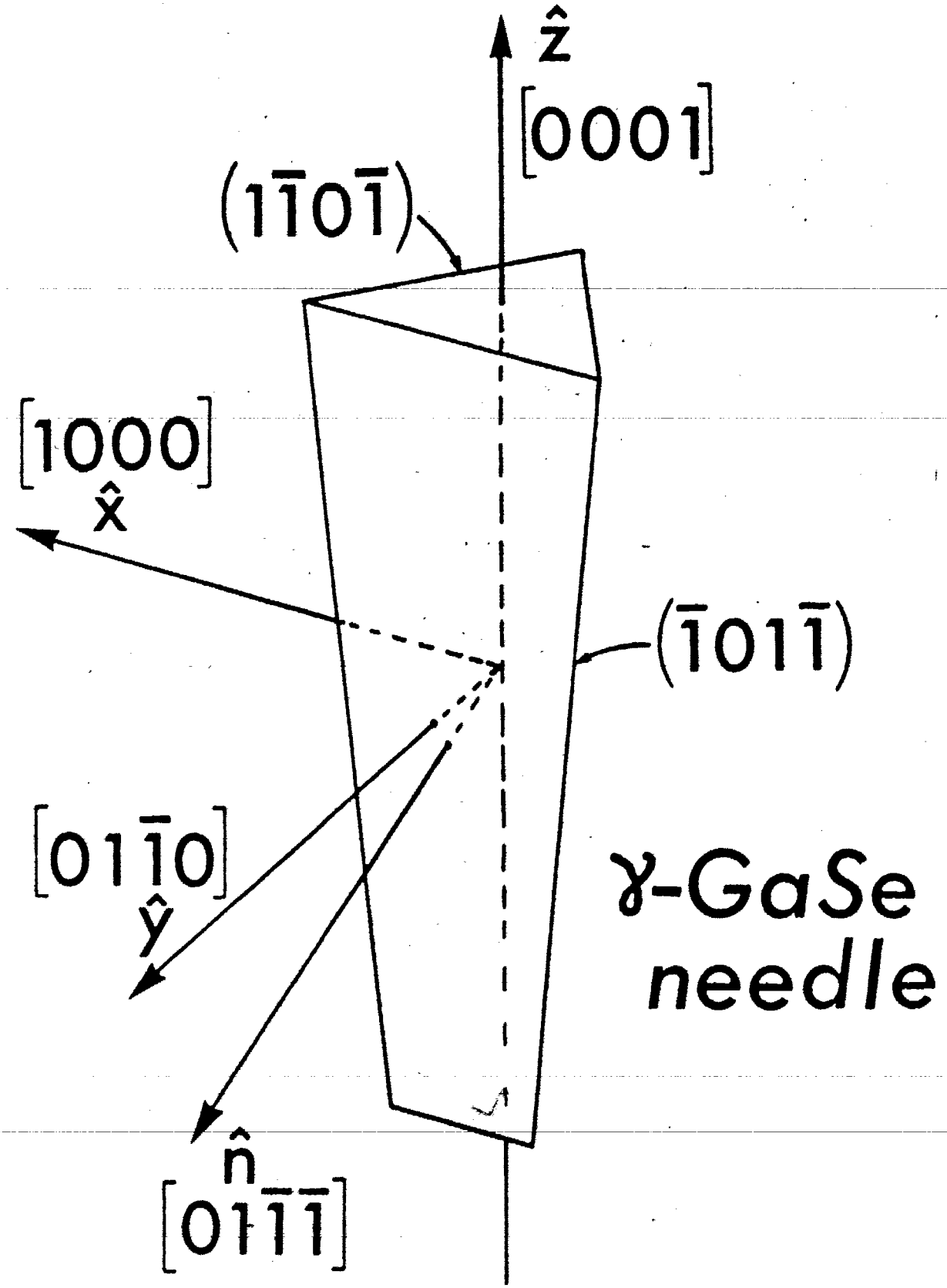

Figure 3.7. Diagram of γ-GaSe needle.

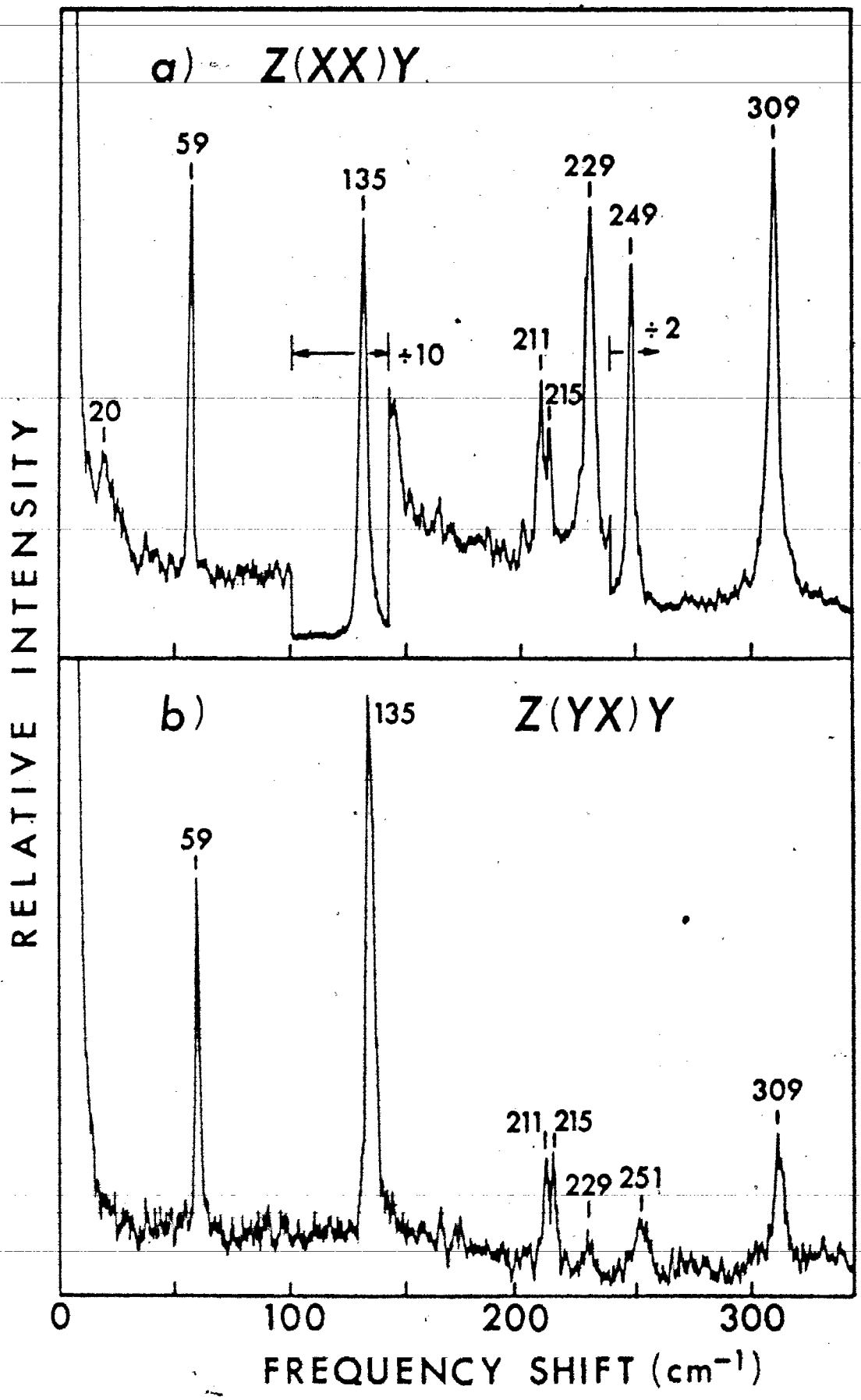

Figure 3.8. Raman Spectra of γ-GaSe: Z(XX)Y and Z(YX)Y. Spectra taken at 6328 A at 81 °K.

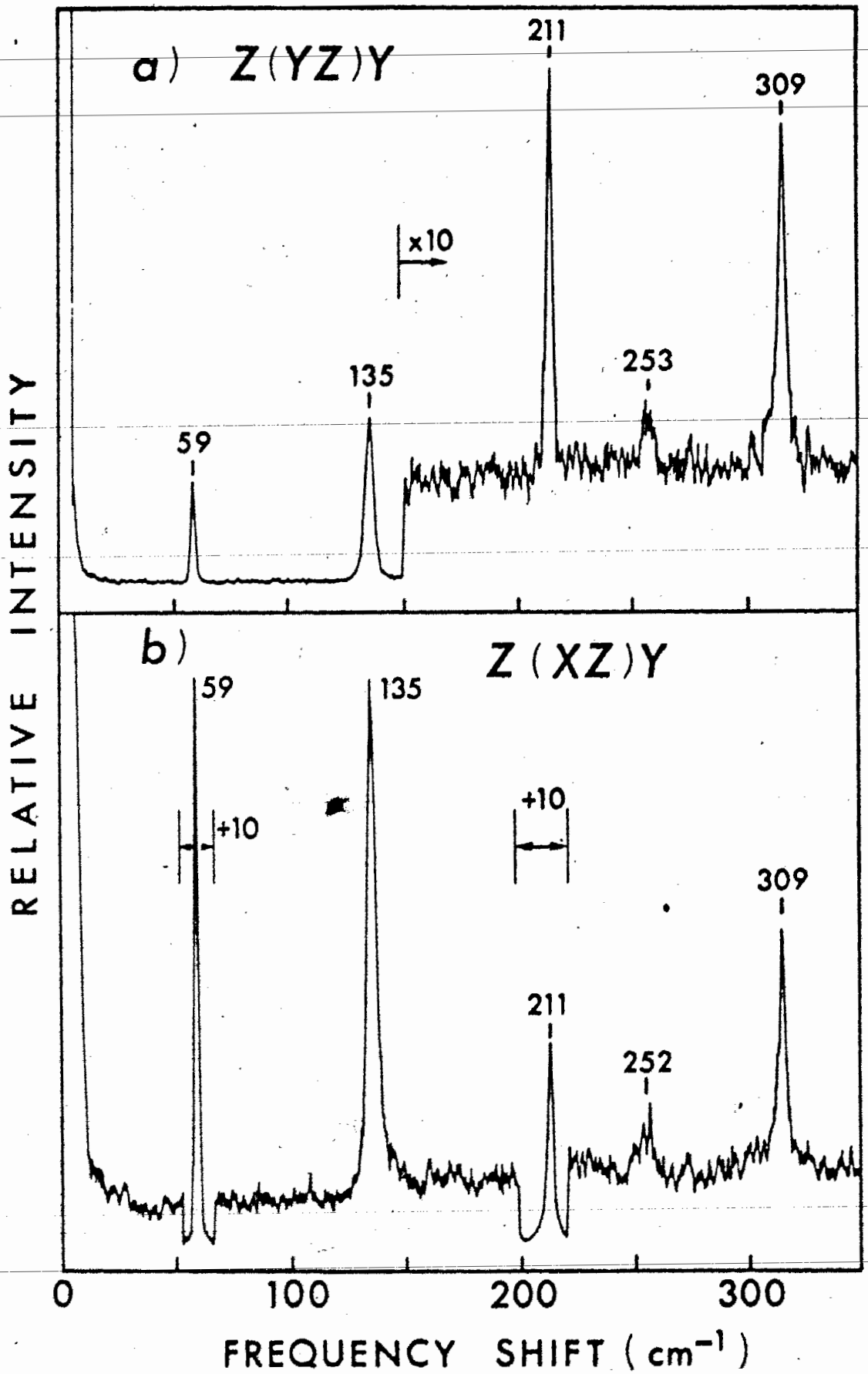

Figure 3.9. Raman Spectra of γ-GaSe: Z(YZ)Y and Z(XZ)Y. Spectra taken at 6328 Å at 81 °K.

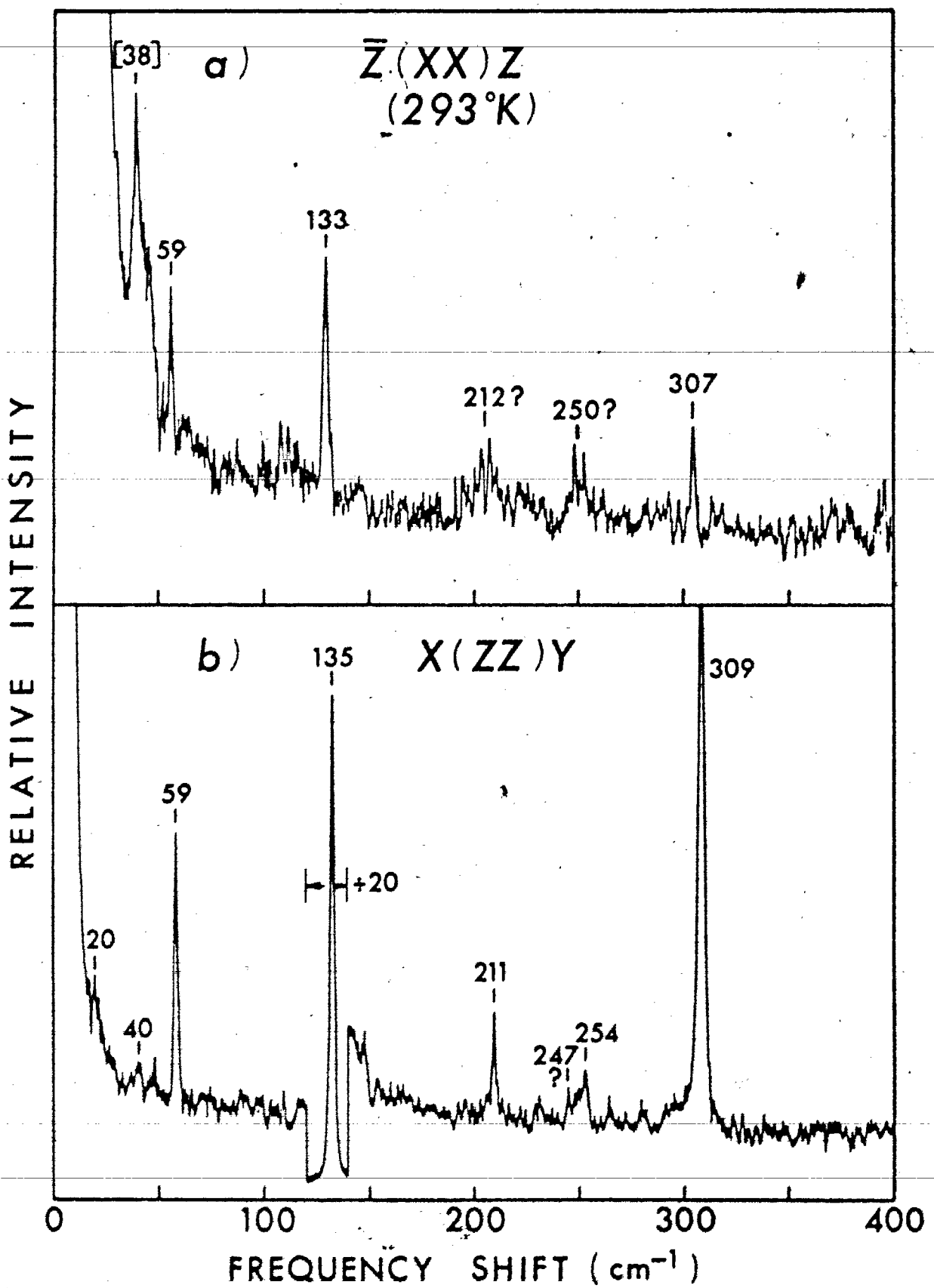

Figure 3.10. Raman Spectra of γ-GaSe: $\bar{Z}(XX)Z$ and $X(ZZ)Y$. Both spectra taken at 6328 A. Top spectrum recorded at room temperature and bottom spectrum at 81 °K. Possible ghosts indicated by brackets.

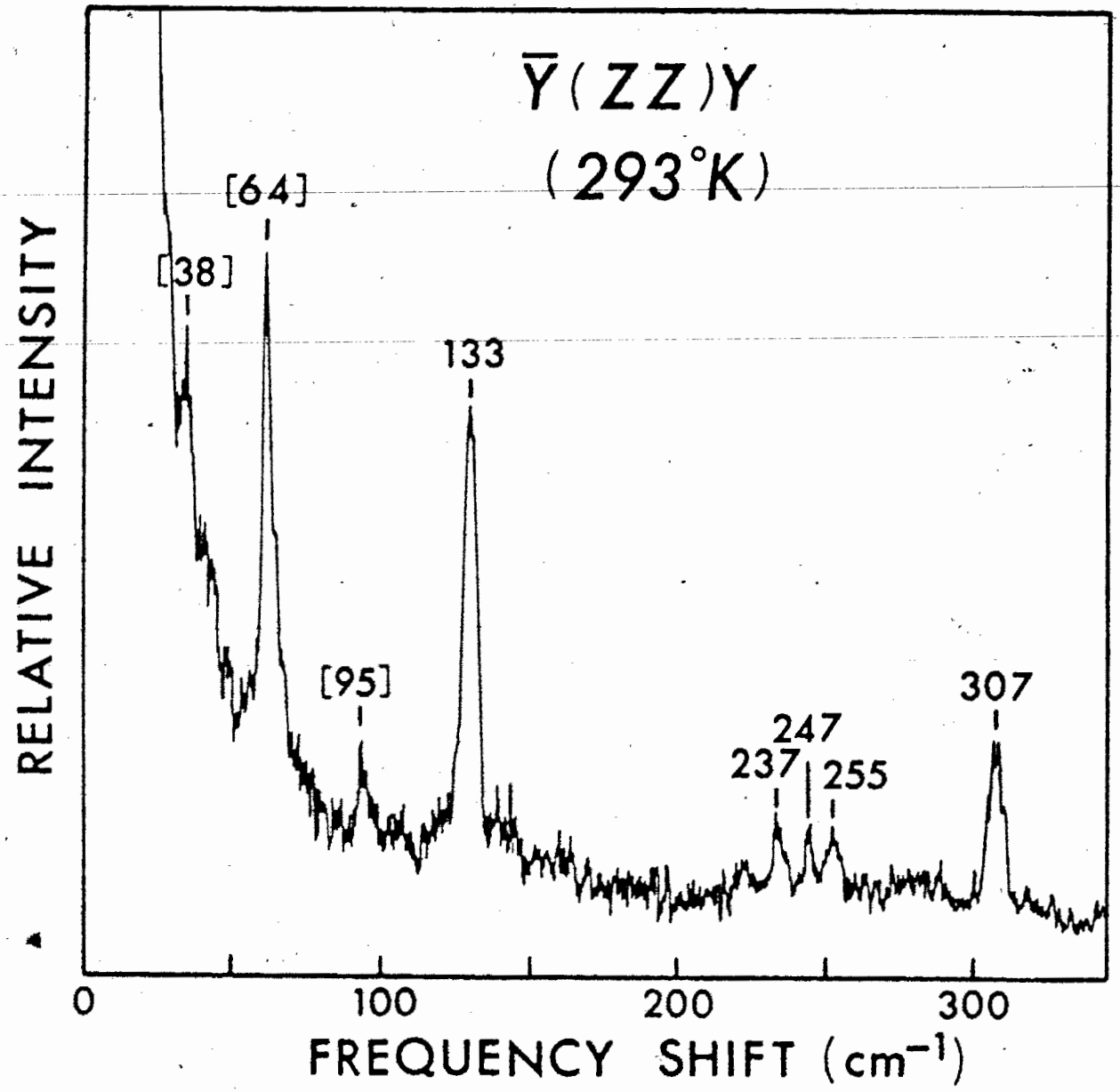

Figure 3.11. Raman Spectrum of γ-GaSe: $\bar{Y}(ZZ)Y$. Spectrum taken at 6328 A at room temperature. Possible grating ghosts indicated by brackets.

TABLE 3.3 - Assignments and Frequencies of Vibration for γ - GaSe. All frequencies are ±1.0 cm^{-1} unless otherwise noted. Selection rules for the vibrations are given in Table 2.2.

Irreducible Representation	Raman Frequencies (cm^{-1})	
	$\tilde{\nu}$ (293 °K)	$\tilde{\nu}$ (81 °K)
E (1)	20.9	20.7
A_1(1) (?)	38.3 ± 2.0	40.4 ± 2.0
E (3)	59.5	59.4
A_1(3)	133.5	135.0
E (4)	208.7	211.0
E (2) TO	213.9	215.2
A_1(2) TO	235.7	-
A_1(2) LO	246.5	247.8
E (2) LO	253.2	255.5
A_1(4)	307.4	309.5

Z(YX)Y geometries. The diagonal spectrum (a) shows the mixed E(2) - A_1(2) LO mode to be relatively strong at 249 cm^{-1} and the mixed A_1(2) - E(2) TO mode at approximately one half the LO intensity. The TO mode is at 229 cm^{-1}. All A_1 symmetry modes appear quite strong in this spectrum. Figure 3.8(b) shows the YX geometry which is generally much weaker than the above spectrum.

Figure 3.9 shows the two other off-diagonal elements Z(YZ)Y (Figure 3.9(a)) and Z(XZ)Y (Figure 3.9(b)). In both these spectra the E symmetry phonons at 59 cm^{-1} and at 211 cm^{-1} are quite strong. Figures 3.10 and 3.11 show two diagonal backscattering geometries $\bar{Z}$(XX)Z and $\bar{Y}$(ZZ)Y both taken at room temperature and a right angle spectrum X(ZZ)Y. One feature to note is the peak at 38 cm^{-1} in the room temperature spectra. This peak is found to be strong only in backscattering spectra and has been tentatively identified as the A_1(1) compressional vibration, which was inactive in the ε-polytype. It is somewhat disconcerting that the peak should appear so strongly in backscattering and only very weakly (Figure 3.8(a)) in other diagonal geometries. Because of this fact, and since one must always be reticent about assignments of low energy peaks in backscattering because of the possible high intensity grating ghostswhich may occur from specular reflections off the crystal, the identification of the A_1(1) "rigid-layer" mode must be termed tentative. The other feature to note in the backscattering spectrum from the Y face is the observation

of the $A_1(2)$ TO phonon at 237 cm^{-1}.

The frequencies obtained for the normal modes of vibration for the γ-polytype are shown in Table 3.3. The frequencies given for the $A_1(2)$ and E(2) LO and TO phonons are the limiting values seen in the experiment and represent pure A and pure E symmetry vibrations.

3.3 Discussion

3.3.1 β-GaS

As was seen in Table 2.2, of the 24 normal modes of vibration of the β-polytype, only six are Raman active. These six modes have been identified and assigned to the spectral features in the Raman spectrum according to their symmetry properties with no disagreement with previous results (Van der Ziel et al., 1973). The six Raman active modes are all even in symmetry as this is a centrosymmetric crystal and thus represent the phonons in the lower row of Figure 2.6. This is an important observation because not only does it identify the primary intralayer vibrations but also bears some significance to the identification of "conjugate" modes in GaSe.

3.3.2. ε-γ GaSe

From the similarities between the structures of GaS and GaSe in the layers, one would expect that the spectra observed should also be similar with the frequencies of vibration scaled by the ratio of the reduced mass of the gallium-selenium pair to the gallium-sulphur pair. Roughly, if the elastic constants are equal one would have

$$\frac{\omega_{GaS}}{\omega_{GaSe}} = \sqrt{\frac{M_{Se}^{*}}{M_{S}^{*}}} = \sqrt{\frac{M_{S} + M_{Ga}}{M_{Se} + M_{Ga}} \left(\frac{M_{Se}}{M_{S}} \right)} = 1.356 \qquad (3.1)$$

This ratio is quite well obeyed for several modes in these two compounds. The frequencies of the corresponding vibrations and their ratios is given in Table 3.4.

One mode in the ε-γ spectra of GaSe is, however, not

TABLE 3.4 - Ratios of Frequencies of Vibration of Corresponding Modes in GaS and GaSe.

Vibrational Mode			
GaS	GaSe	$\tilde{\nu}_{GaS}/\tilde{\nu}_{GaSe}$	% Error*
E_{2g}^2	E´ (1)	1.13	16.7%
E_{1g}^1	E´´(1)	1.25	7.8%
A_{1g}^1	A_1´(1)	1.40	3.2%
E_{1g}^2	E´´(2)	1.37	1.0%
E_{2g}^1	E´ (2) TO	1.38	1.8%
A_{1g}^2	A_1´(2)	1.17	13.7%

* This is the percentage difference from the rough estimate of 1.36 obtained from the ratio of the reduced mass.

comparable to β-GaS in this manner and this is the mode at 254 cm^{-1}. From symmetry consideration this mode was identified in a previous work (Irwin et al., 1973) as the split off LO phonon $E'(2^2)$ from the E'TO at 215 cm^{-1}. On the other hand Hayek et al. (1973) assigned this peak and one they observed at 247 cm^{-1} as an E'' phonon conjugate pair. The results of the work on the Resonant Raman effect and the spectra taken on the γ-polytype will show that this conclusion is erroneous, and in fact is a manifestation of the RRE.

With the use of the selection rules, the assignments made in Table 3.2 identify again six modes (plus the additional split off LO phonon). Group theory (Appendix A) predicts that there are eleven Raman active phonons:

$$\Gamma_{Raman} = 4A_1' \oplus 4E'' \oplus 3E'$$

To explain why only six features (plus the LO phonon) are observed, one must return to the argument of conjugate modes and refer to Figure 2.7. In ε-GaSe the A_2'' modes are Raman inactive and thus only six pairs of modes of Figure 2.7 can be Raman active. Since the $E''(1^1)$ is an acoustic mode, that leaves eleven Raman active phonons. Each remaining column then consists of two modes which are nearly degenerate in energy by the argument of the weak coupling between the layers, which leads to equation 2.32. One can, on the basis of the symmetry of the modes and with comparison to GaS through Table 3.4, make assignments of each spectral peak to one pair

of conjugate modes. From equation 2.32 one can estimate the frequency difference between each pair of conjugate modes. With ω_i, the coupling frequency, being the rigid-layer frequency for the E symmetry modes (19.5 cm^{-1}) and 36.7 cm^{-1} (Irwin et al., 1973) for the A symmetry modes, the only experimentally resolvable splittings (that is, $\Delta\omega > 1$ cm^{-1}) would occur for the 60 cm^{-1} E' phonon or the 135 cm^{-1} A_1' phonon. In spite of a careful search for these satellite lines, no experimental evidence of conjugate modes was found. One must conclude that the conjugate modes were either too weak to observe or had experimentally unresolvable splittings. Because of this, one can not conclusively determine whether the Raman mode being observed is from the upper row or lower row of Figure 2.7.

The work on the crystals of ε-γ GaSe demonstrates that the Raman activity of the modes is consistent with the conclusion that these large plate crystals are primarily of the ε-polytype. The degree of γ-polytypism in these samples can be estimated from the work described in the following section.

3.3.3 γ-GaSe

From the group theoretical prediction of Section 2.4, one would expect all the phonons in the C_{3v}^5 γ-polytype to be both Raman and infrared active. The work, then, on the γ-polytype needles serves both as corroboration of the previous conclusions about the ε-polytype and also adds much new information about the modes previously inactive. There are 36 normal

modes of vibration in the γ-polytype. Because of the double degeneracy of the E modes and because of the near degeneracy of the conjugate modes, there are only eight very distinct frequencies if one ignores the LO phonons. Of these, six are vibrations of the form of the active phonons the β- and ε-polytypes. The remaining two are the A_1 vibrations which are derived from the A_2'' symmetry of the ε-polytype. Thus, one expects the rigid layer compressional vibration $A_1(1)$ (A_2'' (1) in ε-GaSe) to become visible as well as the $A_1(2)$ vibration. This latter vibration had manifested itself in the ε-polytype only in the Resonant Raman effect when a peak near 247 cm^{-1} appeared in spectra taken at room temperature with the He-Ne laser. This phonon was interpreted to be the A_2'' (LO) since the LO phonon should predominantly be affected in the RRE. The associated TO phonon was not observed in the ε-polytype since it was Raman forbidden. Previous infrared absorption measurements indicated, however, a Reststrahlen edge for $\vec{E} \| \vec{c}$ at approximately 237 cm^{-1} (Leung et al., 1966; Wieting and Verble, 1972).

The Raman spectrum of γ-GaSe shown in Figures 3.8 - 3.11 displays these new features. The $A_1(2)$ TO and LO phonons do not show a unique frequency dependence but instead mix with the E(2) TO and LO phonons as a function of the angle between the phonon propagation vector and the c-axis which will be discussed in the following section. The second new feature is the observation of the weak peak near 40 cm^{-1} which has been

tentatively identified as the $A_1(1)$ rigid layer compressional vibration. This identification is made because the peak only appears in diagonal spectra and thus has the symmetry characteristics of A phonons. This, plus the previous identification of the A_2'' (1^2) mode in far infrared absorption at 36.7 cm^{-1} (Irwin et al., 1973) supports the $A_1(1)$ assignment.

The intensities of the other phonons in the γ-polytype however, show a striking similarity to the behaviour of the phonons in the mixed ε-γ crystals. In particular the E(3) 59 cm^{-1} and E(4) 211 cm^{-1} vibrations are strongest in XZ or YZ spectra. This behaviour is very much like the behaviour of the E'' phonons of the ε-polytype which are only active with the above components.

As in the ε-polytype, this polytype displays no experimental evidence for conjugate modes in the spectrum. The arguments which applied to the ε-polytype can again be applied here with some care. The γ-polytype has triplets of conjugate modes (except for $A_1(1)$ and E(1) which are doublets), and the argument of two simple coupled oscillators (Wieting and Verble, 1972) must be altered somewhat. The solution of the problem of three simple coupled oscillators of frequency ω_o and coupling constant $C_i = \omega_i^2 M$ gives the frequencies:

$$\omega^2 = \omega_o^2,\ \omega_o^2 + \omega_i^2,\ \omega_o^2 + 3\,\omega_i^2 \qquad (3.2)$$

This approximation again reveals that the order of magnitude of the splitting of the conjugate modes would be small and

unresolvable except for the lowest lying modes, which experimentally show no evidence of satellites. The linear chain model of Wieting (1973) cannot simply be applied to the γ-polytype since a linear chain constructed of two types of atoms and only three spring constants does not differentiate between the ε- and γ-stackings. One must conclude that conjugate modes were not seen because they are either too weak in the Raman spectrum and/or have unresolvable splittings.

Finally, one can draw some conclusion about the amount of γ-polytypism in the large ε-γ plate crystals. Until this work was completed, no estimate of the degree of admixing had been made. The conclusions of the previous work on these crystals (Irwin et al., 1973) was that the degree of γ-polytypism must be small since the selection rules for the ε-polytype are well obeyed. The strength of the A_1 phonons in γ which are compatible with A_2'' vibrations of ε indicates that these phonons are an adequate indicator of the degree of γ-polytypism in the large crystals. From the strength of the $A_1(2)$ TO line in the γ-polytype, one must conclude that the amount of γ-polytypism in the ε-γ crystals is less than 5%.

3.3.4 Angular Dependence of the Scattering

As was shown in Section 2.4, one expects the polar phonon frequencies in a piezoelectric crystal to be strongly dependent on the direction of phonon propagation as well as polarization of the phonon. In particular one would expect

the phonon frequencies of the LO and TO phonons in an anisotropic polar crystal to vary as the angle θ, between the direction of phonon propagation and the c-axis is varied (c.f. equation 2.25 and Figures 2.4 and 2.5). As was seen in the preceding sections, the frequencies of the LO and TO phonons in the ε- and γ-polytypes in many cases have values which are indicative of the phonon propagating in a non-symmetry direction. It was possible in the γ-needles to measure this dispersion as a function of the angle of propagation of the phonon, θ.

The particular geometries of interest involved are those where the light enters the crystal along the c-axis of the needle and is viewed at some angle δ with respect to the y-axis.

By varying this viewing angle δ one is then able to adjust the angle between the incident and scattered beams inside the crystal. By doing this one effectively samples phonons with different propagation directions relative to the c-axis and makes it possible to study the frequencies of angularly dispersive phonons. The geometry of the scattering is shown in Figure 3.12. The XX polarization component was selected for these measurements for two reasons. First, it gives a strong spectrum and, secondly, since the polarization is perpendicular to the c-axis, there are minimal birefringent effects in either the incident or scattered beams. Thus only one index of refraction, n_o, is necessary. Since no

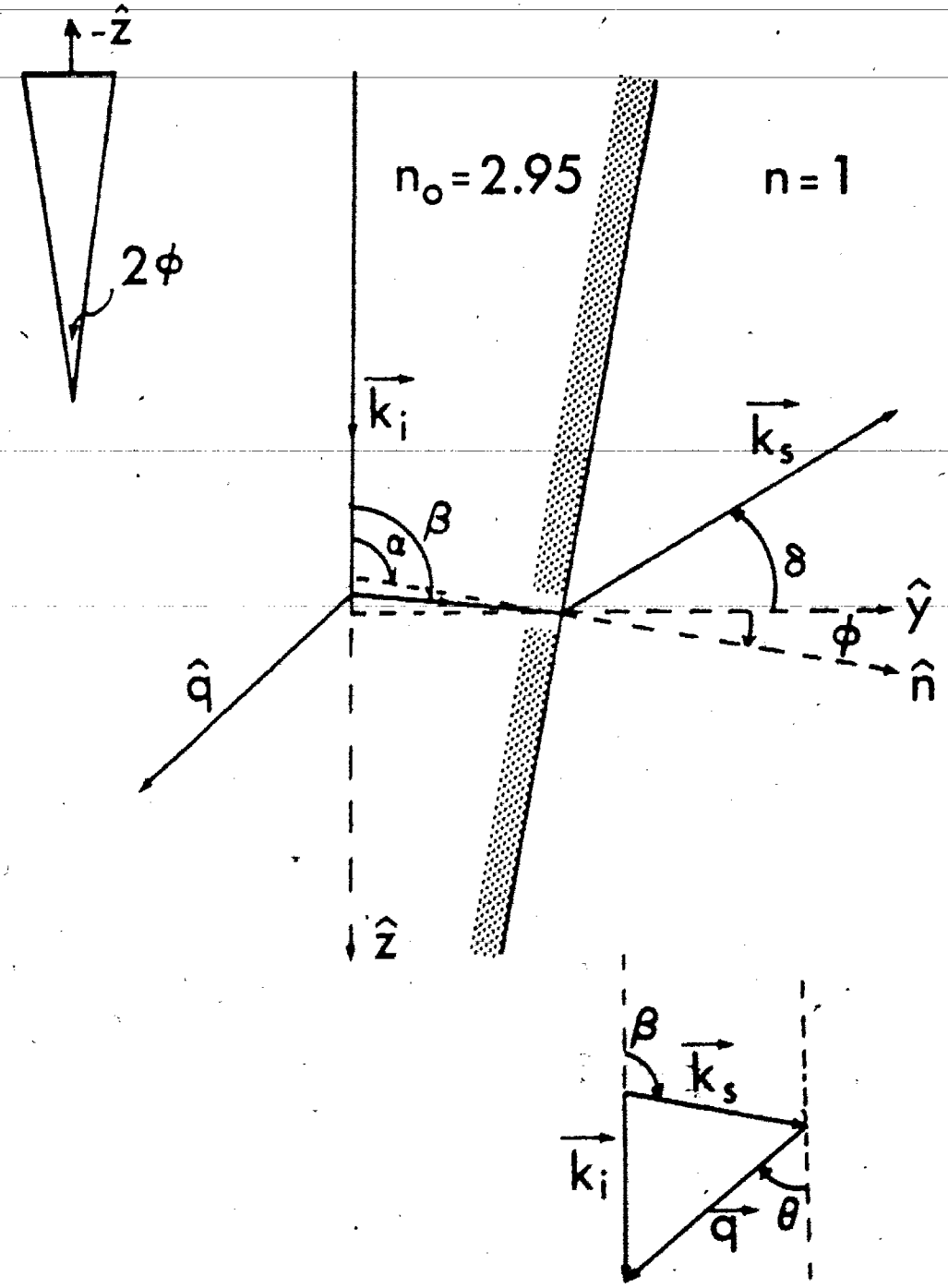

Figure 3.12. The scattering geometry for arbitrary viewing angle with respect to the γ-needle face. (Inset above) The angle ϕ is half the apex angle of the needle. (Inset below) Momentum conservation diagram showing $\theta = \beta/2$ if $|\vec{k}_i| \simeq |\vec{k}_s|$.

measurements of the indices of refraction of the γ-polytype have been made, the indices of refraction used here are from the ε-γ data of Wasscher and Dieleman(1972) who give $n_o \cong 2.95$. From Snell's law one has, if $\varphi = \alpha - \beta$,

$$\sin(\phi + \delta) = (\sin \varphi)\, n_o \qquad (3.3)$$

and since,

$$\alpha = \frac{\pi}{2} + \phi \qquad (3.4)$$

then,

$$\beta = \alpha - \varphi = 90^\circ + \phi - \varphi \qquad (3.5)$$

and,

$$\theta = \beta/2 = 45^\circ + (\phi - \varphi)/2 \qquad (3.6)$$

Data for intermediate propagation angles θ were taken by letting $\delta = +45^\circ, 0^\circ, -45^\circ$. The frequencies measured at room temperature and are shown in Figure 3.13.

The limiting frequencies in the dispersion of the $A_1(2)$ and E(2) modes were obtained by backscattering and right angle scattering in the pure symmetry directions (i.e. both $\vec{k}_i$ and $\vec{k}_s$ either parallel or perpendicular to the c-axis) and were given in Table 3.3. The values thus obtained give the frequencies necessary to calculate the dispersion of the LO and TO modes (of equation 2.25) if the dielectric constants are known. The dielectric constants for the ε-polytype have been given by Leung et al (1966):

$$\epsilon_{\parallel}^{o} = 7.6 \qquad \epsilon_{\parallel}^{\infty} = 7.1$$
$$\epsilon_{\perp}^{o} = 9.8 \qquad \epsilon_{\perp}^{\infty} = 7.45$$

The theoretical curve is plotted in Figure 3.13. The agreement with the theoretical curve is excellent.

Several points of clarification are in order at this point. The range of measured angles shown in Figure 3.13 could not be extended in practice since scattering in any z( )Y* geometry (where Y* is some direction viewed from the y face, i.e. $-\frac{\pi}{2} \leq \delta \leq \frac{\pi}{2}$) limits the phonon propagation to an approximately 14° band about 45° because of the large index of refraction. Because, however, the three intermediate angles fall on the most dispersive portion of the curve, it is felt that they give a reliable test of the theoretical predictions here.

From these results and the agreement of the observed Raman symmetries of the LO and TO phonons with the theory of Loudon for the electrostatic limit (Case I), it seems evident that GaSe behaves as a Case I uniaxial crystal even though the limits for Case I as set out by Loudon are not completely satisfied (that is, $|\omega_{\parallel}^{\ell} - \omega_{\parallel}|$ is not >> $|\omega_{\parallel} - \omega_{\perp}|$). This conclusion contains implications that must be considered for the theory of the Resonant Raman effect. The primary fact to retain from this conclusion is that the electrostatic effects dominate the behaviour of the polar phonons. In this limit

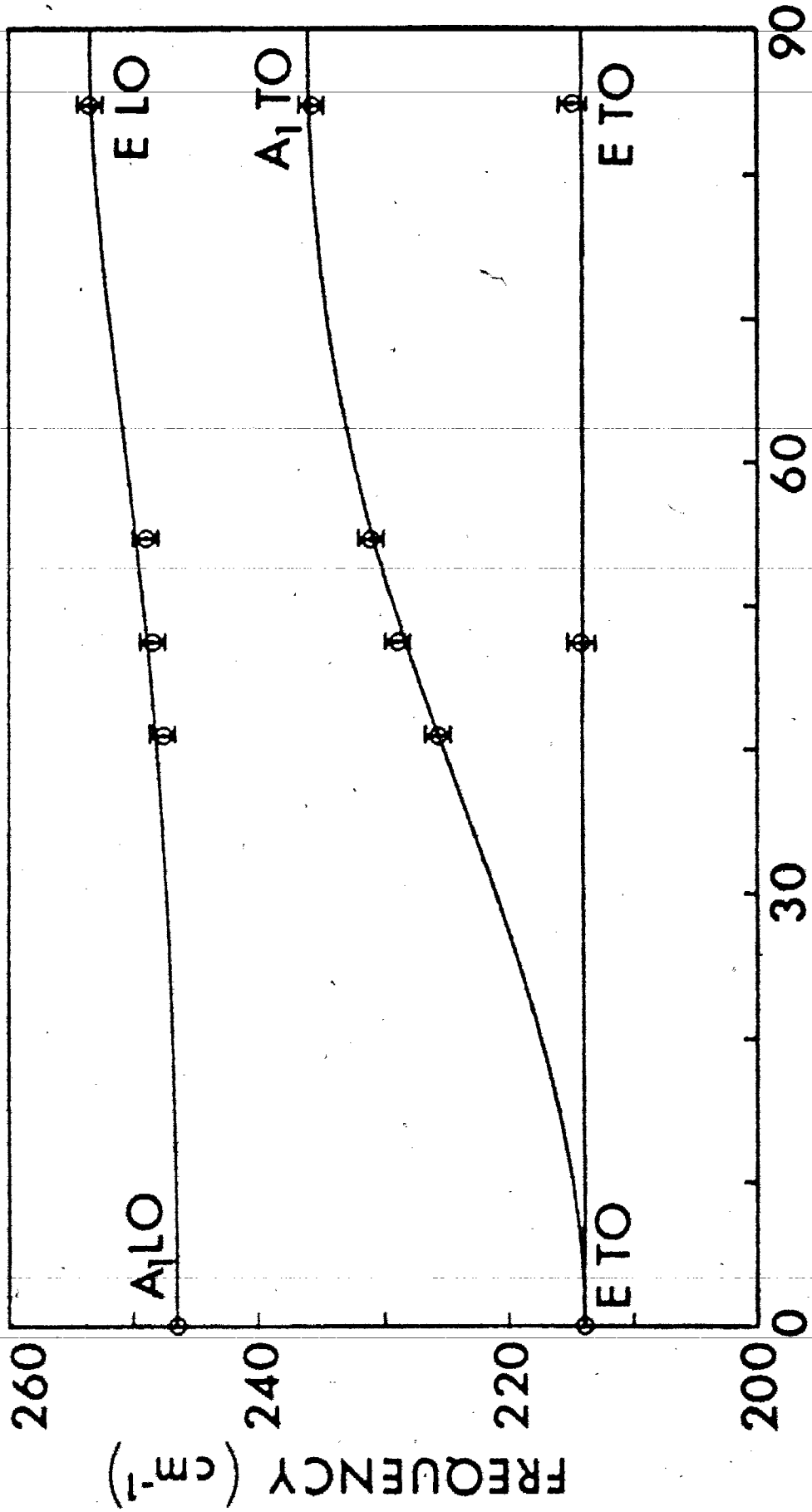

Figure 3.13. Dispersion of LO-TO phonons in γ-GaSe vs. propagation angle. The solid curve is calculated from equation 2.25.

to a good approximation, the electric field associated with the polarization disturbance (the polar phonon) is longitudinal (Loudon, 1964) and thus can, also to a good approximation, be treated as isotropic.

CHAPTER IV

THE RESONANT RAMAN EFFECT IN GaSe - THEORY

4.1 Introduction

From the work of Loudon described in Section 2.2, the existance of singularities in the Raman scattering tensor suggested that the Resonant Raman Effect (RRE) should exist in crystals. There are various electronic states in semiconducting crystals which could feasibly be responsible for the RRE. The most obvious would be the interaction of a phonon with isolated electrons which have been promoted to the conduction band by the incident light. Thus, the existence of an energy gap provides one frequency region to focus the study of the RRE. In semiconductors, however, there are various complications which also involve this energy region. The electron which has been promoted to the conduction band can be Coulomb attracted to the hole which is left behind in the valence band. The energy of this correlated state, the exciton, is usually very close to the gap energy itself. The difference in energy is the exciton binding energy, E_{ls}, which is typically 1 to 30 meV. Due to this small energy difference, one must perform quite sensitive measurements as a function of energy in order to distinguish between these two possible contributions to the RRE.

Additionally, one can have free electrons or holes bound to ionised donors or acceptors in semiconductor. Excitons can also be bound to neutral or ionised impurities. All these

states can feasibly be responsible for the RRE and are very difficult to differentiate with measurements taken at only a few energy points as is done with the discrete lines of gas lasers. It is primarily for this reason, i.e. the uncertainty of the type of intermediate electronic state in the scattering (and thus the type of interaction between the electrons and the lattice), that the theory of the RRE was unable to provide any reasonable agreement with the experimental results until an extensive amount of experimental evidence was accumulated.

Although the list of crystals and number of observations of the RRE in solids is now far too long to list here, the early work was confined primarily to Bell Laboratories. Most of the original observations were done on two crystals, CdS and ZnSe, starting with the original study of CdS by Leite and Porto (1966). CdS and ZnSe were first choices since they gave strong multiple phonon Raman spectra (that is, gave off photons corresponding to the creation of more than one optical phonon) and since the band gaps of these compounds were relatively near the lines of existing gas lasers (Argon ion, Krypton ion, and Helium-Cadmium). The earliest work (Pinczuk, 1968; Leite et al., 1969a; Leite and Scott, 1969b; Leite et al., 1969c; Scott et al., 1969, 1970) was primarily concerned with the multiphonon RRE. In CdS up to nine multiple LO phonon peaks were observed. The last three of the above works attempted to define the intermediate state in the interaction and it was observed that when a multiple phonon

line was resonant with the excitonic energy level that line was enhanced (Scott et al., 1970). Because only a few discrete laser lines were available, the quantitative examination of the scattering cross-section as a function of incident photon energy, however, remained somewhat sketchy.

With the advent of the tunable dye laser, it becomes possible to study the behaviour of the cross-section over a wide energy range with the only limitation on the energy sensitivity being the width of the dye laser line itself which is typically .1 meV or less. When this work was initiated there had been no quantitative results for the RRE obtained with a tunable dye laser. GaSe was an obvious choice as a subject for the RRE since its bandgap at 77°K lies midway in the tuning range of Rhodamine 6G dye lasers (5400 Å to 6400 Å). As such it is one of the very few semiconductors which could be studied with such a laser. The tunable dye laser is still a relatively novel tool, although new dyes have now been introduced which expand the available wavelength range. To the date of this writing, the only quantitative measurements of the Raman cross-section using a dye laser have been in Cu_2O (Yu et al., 1973; Compaan and Cummins, 1973), InSb (Yu and Shen, 1974); CdS (Damen and Shah, 1971) and the present work in GaSe (Hoff and Irwin, 1974).

The primary objective of this research was to determine the frequency dependence of the Raman cross-section and thus identify the intermediate state(s) in the scattering process.

The next two chapters will present the results of the work on the Resonant Raman spectrum of GaSe. The theory of Martin (1971b, 1973) for the one-phonon RRE will be presented along with a discussion of the probable intermediate states in the scattering process. Chapter V begins with the outline of the procedure for obtaining the scattering cross-section from the experimental spectra. The results of the experiments on the relative scattering efficiency for Raman scattering in GaSe will be presented. Of particular interest is the resonant enhancement of the $E'(LO)$ and $A_2''(LO)$ phonons of ε-GaSe in a geometry where neither is allowed. The former proves to be an example of selection rule breakdown and the latter is an example of the breaking of Raman inactivity in resonance. Both of these effects have been predicted by Martin (1971b) on the basis of a q-dependent scattering mechanism and the present results enable a quantitative comparison to be made with Martin's theory. Although several such comparisons have been attempted in the past (Colwell and Klein, 1970; Martin and Damen, 1971a; Williams and Porto, 1973), the results are sketchy for the reasons explained above. More importantly the crucial aspect of the angular dependence (Martin, 1971b) has been investigated in only one instance (Colwell and Klein, 1970) with negative results. The present work will discuss a similar investigation of the angular dependence in GaSe, with similar negative results.

The resonance behaviour of the non-polar modes will also be presented. These modes exhibit a pronounced anti-resonance as the light frequency approaches the band edge. This behaviour is similar to that observed in CdS (Ralston et al., 1970; Damen and Scott, 1971) where an empirical model was used to explain the data. An effort has been made to describe the results obtained here in terms of this model.

4.2 Theoretical Considerations

The theoretical description of the first order RRE has been the cause of much speculation. The crucial questions can be limited however to two, that is, what is the intermediate electronic state in the scattering and what is the nature of the interaction of this state with the lattice? Early work by Grechko and Ovander (1962) and Ovander (1962a, 1962b) treated the scattering in terms of molecules neglecting energy band effects. This is not practical in semiconductor crystals where the scattering is resonant near the band edge. Loudon (1963,1964) developed the results of Section 2.2, and using the assumption that free electrons and free holes are the intermediate states, came up with an expression for the scattering cross-section near resonance (Loudon, 1965). Loudon in this latter paper chose the deformation potential as the coupling between the electrons (or holes) and the lattice. The deformation potential, the reader will recall (Ziman, 1960, Sect. 5.6), is the change

in energy of the electron in a lattice which is allowed to be perturbed by some dilatation (a lattice vibration, for example). Thus, the motion of the ions in the lattice gives a spatially varying potential which couples to the electrons (or holes) in the crystal. Loudon further chose to treat all phonons as having zero wavevector. In that limit, the contributions to two-band (intraband) Fröhlich scattering from the electrons and holes exactly cancel and possibly for this reason Loudon ignored the Fröhlich contribution to the RRE in this later paper.

Ganguly and Birman (1967) developed a fuller treatment of the Raman effect in crystals. They included excitons as the primary intermediate state and treated both the deformation potential interaction and the Fröhlich interaction. The result was interpreted only for strictly $\vec{k} = 0$ phonons and thus they found that there was no contribution to the RRE from intraband Fröhlich scattering.

Several workers then followed with a treatment of the effect in terms of polaritons, that is, mixed states of the photon, electron, and phonon in the dielectric crystal (Mills and Burstein, 1969; Bendow and Birman, 1970, 1971). This approach is computationally difficult and provides somewhat inadequate results for the resonance behaviour in that the resonances predicted by the theory are sharper in energy than those seen experimentally. These papers treated the electron-phonon coupling in terms of the deformation potential. Hamilton (1969) included the

possibility of the Fröhlich interaction (the interaction of the electrons or holes in a polar crystal with the electric field caused by the ionic displacements, e.g. equation 2.19) as the coupling between the electrons and phonons, but his calculation was valid only for light incident at frequencies greater than the band gap energy.

Martin (1971a, 1971b, 1973) treated the Resonant Raman effect through the formalism developed by Ganguly and Birman (1967). Martin, however, extended their results to include wavevector dependent effects and found that intraband Fröhlich scattering could become the dominant mechanism for the RRE. His results are computationally much simpler and include both the deformation potential and Fröhlich interaction.

Because of this relative simplicity and since these results synthesize much of the earlier work, the theory presented in this section will follow this treatment (Martin, 1971b). In doing this, an expression for the Raman cross-section as a function of frequency will be developed. Much of the work will draw on Loudon's results of Section 2.2 and the reader will have to refer to these equations for further details. Although there are six possible time orderings of the scattering event seen in Figure 2.1 and equation 2.10, only the third term (c) will be considered quantitatively here. This normally considered term is the only term which possesses a second order singularity, that is, the denominator goes to zero at two approximately equal frequencies.

The terms (b), (d), and (f) are non-resonant at the band gap frequency and thus are assumed small. The two other terms are neglected for two reasons. In both (a) and (e) there is only a first order singularity when one term in the denominator becomes quite small as ω_i approaches ω_α or ω_β (which are assumed to be near the band gap frequency). The other term in each denominator will remain relatively large and thus, term (c) should be predominant. The second reason is that in two-band scattering (i.e. only one valence and one conduction band), the combination of dipole matrix elements $P_{0\beta}P_{\beta\alpha}$ and $P_{\beta\alpha}P_{\alpha 0}$ in terms (a) and (e) cause these terms to go to zero (Ganguly and Birman, 1967).

Process (c) consists of an incident photon of energy $\hbar\omega_i$, polarization $\hat{\epsilon}_i$ and wavevector $\vec{k}_i$ scattering to a state s of energy $\hbar\omega_s$, polarization $\hat{\epsilon}_s$, and wavevector $\vec{k}_s$. It is assumed that the index of refraction is constant over the scattering region, i.e. $n(\omega_i) = n(\omega_s)$. This is a very good approximation in GaSe in all but an approximately 20 Å region about the exciton (Wasscher and Dieleman, 1972; Salaev et al., 1972).

The scattering probability per second is by Fermi's Golden Rule:

$$W = \frac{2\pi}{\hbar} \rho(\beta) \, |W_{\beta\alpha}|^2 \qquad (4.1)$$

where α and β are the initial and final states and $\rho(\beta)$ is the photon field density in the state β. If the wavefunctions are box normalized to the volume of the crystal, V, the density of photon states is:

$$\rho_{\hbar\omega_s, d\Omega} = V \frac{\omega_s^2 \, d\Omega}{(2\pi)^3 \hbar c_s^3} \quad ; \quad c_s = \frac{c}{n_s} \qquad (4.2)$$

The scattering probability per unit solid angle per unit length is W/(flux of incident photons ·L· dΩ). The flux of photons across and area A (= V/L) is (c/n)/L so the scattering probability per unit length per unit solid angle is:

$$\frac{S}{L} = \frac{W \, L}{\frac{c}{n} \, L \, d\Omega} = \frac{W}{\frac{c}{n} \, d\Omega} = \frac{n}{c} \frac{W}{d\Omega}$$

$$= \frac{2\pi}{\hbar} \frac{V\omega_s}{(2\pi)^3} \frac{n^4}{\hbar c^4} |W_{fi}|^2$$

$$= V \left(\frac{\omega_s n^2}{2\pi\hbar c^2} \right)^2 |W_{fi}|^2 \qquad (4.3)$$

Martin defines a scattering cross-section per unit cell:

$$\sigma = \Omega \left(\frac{S}{L} \right) = \left(\frac{n^2 \omega_s}{2\pi\hbar c^2} V^{\frac{1}{2}} \Omega^{\frac{1}{2}} \right)^2 |W_{fi}|^2 \qquad (4.4)$$

Factoring out the free electron Compton cross-section (classical radius of the electron squared):

$$\sigma_o = \left(\frac{e^2}{mc^2} \right)^2 = 7.95 \times 10^{-26} \text{ cm}^2$$

one gets:

$$\sigma = \sigma_o \left(\frac{n^2 \omega_s m V^{\frac{1}{2}} \Omega^{\frac{1}{2}}}{2\pi\hbar e^2} \right)^2 |W_{fi}|^2 \qquad (4.5)$$

Much of what has been achieved so far is redundant with the equations 2.5 - 2.10, except that there is some shifting of constants (i.e. $W_{fi} \neq W$). However, since the factors of the Hamiltonian of W_{fi} above are the same as equations 2.6,

2.7 and 2.8, one comes to a common meeting ground by writing for each mode ν:

$$\sigma_\nu = \sigma_o\left(\frac{\omega_s}{\omega_i}\right) \left| \sum_{\alpha\ \beta} e_s^\alpha\ R_\nu^{\alpha\beta}(\vec{q},\ \omega_i)\ e_i^\beta \right|^2 \qquad (4.6)$$

which is of the form of equation 2.30. The problem then reduces to one of deducing the form of the Raman tensor, $R_\nu^{\alpha\beta}$, by calculating the three matrix elements of $|W_{fi}|$. To do this one must have a proper description of the electronic states in the scattering process. The present work will use the Wannier exciton representation, and since the development of this representation is quite lengthy only the results will be employed here. For a more complete background to these results the reader is referred to Knox's Theory of Excitons (1963).

The states of concern in the scattering event diagrammed in Figure 2.1(c) are single excited electronic states for which one can write the electronic part of the wavefunction in momentum representation as:

$$|\lambda,\ \vec{K}\rangle = \sum_{\substack{c,v \\ \vec{k}}} U_{\lambda\vec{K},cv}(\vec{k})\ \Phi_{\vec{K},cv}(\vec{k}) \qquad (4.7)$$

The adiabatic approximation has been employed in that it is assumed that the wavefunctions are slowly varying and separable into a correlation (or overlap) function between the electron and hole $U_{\lambda\vec{K},cv}$ and a product function of the valence band Bloch state replaced by a conduction band Bloch state:

$$\phi_{\vec{\kappa},cv}(\vec{k}) = A\, \Psi_{c\vec{k}_1}\Psi_{v\vec{k}_1} \cdots \Psi_{c\vec{k}_e}\Psi_{v\vec{k}_h} \cdots$$
$$\cdots \Psi_{c\vec{k}_n}\Psi_{v\vec{k}_h} \qquad (4.8)$$

The exciton momentum can be written as $\vec{\kappa} = \vec{k}_e - \vec{k}_h$ and thus one can write these Bloch states as:

$$\Psi_{c,\vec{k}_e}(\vec{r}) = \Psi_{c,\vec{k}+\frac{1}{2}\vec{\kappa}}(\vec{r}) = e^{i(\vec{k}+\frac{1}{2}\vec{\kappa})\cdot\vec{r}}\, u_{c,\vec{k}+\frac{1}{2}\vec{\kappa}}(\vec{r}) \qquad (4.9)$$

$$\Psi_{v,\vec{k}_h}(\vec{r}) = \Psi_{v,\vec{k}-\frac{1}{2}\vec{\kappa}}(\vec{r}) = e^{i(\vec{k}-\frac{1}{2}\vec{\kappa})\cdot\vec{r}}\, u_{v,\vec{k}-\frac{1}{2}\vec{\kappa}}(\vec{r}) \qquad (4.10)$$

where the small u's are the periodic band functions.

The calculation can be further simplified by making two approximations. The first approximation is the use of an isotropic effective mass, thus assuming spherical bands. While GaSe is an anisotropic material with non-spherical bands (Schlueter, 1973), this approximation turns out to be reasonably valid since, in the end, the relatively small q of the phonon restricts the momentum to the centre of the zone and band dispersion effects are negligible. Furthermore, the calculation will show that to lowest order in the wavevectors, only spherical excitonic states are involved in the scattering and thus an isotropic effective mass is in keeping with this approximation. The second approximation is to neglect the $\vec{k}$ dependence of the band functions. For the reasons given above, this is also valid since near $\vec{k} = 0$ the functions u_c and u_v are slowly varying. Thus one sets:

$$u_{v,\,\vec{k}-\frac{1}{2}\vec{\kappa}} = u_{v,\,-\frac{1}{2}\vec{\kappa}} \qquad (4.11)$$

$$u_{c,\,\vec{k}+\frac{1}{2}\vec{\kappa}} = u_{c,\,\frac{1}{2}\vec{\kappa}} \qquad (4.12)$$

If one restricts the calculation for two sets of bands cv and c'v' and assume that $m_c^* = m_{c'}^* = m_e^*$ and $m_v^* = m_{v'}^* = m_h^*$, then one can transform the correlation function $U_{\lambda\vec{\kappa},cv}$ to the centre-of-mass system of the exciton to give (Knox, 1963):

$$\Psi_n(\vec{r}) = e^{-i\alpha\vec{\kappa}\cdot\vec{r}}\, V^{-\frac{1}{2}} \sum_{\vec{k}} U_{n,\vec{\kappa}}(\vec{k})\, e^{i\vec{k}\cdot\vec{r}} \qquad (4.13)$$

Here the band index λ has been broken up into valence band and conduction band indices v,c and exciton index n. The constant

$$\alpha = \tfrac{1}{2}\,\frac{m_e^* - m_h^*}{m_e^* + m_h^*}$$

relates the position of the centre-of-mass relative to the position of the electron and hole (Knox, 1963).

In this coordinate system, the excitonic eigenvalues are solutions of the equation:

$$\left(-\frac{\hbar^2}{2\mu}\nabla^2 + V(\vec{r}) - E_n \right)\Psi_n(\vec{r}) = 0 \qquad (4.14)$$

where $\mu^{-1} = (m_e^*)^{-1} + (m_h^*)^{-1}$ and $V(\vec{r})$ is the electron-hole potential. If $V(r) = -e^2/\epsilon r$, one has Coulomb correlated excitons and the solutions for the energy of the exciton are:

$$E_{\lambda,\vec{\kappa}} = E_g + E_n + \frac{\hbar^2\kappa^2}{2(m_e^* + m_h^*)} \qquad (4.15)$$

where in the hydrogenic limit:

$$E_n = -\frac{\mu e^4}{2\hbar^2 \epsilon^2 n^2} = -\frac{E_{1s}}{n^2} \tag{4.16}$$

and E_{1s} is the exciton Rydberg. $\Psi_n(\vec{r})$ then would be normalized hydrogen wavefunctions with the exciton Bohr radius a_o.

This formalism is convenient for "free" electrons and holes as well since one can set $V(\vec{r}) = 0$ to get completely uncorrelated particles.

With the use of the above results, given any one-electron operator of the form:

$$H = \sum_i f(\vec{r}_i)\, e^{-i\vec{q}\cdot\vec{r}_i} \tag{4.17}$$

where $\vec{r}_i$ is any general position coordinate, $\vec{q}$ a general momentum coordinate and $f(\vec{r}_i)$ any periodic one-electron operator, one can derive the following matrix elements (Martin, 1971b):

$$\langle \lambda\, \vec{\kappa} \,|f(\vec{r}_i)e^{-i\vec{q}\cdot\vec{r}_i}|0\rangle = \delta_{0,\vec{\kappa}+\vec{q}}\, V^{\frac{1}{2}}\, \Psi_n(\vec{r}=0) \cdot (u_{c,-\frac{1}{2}\vec{\kappa}}|f(\vec{r}_i)|u_{v,\frac{1}{2}\vec{\kappa}}) \tag{4.18}$$

and,

$$\langle \lambda'\vec{\kappa}'|f(\vec{r}_i)e^{-i\vec{q}\cdot\vec{r}_i}|\lambda\kappa\rangle = \delta_{\vec{\kappa},\vec{\kappa}'+\vec{q}}\Big[\{\delta_{vv'} f_{n'n}(\alpha_e\vec{q}) \cdot (u_{c',-\frac{1}{2}\vec{q}}|f(\vec{r}_i)|u_{c,\frac{1}{2}\vec{q}})\} - \{\delta_{cc'} f_{n'n}(\alpha_h\vec{q}) \cdot (u_{v,-\frac{1}{2}\vec{q}}|f(\vec{r}_i)|u_{v',\frac{1}{2}\vec{q}})\}\Big] \tag{4.19}$$

In these important equations, one has:

$$f_{n',n}(\vec{q}) = \int \psi_{n'}^{*}(\vec{r})\ e^{i\vec{q}\cdot\vec{r}}\ \psi_{n}(\vec{r})\ d^{3}\vec{r}$$

$$\alpha_e = -\frac{m_h^*}{(m_e^* + m_h^*)} \quad ; \quad \alpha_h = \frac{m_e^*}{(m_e^* + m_h^*)} \tag{4.20}$$

and (| |) denotes integration over the unit cell.

With the use of 4.18 and 4.19, 4.6, 2.5 and 2.8, one obtains the Raman tensor:

$$R_{\nu}^{\alpha\beta}(\vec{q},\ \omega_i) = \Omega^{\frac{1}{2}} \sum_{c',c,v',v} \frac{P_{v',c'}^{\alpha} P_{cv}^{\beta}}{m} \left\{ \delta_{v',v}\theta_{cc'}^{\nu}(\vec{q}) \cdot F_{c',v',cv}(\alpha_e\vec{q},\omega_i) - \delta_{cc'}\theta_{vv'}^{\nu}(\vec{q}) F_{c',v',cv}(\alpha_h\vec{q},\ \omega_i) \right\}$$

$$+ \ . \ . \ . \ . \tag{4.21}$$

Here

$$\theta_{m',m}^{\nu}(\vec{q}) = (u_{m,0} | \theta^{\nu}(\vec{r}) |\ u_{m',0}) \tag{4.22}$$

and

$$F_{c',v',cv}(\vec{q},\omega_i) = \sum_{n',n} \frac{\psi_{n'}(0)\ f_{n',n}(\vec{q})\ \psi_{n}(0)}{(E_{c',v'} + E_n - \hbar\omega_i + \hbar\omega_o)(E_{cv} + E_n - \hbar\omega_i)} \tag{4.23}$$

One can note that terms of order higher than first in the wavevectors have been dropped in eq. 4.21. This gives rise to the scattering amplitude F being proportional to $\psi_n(0)$ which means that only s-excitonic states take part in the scattering process (since only $\psi_{n_s}(0) \neq 0$).

The Raman scattering tensor of 4.21, then, will be correct for any type of electron-phonon interaction $\theta_{m',m}^{\nu}$ and

for scattering between two sets of bands. This work will concern itself primarily with the Fröhlich interaction for intraband scattering since GaSe has a single valence and single conduction band at $\vec{k} = 0$ (Schlueter, 1973) and since Fröhlich scattering should be predominant for polar LO phonons. For the intraband Fröhlich interaction $\Theta^{\nu}_{m'm} = \frac{\gamma}{q}\delta_{m'm}$, where for a purely longitudinal phonon in a two atom per unit cell crystal (Fröhlich, 1954):

$$\gamma = -ie\left(\frac{1}{\epsilon_\infty} - \frac{1}{\epsilon_o}\right)^{\frac{1}{2}}(2\pi\hbar\omega_o)^{\frac{1}{2}} \qquad (4.24)$$

This form of the Fröhlich potential is valid as well in any crystal with more than two atoms per unit cell for any vibration where all atoms of a given species move together (Ganguly and Birman, 1967). Thus, it is valid in this form for the $A_2'(2)$ and $E'(2)$ phonons of GaSe.

The Raman tensor becomes:

$$R^{\alpha\beta}_{\nu}(\vec{q},\omega_i) = \Omega^{\frac{1}{2}}\delta_{cc'}\delta_{vv'}(P^{\alpha}_{vc}P^{\beta}_{cv}/m)\,\gamma q r_p^{\,2} H_{cv}(\vec{q},\omega_i) \qquad (4.25)$$

where

$$H_{cv}(\vec{q},\omega_i) = (qr_p)^{-2}\{F_{cvcv}(\alpha_e\vec{q},\omega_i) - F_{cvcv}(\alpha_h\vec{q},\omega_i)\} \qquad (4.26)$$

The rationale for writing the Raman tensor in this form is that the $\vec{q}$-dependence of the scattering is displayed explicitly. The function H is independent of $\vec{q}$ as $\vec{q} \to 0$ and the Raman tensor is thus proportional to $\vec{q}$. Here r_p, the polaron radius, is given by:

$$r_p = (\hbar/8\pi^2\mu\omega_o)^{\frac{1}{2}}$$

and thus qr_p is a dimensionless quantity.

For deformation potential (dp) scattering, the matrix element is:

$$\theta^{\nu}_{mm'}(\vec{q}) = \langle u_{m,0} \left| \left(\frac{\hbar\Omega}{2ma^2\omega_o}\right)^{\frac{1}{2}} D^{\nu}(\vec{r}) \right| u_{m',0} \rangle \qquad (4.27)$$

for a two atom per unit cell crystal where $D^{\nu}(\vec{r})$ is the dp (Bir and Pikus, 1961). This potential is short range (on the order of the interatomic spacing) and all q dependences can be set equal to zero in evaluating the matrix elements. Thus,

$$R^{\alpha\beta}_{\nu}(\vec{q},\omega_i) = \Omega^{\frac{1}{2}}(P^{\alpha}_{v'c'}P^{\beta}_{cv}/m)(\delta_{cc'}\theta^{\nu}_{vv'} - \delta_{vv'}\theta^{\nu}_{cc'})$$

$$\cdot F_{c'v'cv}(0,\omega_i) \qquad (4.28)$$

The Raman tensor in this case is q-independent as $\vec{q}\to 0$. Another important facet in the Fröhlich case is that for intraband scattering, that is $c' = c$, $v' = v$, the middle matrix element is diagonal in the electronic state and thus the Raman tensor has only diagonal components ($\hat{\epsilon}_i = \hat{\epsilon}_s$).

The problem of finding the scattering cross-section as a function of frequency has thus been reduced to the computation of the functions $F_{c'v'cv}(\vec{q},\omega_i)$ and $H_{cv}(\vec{q},\omega_i)$. To the extent of the approximations made so far, all the frequency dependence of the scattering is entirely contained in these functions and one has for the dp case:

$$\sigma_{dp} = A \left| F_{c'v'cv}(0, \omega_i) \right|^2 \qquad (4.29)$$

and for the Fröhlich case:

$$\sigma_f = B \left| H_{cv}(\vec{q}, \omega_i) \right|^2 \qquad (4.30)$$

To calculate these quantities, Martin (1971b) transforms the sum in equation 4.23 into an integral over the Green's functions for the internal motions. Defining a Green's function for equation 4.14:

$$\left(-\frac{\hbar^2}{2\mu} \nabla^2 + V(\vec{r}) - E \right) G_E(\vec{r}, \vec{r}') = \delta(\vec{r} - \vec{r}') \qquad (4.31)$$

one can write:

$$G_E(\vec{r}, \vec{r}') = \sum_n \frac{\Psi_n(\vec{r})\ \Psi_n(\vec{r}')}{E_n - E} \qquad (4.32)$$

Thus, simply the needed equation for F becomes:

$$F_{c'v'cv}(\vec{q}, \omega_i) = \int d^3r\ G_{E_2}(0, \vec{r})\ e^{i\vec{q}\cdot\vec{r}}\ G_{E_1}(\vec{r}, 0) \qquad (4.33)$$

where

$$E_1 = \hbar\omega_i - E_{cv} - \hbar^2 k_i^2/2(m_e^* + m_h^*) \qquad (4.34)$$

$$E_2 = \hbar\omega_i - \hbar\omega_s - E_{c'v'} - \hbar^2 k_s^2/2(m_e^* + m_h^*) \qquad (4.35)$$

Since the momentum terms are small corrections (these energies are typically one microelectron volt over the $\vec{k}$ values of interest) to the exciton energy, they are neglected.

Several solutions of this equation are of interest in this work. First, suppose all correlations were absent, that is, $V(\vec{r}) = 0$. In that case, the solution to 4.31 is:

$$G_E(\vec{r},0) = \frac{2\mu}{\hbar^2}\frac{1}{4\pi r}e^{ikr} \tag{4.36}$$

with

$$k^2 = \frac{2\mu E}{\hbar^2} \tag{4.37}$$

From now on the discussion will be limited to two bands c, v (intraband scattering) so that $E_{c'v'} = E_{cv} = E_g$, then

$$G_{E_2}(0,\vec{r}) = \frac{2\mu}{\hbar^2}\frac{1}{4\pi}\frac{e^{ik_2 r}}{r} \tag{4.38}$$

$$G_{E_1}(\vec{r},0) = \frac{2\mu}{\hbar^2}\frac{1}{4\pi}\frac{e^{ik_1 r}}{r} \tag{4.39}$$

where

$$k_2 = \left(\frac{2\mu}{\hbar^2}\right)^{1/2} E_2^{1/2} = \left(\frac{2\mu}{\hbar^2}\right)^{1/2}(-E_g + \hbar\omega_i - \hbar\omega_o) \tag{4.40}$$

$$k_1 = \left(\frac{2\mu}{\hbar^2}\right)^{1/2} E_1^{1/2} = \left(\frac{2\mu}{\hbar^2}\right)^{1/2}(-E_g + \hbar\omega_i) \tag{4.41}$$

For incident photon energies below the gap, both k_1 and k_2 are imaginary, so taking their imaginary parts, $k_1 = i\,k_1'$ and $k_2 = i\,k_2'$,

$$G_{E_2}\cdot G_{E_1} = \left(\frac{2\mu}{4\pi\hbar^2}\right)^2 \frac{e^{-(k_1'+k_2')r}}{r^2} \tag{4.42}$$

Thus by eq. 4.33,

$$F_{cvcv}(\vec{q},\omega_i) = 2\pi\int_0\int_{-1}^{\infty}\int^{1} r^2 dr\,d(\cos\theta)\left(\frac{2\mu}{\hbar^2 4\pi}\right)^2\frac{e^{-(k_1'+k_2')r}}{r^2}$$

$$\cdot e^{iqr\cos\vartheta}$$

$$= 4\pi\left(\frac{2\mu}{4\pi\hbar^2}\right)^2\int_0^{\infty}\frac{\sin(qr)}{qr}\,e^{-(k_1'+k_2')r}\,dr$$

Letting $a = (k_1' + k_2')/q$ and $x = qr$, one has

$$F_{cvcv}(\vec{q},\omega_i) = \frac{4\pi}{q}\left(\frac{2\mu}{4\pi\hbar^2}\right)^2 \int_0^\infty \frac{\sin x}{x} e^{-ax} dx$$

$$= \frac{4\pi}{q}\left(\frac{2\mu}{4\pi\hbar^2}\right)^2 \cot^{-1} a \qquad (4.43)$$

Employing the radius of the polaron r_p as defined before one has,

$$F_{cvcv}(\vec{q},\omega_i) = \frac{1}{8\pi^2}\left(\frac{\hbar^2}{2\mu}\right)^{-\frac{3}{2}} (\hbar\omega_o)^{-\frac{1}{2}} (qr_p)^{-1}$$

$$\cdot \tan^{-1}\left\{2\pi q r_p\left[\left(\frac{E_g - \hbar\omega_i}{\hbar\omega_o} + 1\right)^{\frac{1}{2}} - \left(\frac{E_g - \hbar\omega_i}{\hbar\omega_o}\right)^{\frac{1}{2}}\right]\right\}$$

(4.44)

This result is identical to that obtained by Loudon (1965). Two things should be noted. First as $\vec{q}\to 0$, the function F is indeed independent of q. Secondly, the function F does not peak at the n = 1 exciton level but rather at the gap, where it remains finite.

A second case which can be examined in detail is the case of the dp interacting with the discrete excitons as the intermediate states. Recall that the function needed is $F(0, \omega_i)$, thus in eq. 4.33 one has:

$$F_{cvcv}(0,\omega_i) = \int d^3r \sum_{n'} \frac{\Psi_{n'}(0)\Psi_{n'}(\vec{r})}{E_{n'} - E_2} \sum_n \frac{\Psi_n(\vec{r}')\Psi_n(0)}{E_n - E_1} \qquad (4.45)$$

where $\Psi_{nlm}(\vec{r},\theta,\varphi) = R_{nl}(\vec{r})\, Y_{lm}(\theta,\varphi)$ are the excitonic (hydro-

genic) wavefunctions. These wavefunctions are orthonormal:

$$\int d^3r \quad \Psi_{n'}(\vec{r}) \; \Psi_n(\vec{r}') \quad = \delta_{n'n} \; \delta(\vec{r} - \vec{r}') \qquad (4.46)$$

so that:

$$F_{cvcv}(0,\omega_i) = \sum_n \frac{|\Psi_n(0)|^2}{(E_n - E_2)(E_n - E_1)} \qquad (4.47)$$

In the course of the derivation of eq. 4.23, it was shown that only s-states take part in the scattering so:

$$Y_{lm}(\theta,\varphi) = Y_{00}(\theta,\varphi) \quad = (\frac{1}{4\pi})^{\frac{1}{2}} \qquad (4.48)$$

and also (Schiff, 1955):

$$R_{nl}(\vec{\rho}) = - \left\{ \left(\frac{2Z}{na_o} \right)^3 \frac{(n-\ell-1)!}{2n\{(n+\ell)!\}^3} \right\}^{\frac{1}{2}} e^{-\frac{1}{2}\rho} \rho^{\ell} \; L_{n+\ell}^{2\ell+1}(\vec{\rho}) \qquad (4.49)$$

where $\rho = \frac{2Z}{na_o} \; r$.

One has then,

$$R_{n0}(0) = - \left\{ \left(\frac{2}{na_o} \right)^3 \frac{(n-1)!}{2n(n!)^3} \right\}^{\frac{1}{2}} L_n^1(0) \qquad (4.50)$$

but (Schiff, 1955):

$$L_n^1(0) = \sum_{k=0}^{n-1} \frac{(-1)^{k+1}(n!)^2 \rho^k}{(n-1-k)!(1+k)!k!} = \frac{(-1)(n!)^2}{(n-1)!} \qquad (4.51)$$

whence,

$$R_{n0}(0) = \left\{ \left(\frac{2}{na_o} \right)^3 \frac{n!}{2n(n-1)!} \right\}^{\frac{1}{2}} = \left(\frac{4}{n^3 a_o^3} \right)^{\frac{1}{2}} \qquad (4.52)$$

Finally from 4.47, 4.48, and 4.52,

$$F_{cvcv}(0,\omega_i) = \frac{1}{\pi a_o^3} \sum_n \frac{1}{n^3} (E_g - \frac{E_{1s}}{n^2} - \hbar\omega_i + \hbar\omega_o)^{-1} \cdot (E_g - \frac{E_{1s}}{n^2} - \hbar\omega_i)^{-1} \qquad (4.53)$$

which agrees with the result of Ganguly and Birman (1967). This function has been shown in Figure 4.1 along with the result for the uncorrelated pairs. In both cases, the factor of $(\pi a_o^3)^{-1}$ has been removed to permit direct comparison. The fluctuations in the function at excited excitonic states (Figure 4.1) arise from the fact that for certain frequencies between n = 1 and n = ∞ various terms in the sum of equation 4.53 are negative and one gets cancellations. This behaviour carries over in the more complete calculation (Martin, 1971b) and these "nulls" between the various excited states of the exciton can serve to distinguish between dp and Fröhlich enhanced scattering. The sum in 4.53 has been summed only through n = 5 in the above figure, but there is no appreciable effect of extending the sum further.

Two other cases which can be solved easily which are of particular interest involve the Fröhlich scattering amplitude $H_{cv}(\vec{q}, \omega_i)$. First, the simple case of a single 1s exciton state as the intermediate state can be calculated. In this case:

$$G_{E_1}(r,0) = \frac{\Psi_1(r)\Psi_1(0)}{E_{1s} - E_1} \qquad (4.54)$$

$$G_{E_2}(0,r) = \frac{\Psi_1(0)\Psi_1^*(r)}{E_{1s} - E_2} \qquad (4.55)$$

where

$$\Psi_1(r) = (\pi)^{-\frac{1}{2}} (a_o)^{-\frac{3}{2}} e^{-r/a_o} \qquad (4.56)$$

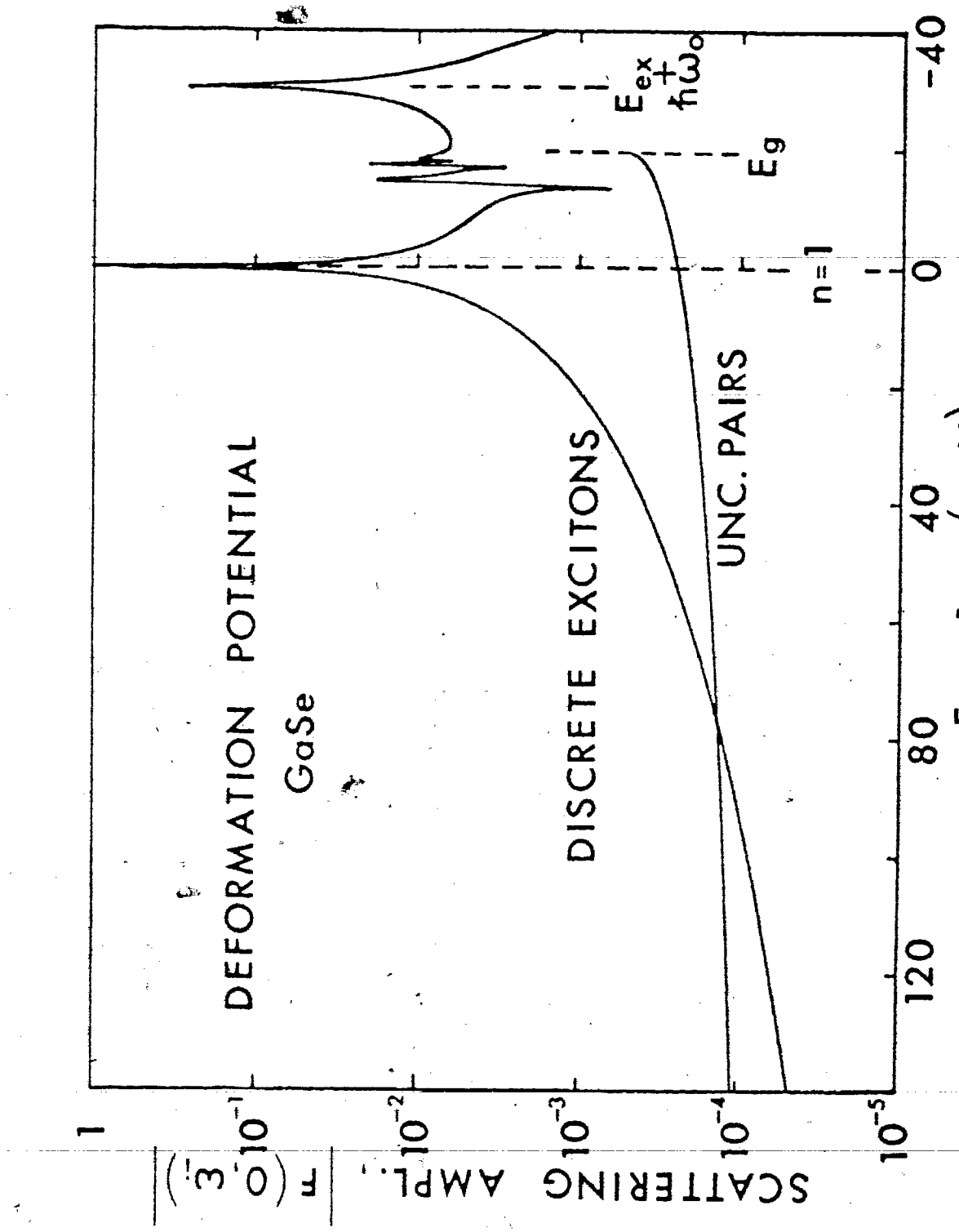

Figure 4.1. Scattering amplitude for deformation potential scattering. Shown are the contributions from the discrete excitons and uncorrelated pairs.

Then

$$F_{cvcv}(q,\omega_i) = \frac{2\pi}{\pi a_o^3}\int_0^{\infty}\int_{-1}^{1} \frac{r^2 d(\cos\theta)\,dr\; e^{iqr\cos\theta} e^{-2r/a_o}}{D\;\pi a_o^3} \qquad (4.57)$$

where

$$D = (\hbar\omega_i + E_{ls} - E_g)^{-1}\;(\hbar\omega_i + E_{ls} - E_g - \hbar\omega_o)^{-1}$$

which becomes

$$F_{cvcv}(q,\omega_i) = \frac{4}{\pi a_o^6 D}\int_0^{\infty} \frac{\sin(qr)}{qr}\, r^2\, e^{-2r/a_o} dr \qquad (4.58)$$

Finally then

$$F_{cvcv}(q,\omega_i) = \frac{1}{\pi a_o^3 D}\left(\frac{1}{1 + \frac{a_o^2 q^2}{4}}\right) \qquad (4.59)$$

which agrees with the result of Toyazawa (1958).

So for the Fröhlich amplitude, one has:

$$H_{cv}(q,\omega_i) = (qr_p)^{-2}\left\{F_{cvcv}(\alpha_e q,\omega_i) - F_{cvcv}(\alpha_h q,\omega_i)\right\}$$

$$= (\pi a_o^3)^{-1}(qr_p)^{-2}\left\{\left(1 + \frac{\alpha_e^2 a_o^2 q^2}{4}\right)^{-1} - \left(1 + \frac{\alpha_h^2 a_o^2 q^2}{4}\right)^{-1}\right\}\cdot(E_g - E_{ls} - \hbar\omega_i)^{-1}$$

$$\cdot(E_g - E_{ls} - \hbar\omega_i + \hbar\omega_o)^{-1} \qquad (4.60)$$

The important thing to note about this result is that the frequency dependence is the same as would be obtained for the dp case for n = 1 only (eq. 4.53).

In Figure 4.2 this function has been plotted against the result for the uncorrelated electrons and holes using the values of Table 4.1. The result for the exciton is

TABLE 4.1 - Material Parameters of GaSe. Where appropriate, values correspond to right angle scattering at 5900 A.

$E_g = 2.120$ eV [a]	$\varepsilon_o = (\varepsilon_\perp \varepsilon_\parallel)_o^{1/2} = 8.63$ [c]
$E_{ls} = 19.6$ meV [a]	$\varepsilon_\infty = (\varepsilon_\perp \varepsilon_\parallel)_\infty^{1/2} = 7.27$ [c]
$h\omega_{LO}(A_2'') = 30.6$ meV [b]	$a_o = \frac{R_\infty \, a_{Bohr}}{\varepsilon_o \, E_{ls}} = 42.5$ Å
$h\omega_{LO}(E') = 31.6$ meV [b]	$r_p = 4.93$ Å
$m_h^\parallel = 0.2\ m_o$ [d]	$m_h^\perp = 0.8\ m_o$ [d]
$m_e^\parallel = 0.3\ m_o$ [d]	$m_e^\perp = 0.17\ m_o$ [d]
$\mu_\perp = 0.14\ m_o$ [d]	$\mu_\parallel = 0.12\ m_o$ [d]
$m_e^* = (m_e^\parallel m_e^\perp)^{1/2} = 0.23\ m_o$	$m_h^* = 0.4\ m_o$
$\mu = (\mu_e^\perp \mu_e^\parallel)^{1/2} = 0.13\ m_o$	$\mu = (\frac{1}{m_e^*} + \frac{1}{m_h^*})^{-1} = .14\ m_o$
$\gamma = \frac{m_h^* - m_e^*}{m_h^* + m_e^*} = 0.27$	$q\ a_o = 0.18$
$n_\parallel \simeq 2.8$ [e]	$n_\perp \simeq 2.95$ [e]

a) Mercier et al. (1973); b) This work; c) Leung et al. (1969); d) Ottaviani et al. (1974); Wasscher and Dieleman (1972).

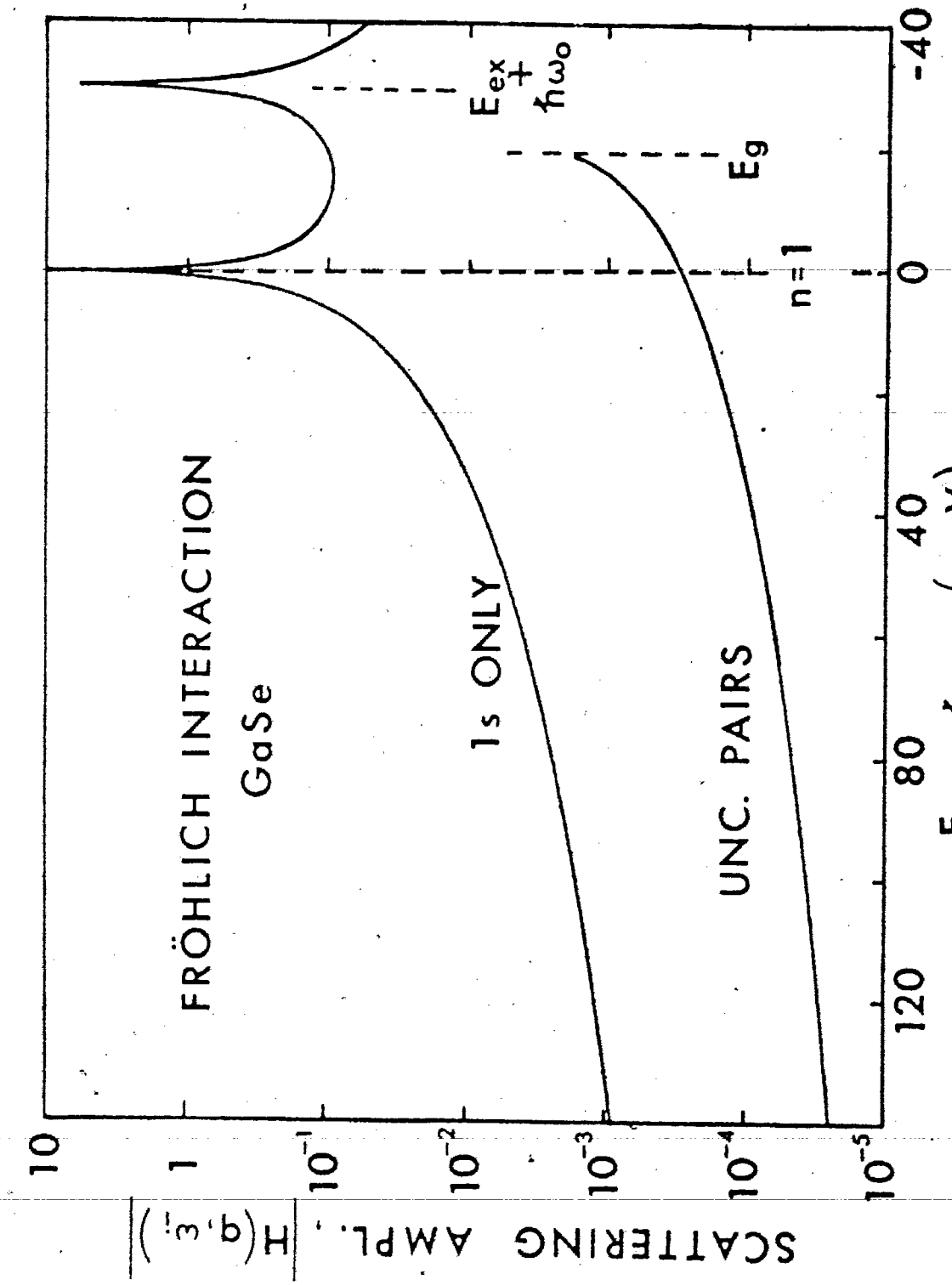

Figure 4.2. Scattering amplitude for Fröhlich scattering. Shown are the contributions from the 1s exciton state only and the uncorrelated pairs.

approximately two orders of magnitude larger than the "free" electrons and holes. This factor arises mainly from the prefactor $(a_o/r_p)^2$ obtained for eq. 4.60 by expanding the q-dependent bracket for small q. This prefactor is indicative of the spatial extent of the two interactions (with isolated electrons or holes or with the large Wannier excitons).

Finally the calculation can be done completely. To this point, each possible intermediate state has been treated distinctly. Unfortunately, the sum of equation 4.23 must be done over a complete set of electronic states. When Coulomb correlations are included in 4.14, the wavefunctions $\Psi_n(r)$ must include the effects of "free" electrons and holes under the perturbation of a coulombic potential (Coulomb scattering). In this case, the wavefunctions of the hydrogen atom do not form a complete set even if a spherical wave state for the continuum (the "uncorrelated" statefunction) is added. This can be visualized in terms of the hydrogen atom since the ionisation of the electron from the atom cannot be described in terms of a spherical wavefunction. Although the ionised electron is "free" it still experiences the effect of a Coulomb potential and one must include coulombic scattering into the wavefunction. The proper wavefunction is a confluent hypergeometric function (Schiff, 1955) which is not necessary to write down here. The problem of finding the Green's function (eq. 4.32) for the Coulomb

correlated case has been done by Hostler (1963) who ob-

$$G_E(r,0) = \frac{1}{4\pi r}\frac{\hbar^2}{2\mu}\Gamma(1-\kappa)\,W_{\kappa,\frac{1}{2}}(\rho) \qquad (4.61)$$

where $\rho = \frac{2r}{\kappa a_o}$ and $\kappa = (E_{ls}/E)^{\frac{1}{2}}$, and $W_{\kappa,\frac{1}{2}}(\rho)$ is a Whittaker function of the first kind (Whittaker and Watson, 1963). The solution of 4.33 is now quite complicated and can only be performed numerically. Fortunately, the calculation has been done in a parameterized form (Martin, 1973). In that work the function $H_{cv}(\vec{q},\omega_i)$ has been given as a function of the parameter $\Delta_o = \hbar\omega_o/E_{ls}$ and a reduced energy parameter

$$\Delta_i = \frac{E_g - \hbar\omega_i}{\hbar\omega_o} \qquad (4.62)$$

A series of curves of $H_{cv}(\vec{q},\omega_i)$ is plotted in Figures 4.3(a) and 4.3(b). Figure 4.3(a) shows the scattering amplitude for the region below the n = 1 state of the exciton and Figure 4.3(b) shows the region between the n = 1 and n = 2 states of the exciton. For GaSe the value of Δ_o is 1.58 for the A_2''(LO) phonon.

This completes the necessary calculations for the resonant cross-sections as a function of energy for GaSe. One point that should be clarified is Martin's use of the notation "Total" to describe the result obtained with the Green's function, eq. 4.61, while in the same diagram (Figure 3 of Martin, 1971b), he has the partial contributions due to discrete excitons and uncorrelated pairs. This is misleading

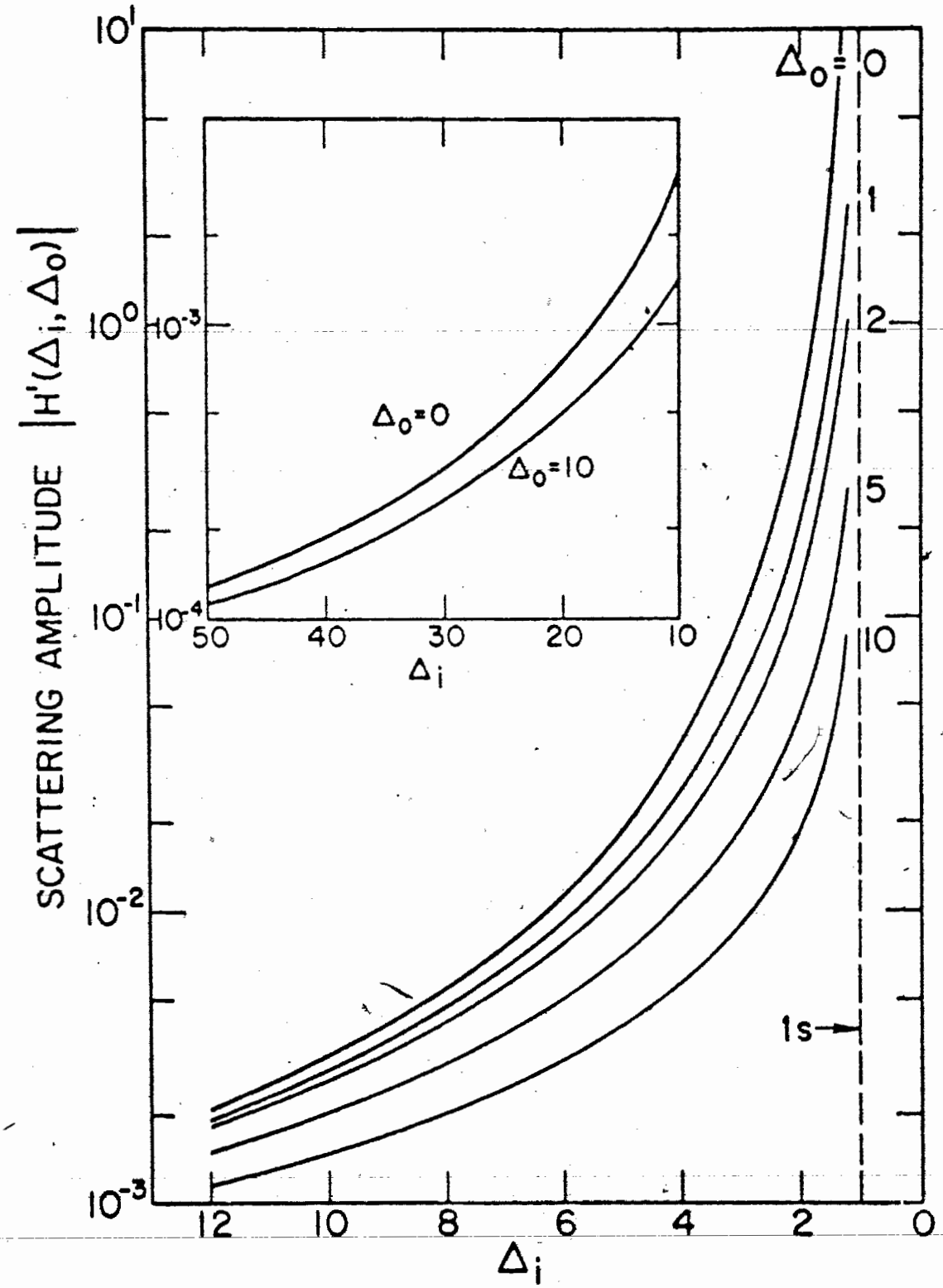

Figure 4.3 (a). The scattering amplitude for Fröhlich scattering for incident photon energies below the n = 1 state of the exciton. The curves are given as functions of the parameters Δ_0 and Δ_i (see text) (After Martin, 1973).

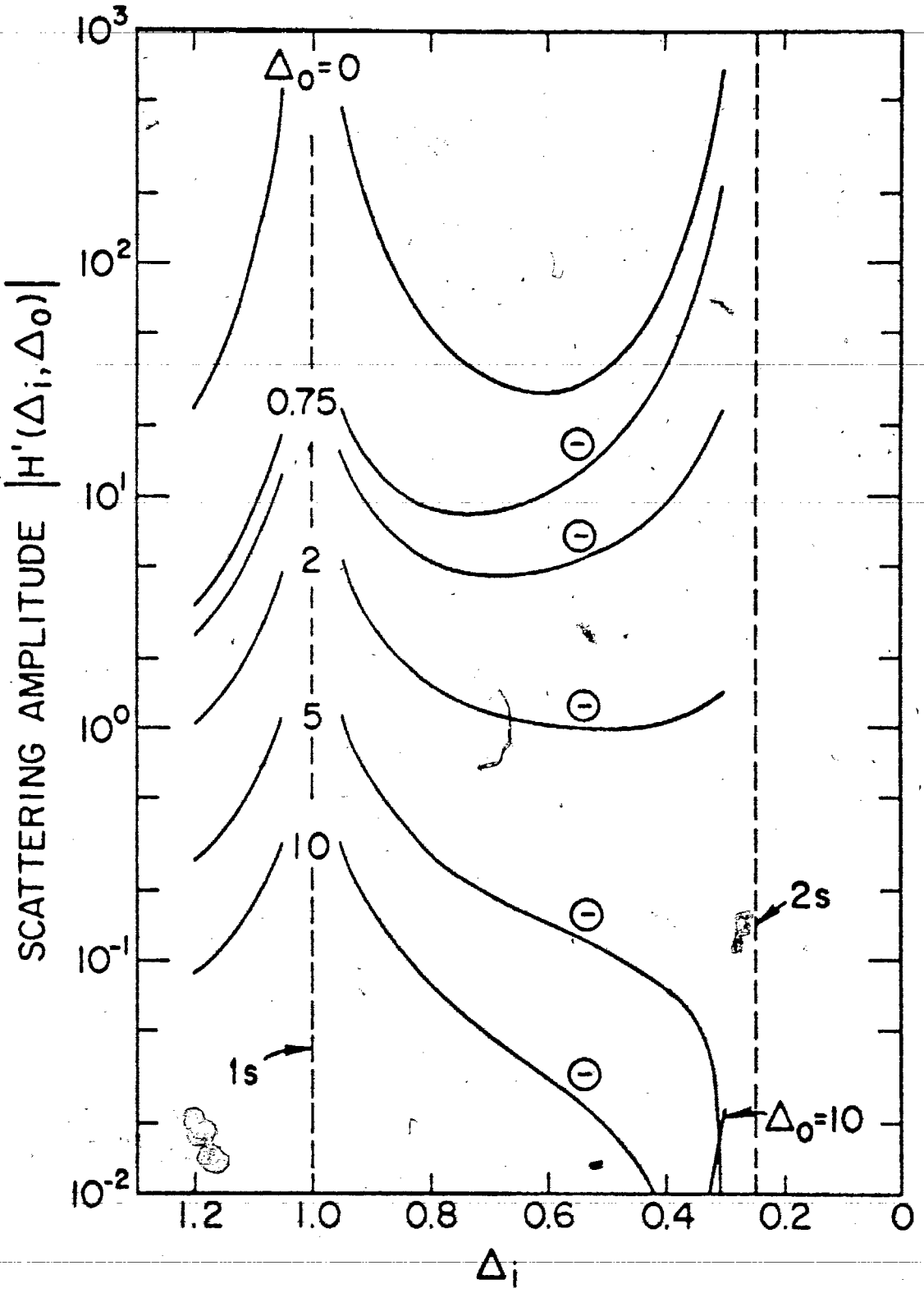

Figure 4.3 (b). The scattering amplitude for Fröhlich scattering for incident photon energies between the n = 1 and n = 2 exciton states. The curves are given as functions of the parameters Δ_o and Δ_i (see text) (After Martin, 1973).

since it is not a total as in the sum of the contributions but rather the result of a more complete calculation. As a result, there is considerable cancellation due to free electrons and holes in the Fröhlich scattering efficiency, and the result is a much sharper resonance than that for the discrete excitons only. This will be an important consideration later.

CHAPTER V

THE RESONANT RAMAN EFFECT IN GaSe-EXPERIMENT

5.1.1 Crystals

The crystals used in the experiments on the RRE in GaSe consisted of a large plate crystal described in Section 3.1.1 and two thin slices taken from the crystal. The large crystal was approximately 2 mm thick by 7 mm long on the x-edge and two slices both approximately 0.8 mm thick were taken from this edge. These slices were used in the forward-backward scattering experiments and were necessary to obtain $\hat{\epsilon}_i \| \hat{c}$.

5.1.2 Method

The spectra were obtained with the use of a Spectra Physics Model 370 tunable dye laser and with a 50 mW He-Ne laser. All the RRE spectra were obtained at 81 $\pm$ 1°K in a cold finger dewar.

The observed Raman signal was calibrated against the 466 cm^{-1} line of an oriented quartz crystal which was mounted immediately prior to the GaSe crystal in the light path. With both crystals thus imaged on the slit of the spectrometer, the heights of the spectral peaks were then measured and a ratio of the intensity of the Raman line versus the quartz reference line obtained. Since slit widths of approximately 5 cm^{-1} were used in the RRE experiments, the peak heights should represent the intensities of the lines of interest (which have line-widths ~ 3 cm^{-1}). The spectra were analyzed with the photon counting techniques described in Section 3.1.2.

5.1.3 Scattering Efficiency and Absorption Corrections

The scattered efficiency of the GaSe LO phonon lines relative to the 466 cm^{-1} quartz line was calculated for grazing incidence (with the incident light transmitted through the quartz reference) according to the procedure of Callender et al. (1973). The experimental geometry is shown in Figure 5.1(c) and is seen to be a combination of Raman scattering from a quartz reference in a transmission geometry (symbolized in Figure 5.1(a)) and Raman scattering from the GaSe sample at non-normal incidence (Figure 5.1(b)). In each of these geometries the scattering efficiency can be calculated, and the result for the experimental geometry is obtained by combining these results.

Figure 5.1(a) shows the transmission geometry with the signal viewed at 90°. One can write for the scattered intensity per unit length:

$$\frac{dI_s^{in}}{dx} = S\, I_\ell(x)\, \Omega \qquad (5.1)$$

where I_s^{in} = the scattered intensity inside the sample

I_ℓ = the incident laser intensity

S = scattering efficiency per unit length per unit solid angle (S/L as defined by Martin, eq. 4.3)

Ω = solid angle

Now

$$I_\ell(x) = I_o\, (1 - R_\ell)\, e^{-\alpha_\ell x} \qquad (5.2)$$

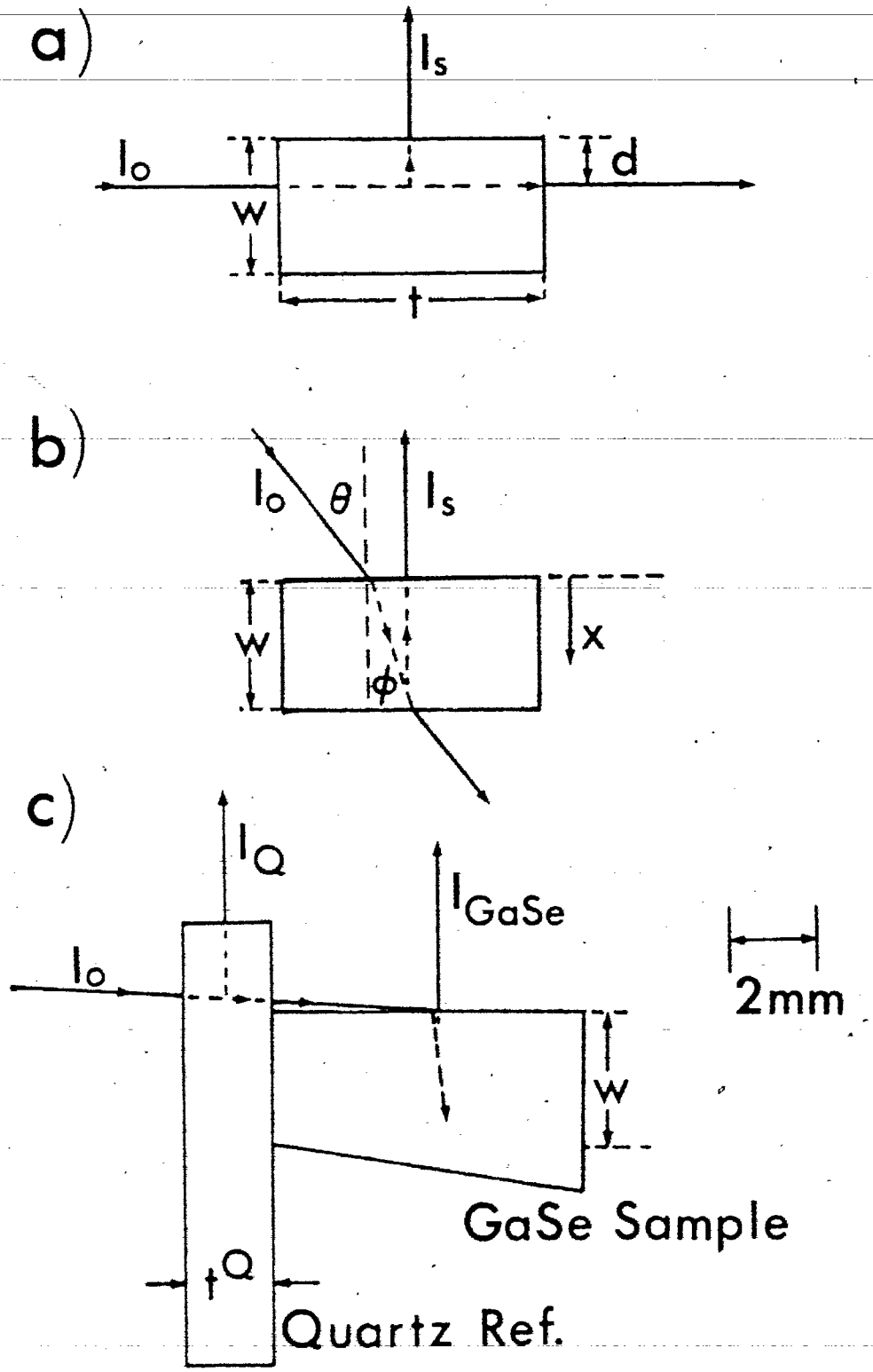

Figure 5.1. Scattering geometry used in RRE. (a) Transmission geometry with light viewed at 90°. (b) Reflection geometry. (c) The experimental geometry drawn roughly to scale.

where I_o = laser intensity outside sample

R_ℓ = reflectance at the laser energy

α_ℓ = absorption coefficient at laser energy

so combining (5.1) and (5.2)

$$\frac{dI_s^{in}(x)}{dx} = S\, I_o\, (1 - R_\ell)\, e^{-\alpha_\ell x} \tag{5.3}$$

Now the scattered beam is also absorbed a certain amount before it leaves the sample:

$$dI_s^{out}(x) = dI_s^{in}(x)\, e^{-\alpha_s d}\, (1 - R_s) \tag{5.4}$$

so integrating (5.3) and using (5.4), one has

$$I_s^{out} = S\, I_o (1 - R_\ell)(1 - R_s) e^{-\alpha_s d} \int_0^t e^{-\alpha_\ell x} dx$$

$$= S\, I_o (1 - R_\ell)(1 - R_s) e^{-\alpha_s d} \left(\frac{1 - e^{-\alpha_\ell t}}{\alpha_\ell} \right) \tag{5.5}$$

whence, finally

$$S = \frac{I_s^{out}}{I_o} \frac{\alpha_\ell}{e^{-\alpha_s d}(1-e^{-\alpha_\ell t})(1-R_\ell)(1-R_s)} \tag{5.6}$$

For the grazing (or non-normal incidence) of Figure 5.1(b) one has a more difficult problem. Suppose that the medium is isotropic (or oriented properly) so that Snell's law applies with only one index of refraction $n(\omega)$, then

$$n \sin \phi = \sin \theta \tag{5.7}$$

$$y = x \sec \phi \tag{5.8}$$

$$dy = dx \sec \phi \tag{5.9}$$

Then, again

$$I_\ell^{in}(y) = I_o\,(1 - R_\ell)\; e^{-\alpha_\ell y} \tag{5.10}$$

$$\frac{dI_s^{in}(y)}{dy} = I_o\,(1 - R_\ell)\; S\;\Omega\; e^{-\alpha_\ell y} \tag{5.11}$$

where $(1 - R_\ell)$ is the transmittance of the surface at the angle ϕ. But the scattered light is in the normal (x) direction:

$$dI_s^{out}(x) = dI_s^{in}(y) e^{-\alpha_s x}(1 - R_s) \tag{5.12}$$

so
$$I_s^{out} = \int_0^w dI_s^{in}(y)\; e^{-\alpha_s x}\; (1 - R_s)\; dy$$

$$= \int_0^w I_o(1-R_\ell)(1-R_s)\Omega S\; e^{-(\alpha_\ell \sec\phi + \alpha_s)x} \sec\phi\; dx$$

$$= \frac{I_o(1-R_\ell)(1-R_s)S\Omega}{\alpha_\ell \sec\phi + \alpha_s}\; \{1 - \exp(-(\alpha_\ell \sec\phi + \alpha_s)w)\}$$

$$\cdot \sec\phi \tag{5.13}$$

or

$$S = \frac{I_s^{out}}{I_o}\; (\alpha_\ell \sec\phi + \alpha_s)\cos\phi \cdot (1 - R_\ell)^{-1}(1 - R_s)^{-1}$$

$$\cdot (\Omega)^{-1}\; \{1 - \exp(-(\alpha_\ell \sec\phi + \alpha_s)w)\}^{-1} \tag{5.14}$$

This result is equivalent to Callender's result (1973) for the reflection geometry if $\cos\phi = \sec\phi = 1$.

One is now in a position to calculate the scattering efficiencyfor the experimental geometry of Figure 5.1 (c). Using the result of eq. (5.6) for the quartz reference (setting $\alpha_\ell^Q = \alpha_S^Q = 0$; $\frac{1-e^{-\alpha_\ell t}}{\alpha_\ell} \to t^Q$) and the result of equation (5.14) for the GaSe at grazing incidence (the approximation

sec ϕ = cos ϕ = 1 is made here and because of the high index of refraction of GaSe this is not a bad approximation), one has:

$$\frac{S_{GaSe}}{S_Q} = \frac{I_{GaSe}}{I_Q} \frac{(\alpha_\ell+\alpha_s)^{GaSe} t^Q (1-R_\ell^Q)^3 (1-R_s^Q)}{\{1 - \exp(-(\alpha_\ell+\alpha_s)w\}^{GaSe} (1-R_\ell)^{GaSe}} \cdot (1 - R_s)^{-1}_{GaSe} \cdot \frac{\Omega^Q}{\Omega^{GaSe}} \qquad (5.15)$$

The solid angles subtended by the optics may not be the same in both cases, but the assumption is made that they are equal outside the samples. This will introduce no frequency dependent error and since the scattered efficiency will prove to be relative rather than absolute, this is a justifiable choice. Inside the sample the ratio of solid angles will just be reduced by the inverse of the ratios of the indices of refraction:

$$\frac{\Omega^Q}{\Omega^{GaSe}} = \frac{n_s^{GaSe}}{n_s^{Quartz}} \qquad (5.16)$$

so that finally

$$\frac{S^{GaSe}}{S^Q} = K \frac{I_{GaSe}}{I_Q} \frac{(\alpha_\ell+\alpha_s)(1 - R_\ell)^{-1}(1 - R_s)^{-1}}{1 - \exp(-(\alpha_\ell+\alpha_s)w)} \qquad (5.17)$$

where

$$K = t^Q (1 - R_\ell^Q)^3 (1 - R_s^Q) \frac{n_{GaSe}}{n_Q} \qquad (5.18)$$

and with

$t^Q = 0.2$ cm $\qquad$ $n^Q = 1.544$

$R_\ell^Q = R_s^Q = .0457$ $\qquad$ $n_e^{GaSe} = 2.6$

(values for quartz from CRC Handbook, 1964; Wasscher and Dieleman (1973) for n_e) one has K = 0.276.

In the equation (5.17) above, then, it is necessary to know the absorption coefficient as a function of frequency as well as the reflection coefficient. Unfortunately, a detailed investigation of the absorption coefficient of GaSe at 77°K has not been carried out with $\vec{E} \| \hat{c}$ because of the impossibility of obtaining thin enough samples with the appropriate orientation. However, oblique incidence methods at room temperature have indicated that the absorption coefficient for $\vec{E} \| \hat{c}$ is about 35 times stronger than for $\vec{E} \perp \hat{c}$ near the exciton (Wasscher and Dieleman, 1972) and a similar result was reached by Bourdon and Khelladi (1971). Thus it is possible to estimate an absorption coefficient for $\vec{E} \| \vec{c}$ from the data available for $\vec{E} \perp \vec{c}$. Such measurements for $\vec{E} \perp \vec{c}$ have been performed at 4.2°K for energies below the exciton by Kamimura et al. (1969) who found a long weak tail due to indirect gap transitions. By using their data (shifted in energy by the band gap shift from 4.2°K to 77°K) and the data for thick samples for $\vec{E} \perp \hat{c}$ (Kurik et al., 1968) (scaled by the factor of 35), a reasonable estimate of the absorption coefficient was made (Figure 5.2). The energy regions covered by these two works (Kamimura et al., 1969; Kurik et al., 1968) are shown in the diagram. The fact that the data of Kamimura is taken at 4.2°K implies that the absorption coefficient in the low energy tail is probably somewhat lower

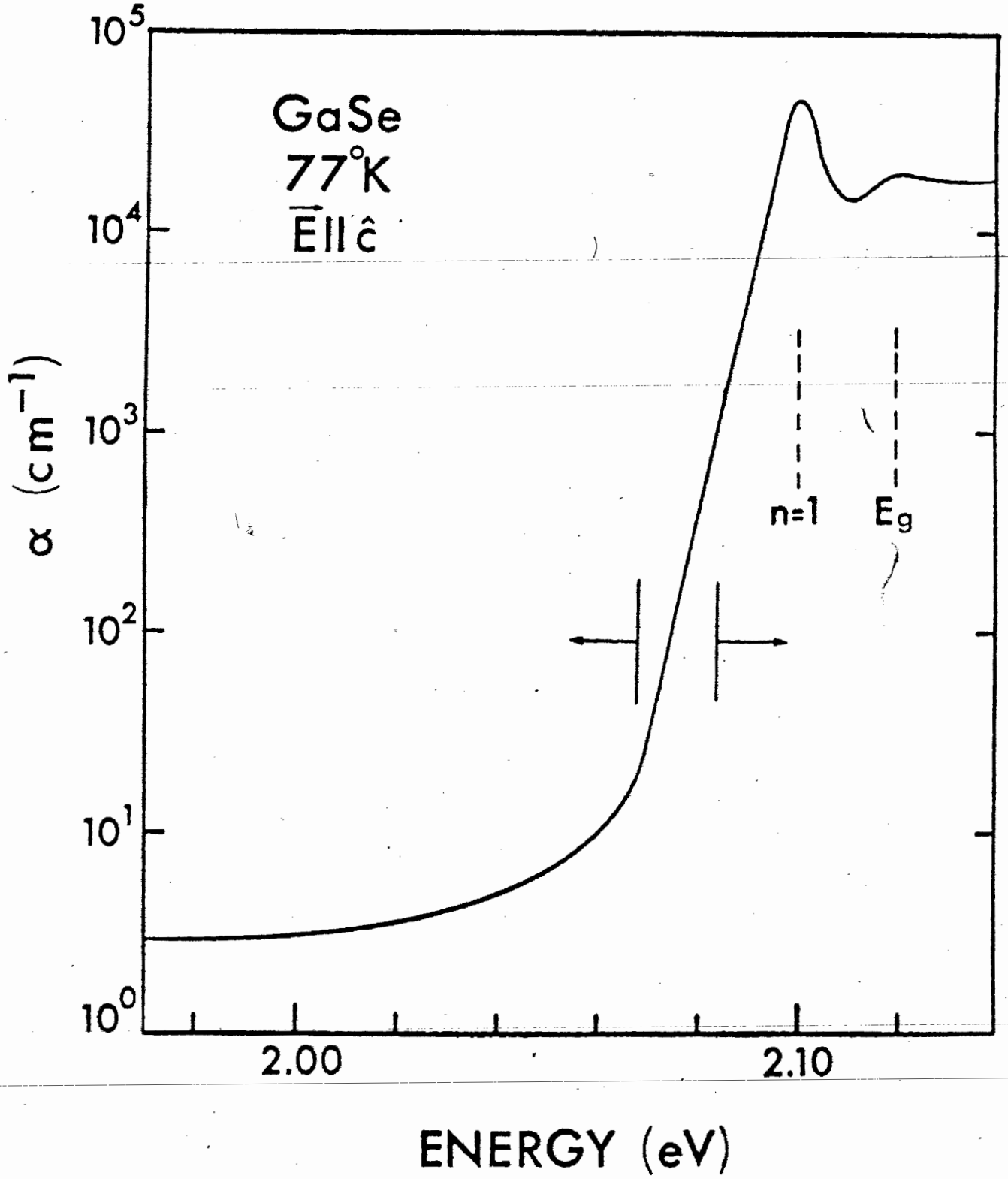

Figure 5.2. Absorption Coefficient of GaSe. To the left of the vertical line is the data of Kamimura et al. (1969) and to the right that of Kurik et al. (1968).

than the true value, since phonon participation in the indirect process would be temperature dependent. On the other hand, an examination of analogous data allows one to argue that this thermal effect will not significantly affect the low energy tail of the absorption curve between 77°K and 4.2°K. For example, in GaP which is also an indirect gap compound, the heights of the absorption steps as the indirect gap is approached do not change significantly over the range 1.6°K to 77°K (Dean and Thomas, 1966). It is also important to note that the sharpness of the exciton line and its tail for $\vec{E} \perp \hat{c}$ in GaSe does not change from 77°K to 1.6°K (Fischer, 1963). Finally, the fact that the portions of the curve from each set of measured data can be joined fairly smoothly provides an additional degree of justification for this procedure. It should be noted that it is in this region of juxtaposition where measurements have not been performed at 77°K, and where the absorption curve is very steep, that the uncertainties in the absorption coefficient will be largest ($\lesssim 30\%$).

The necessary reflectance values for normal incidence were obtained from the $\vec{E} \perp \hat{c}$ measurements (Akhundov et al., 1966). The error introduced by using data obtained in this orientation will be small compared to the overall experimental error. The reflectance values for the angle of grazing incidence were obtained from Fresnel's formula. The index of refraction, n_e, was considered constant throughout the energy interval. As a result of these and the above approximations, the values

obtained for the scattered efficiency should be regarded as relative rather than absolute efficiencies.

5.2 Results

A series of spectra recorded with various laser wavelengths is shown in Figure 5.3. Far from resonance at 6328 Å (Figure 5.3(c)) the spectrum is similar to those shown in Chapter 3 and a list of the modes associated with these features is given in Table 3.2. The resonant behaviour of several of these modes has been investigated in detail and will be described below.

5.2.1 Polar Modes

The resonant behaviour of the A_2''(LO) 247 cm^{-1} mode is the most striking feature of the series of spectra shown in Figure 5.3. This mode is normally Raman inactive as was shown before, and far from resonance (Figure 5.3(c)) it is absent from the spectra. As the exciting wavelength is decreased, however, this mode appears, grows in intensity, and in fact near resonance (Figure 5.3(a)) becomes the dominant feature in (zz) spectra. The E'(LO) mode at 254 cm^{-1}, although a Raman active phonon, is also forbidden by selection rules for the (zz) geometry. It can be seen as going from the relatively weak line in the 6328 Å spectrum (its appearance here is due to sample depolarization) to the second most prominent feature in the GaSe spectrum near resonance. The remaining feature associated with the polar phonons that becomes prominent is the 2E'(LO) mode at 509 cm^{-1}.

The relative scattering efficiency of the two first order modes as a function of excitation energy is shown in Figure

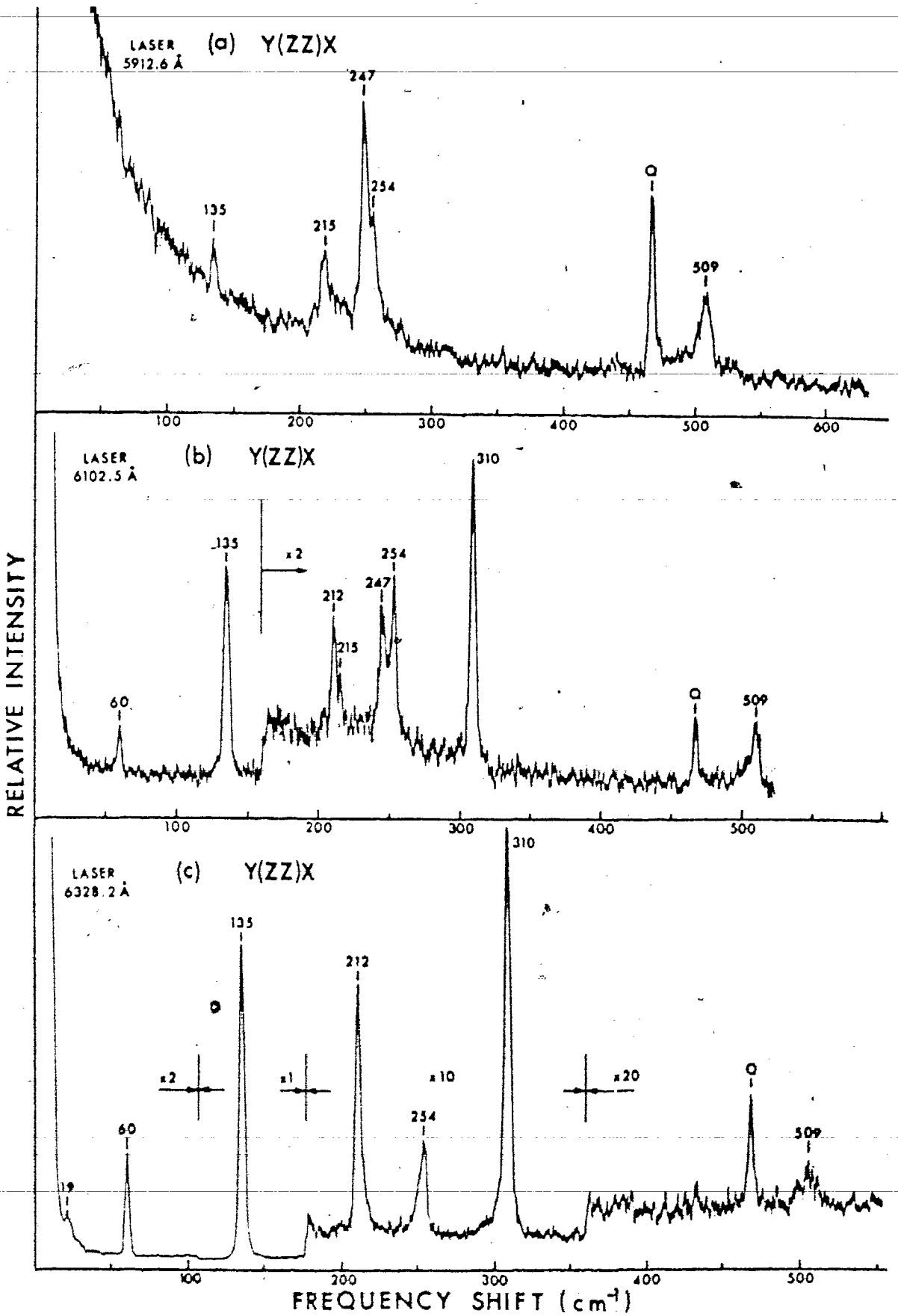

Figure 5.3. Resonant Raman Spectra of GaSe. Spectra correspond to energy shifts, $E_{ex} - \hbar\omega_i$ of a) 4.2 meV; b) 69.5 meV and c) 141.9 meV. All spectra obtained at 81 ^{o}K.

5.4. In this figure, the excitation frequency is written both as the energy difference from the exciton line in meV and as a reduced energy parameter $\Delta_i = (E_g - \hbar\omega_i)/E_{1s}$ where E_g is the band gap energy, $\hbar\omega_i$ the exciting frequency, and E_{1s} is the free exciton Rydberg. This notation allows direct comparison with the theory of Martin (1971b, 1973). At 77°K the exciton energy has been determined previously to be 2.100 eV (Mercier et al., 1973) in absorption. This result is in good agreement with the value of 2.0984 (FWHM 6.3 meV) that we have obtained in emission at 81°K, if the band gap shift of -0.35 meV/°K is included (Fischer, 1963). From Figure 5.4 it is obvious that the scattering efficiency of both polar phonons undergoes a distinct maximum at the n = 1 free exciton.

5.2.2 Non-Polar Modes

Several of the non-polar phonons exhibit a much weaker resonant behaviour than that of the polar modes. The scattering efficiency of the non-polar A_1' (135 cm^{-1}) mode is plotted versus the excitation energy in Figure 5.5. Also included in this figure is the scattering efficiency of the non-polar E'(TO) mode at 215 cm^{-1}. It should be mentioned that the A_1' (135 cm^{-1}) and the A_1' (308 cm^{-1}) modes exhibit the same resonance behaviour and thus only the former is shown. The maximum of the scattering efficiency in each of these cases is approximately a factor of five weaker than that for the polar phonons and this is interpreted as being due to the

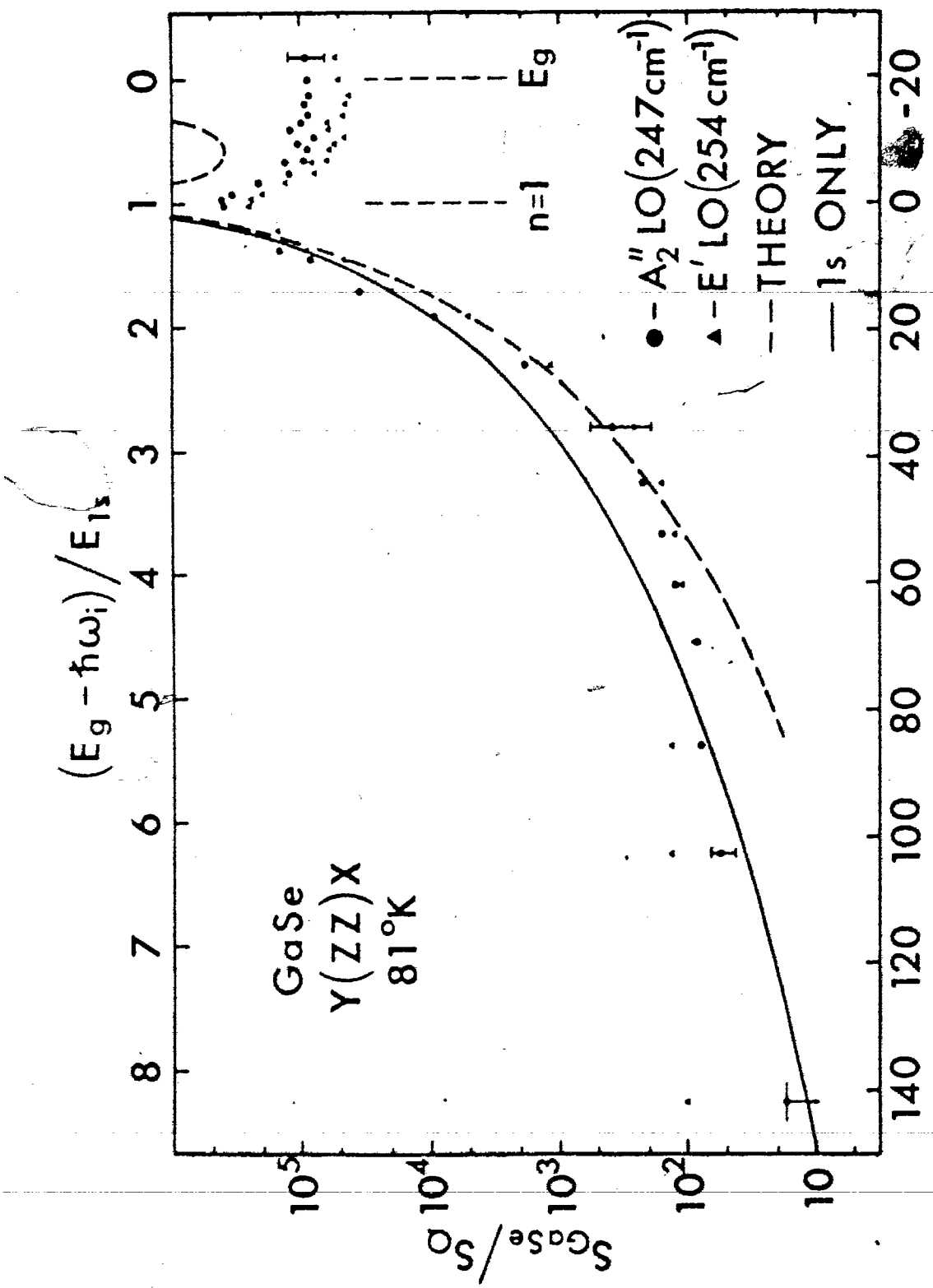

Figure 5.4. Relative scattering efficiency of polar LO modes. The dashed line shows the results of Martin's calculation and the solid line that given by considering only scattering from the 1s excitonic state.

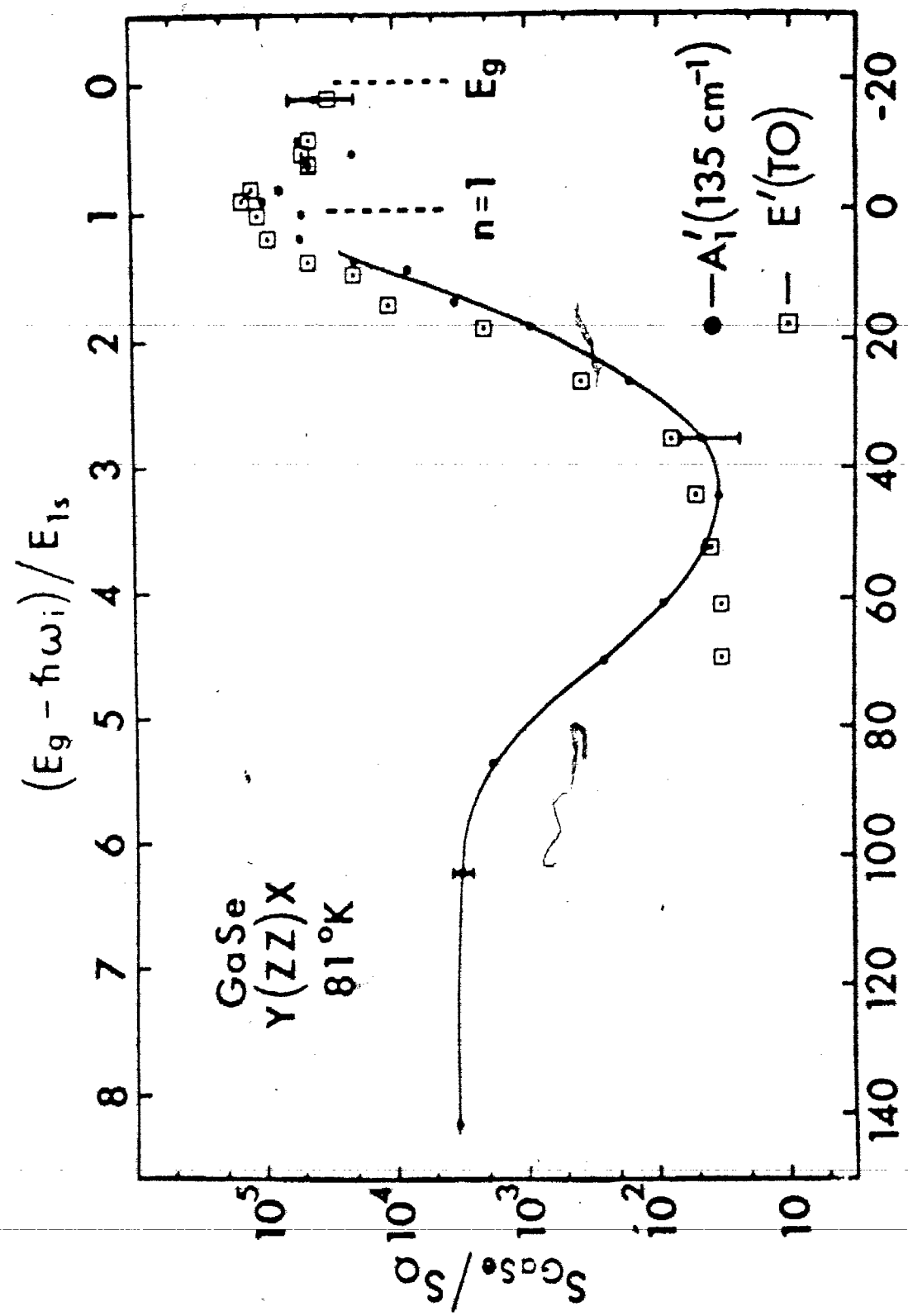

Figure 5.5. Relative scattering efficiency of non-polar $A_1'(135\ cm^{-1})$ and $E'(TO)$ $(215\ cm^{-1})$ modes. The solid line is drawn through the data points for the A_1' phonon as an aid in visualising the antiresonance in the cross-section.

relative strength of the Fröhlich interaction which is active in the polar phonons and the deformation potential interaction which is active for these non-polar phonons.

The striking feature about the behaviour of the A_1' phonons is the antiresonance as the gap is approached. The scattering efficiency from these modes passes through a minimum when the excitation energy is approximately 64 meV below the band gap. This behaviour is qualitatively similar to that observed for the $E_2(1)$ mode in CdS (Ralston et al., 1970; Damen and Scott, 1971).

5.2.3 Angular Dependence

The angular dependence of the scattering efficiency for the polar modes has been investigated in a manner similar to that described by Colwell and Klein (1970). The necessary equation they obtained (which is also easily derived by the ground work of Section 5.1.2) for the backward-forward scattering ratio is:

$$\frac{S_b}{S_f} = \left(\frac{I_b}{I_f}\right) e^{-\alpha_s w}\left(\frac{e^{(\alpha_s-\alpha_\ell)w} - 1}{1 - e^{-(\alpha_\ell+\alpha_s)w}}\right)\left(\frac{\alpha_s + \alpha_\ell}{\alpha_s - \alpha_\ell}\right) \qquad (5.19)$$

which if $\alpha_\ell >> \alpha_s$ reduces simply to

$$\frac{S_b}{S_f} = \left(\frac{I_b}{I_f}\right) e^{-\alpha_s w} \qquad (5.20)$$

The ratio of backward to forward scattering cross sections is shown as a function of energy in Figure 5.6. In the energy region below 50 meV from the exciton, the ratio of backward to forward scattering cross-sections was found to be relatively

constant at a value of ~1.3 ± 0.2 for the E'(LO) phonon. The ratio has a small peak at 30 meV below the exciton going to a value of approximately 3.2 ± 0.4 and returning to a value of about unity 10 meV below the exciton, which is the closest frequency observable in forward scattering.

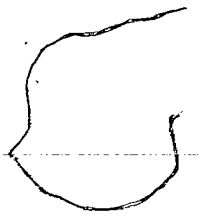

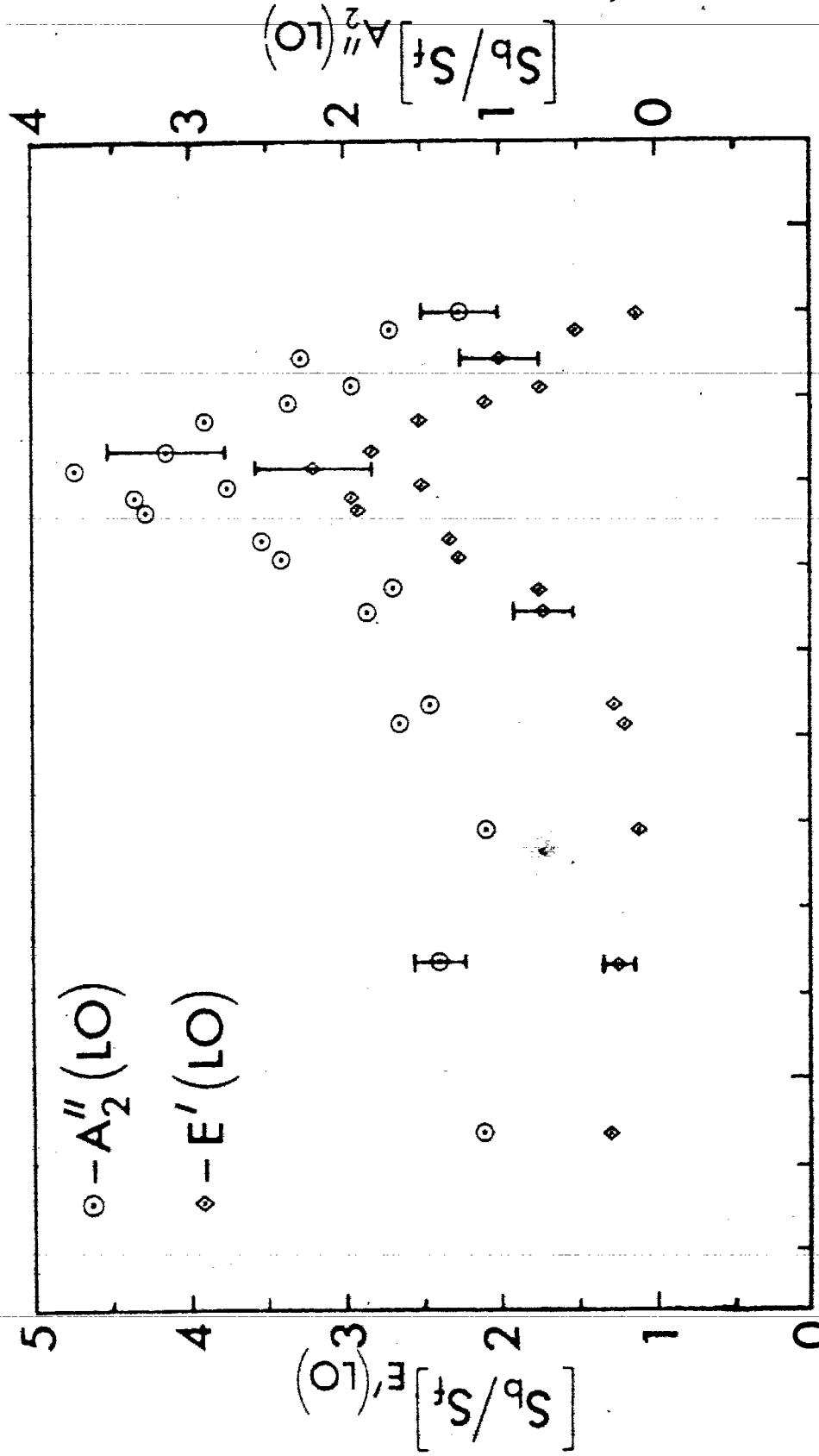

Figure 5.6. Ratio of backward to forward scattering cross-sections. Note that the ordinates for the A_2''(LO) phonon (right scale) is shifted upwards by one unit to aid in distinguishing between the data.

5.3 Discussion

5.3.1 Spectral Features

In Chapter 3, the non-resonant spectrum of GaSe was discussed. Some of the interpretations of the phonon modes drew heavily from the work on Resonant Raman scattering. In particular, the identification of the 247 cm^{-1} mode as the A_2'' (LO) phonon was made conclusive by its dramatic appearance in the Resonant Raman spectrum. In Figure 5.3(c) the typical non-resonant Raman spectrum for the zz geometry is shown ($81^{o}K$). In this orientation only the A_1' (135 cm^{-1}) and the A_1' (308 cm^{-1}) modes are allowed. The other modes appear because of the depolarization introduced by the edges of the crystal. This depolarization, however, has a much smaller effect than the relative amplitudes of the modes with changes in orientation, and consequently the selection rules can be verified.

Hayek et al. (1973) observed the 247 cm^{-1} mode in a zz spectrum with the use of a He-Ne laser at room temperature. They designated this mode as the conjugate to the 254 cm^{-1} mode which they assigned as an E" phonon. The Resonant Raman work here, however, shows that the 247 cm^{-1} mode is observable only in resonance and thus that Hayek's result is a manifestation of the RRE which can be seen with the He-Ne laser at room temperature. Furthermore, when an xz spectrum is taken at wavelengths near that shown in Figure 5.3(b), the 247 cm^{-1} peak disappears and the 254 cm^{-1} peak returns to its relative strength of Figure 5.3(c). Thus, the resonant mode at 247 cm^{-1} is observed only in zz spectra. This behaviour of

the 247 cm^{-1} mode can be easily reconciled with the theory of Martin (1971b) and other experimental observations on forbidden modes (Anastassakis and Burstein, 1971; Williams and Porto, 1973). The result found is that near resonance, where q-dependent scattering predominates, infrared active modes that are normally Raman inactive can become Raman allowed. It should also be noted that the observation of resonance behaviour in only z-oriented spectra, that is $\hat{\epsilon}_i \| \hat{c}$, is consistent with the theory since for GaSe the dipole matrix element, P_{cv}^{β} (equation 4.21), for both the exciton and direct gap transitions is large only for $\hat{\epsilon}_i \| \hat{c}$ (Wasscher and Dieleman, 1972). Since the scattering efficiency is proportional to the Raman tensor squared, there is a fourth power dependence on this dipole matrix element and thus the zz resonance spectrum should be dominant.

5.3.2 Polar Modes (E'(LO) 254 cm^{-1}, A_2'' (LO) 247 cm^{-1})

5.3.2.1 Wavelength Dependence

The observed wavelength dependence of the scattering efficiency for the A_2''(LO) and E'(LO) phonons is compared to Martin's theory in Figure 5.4. In this figure, the curve of the square of the dimensionless scattering amplitude (dashed curve) for $\Delta_o = \hbar\omega_o/E_{1s} = 1.58$ of Figure 4.3 has been plotted by fitting the curve to one data point E'(LO) at $\Delta_i \approx 2$ and this point serves as the only constraint. As can be seen from the figure this curve agrees fairly well with the observed scattering efficiency when the incident photon energy is

within 50 meV or the n = 1 exciton level. For smaller incident photon energies the calculated values become much smaller than the observed scattering efficiencies. In the case of the E'(LO) phonon this discrepancy can be partially explained by a return to the non-resonant intensity of Figure 5.3(c). This explanation is not valid, however, for the 247 cm^{-1} phonon which is normally Raman inactive.

The solid curve, on the other hand, is the result obtained by including only the n = 1 excitonic state as the intermediate state in the scattering (Figure 4.2). This curve has been fitted to the $\Delta_i \approx 2\ A_2''$ (LO) data point and gives a much better result in the long wavelength region where the experimental data is most reliable. The agreement is poorest in the energy region approximately 40 meV below the exciton energy where the measured points fall well below the theoretical curve. In this region, however, one would expect the largest error because of the uncertainty in the absorption corrections as was mentioned in Section 5.1.2. Since the true absorption coefficient is almost certainly larger than the one used in this region, one would expect that the depicted scattering efficiencies at these and lower energies would be somewhat small. This would obviously improve the agreement with the solid curve in the 40 meV region while not seriously affecting the result at longer wavelengths. This would, however, worsen the agreement with the dashed curve representing the complete set of intermediate states. One must conclude

from these remarks that the discrete states of the free exciton are the important intermediate states in the forbidden scattering at 77°K. It should be noted in this regard that in the present work any resonance effects at the higher excited states of the exciton, as well as the sharpness of the resonance at the n = 1 exciton state, will be somewhat muted by thermal effects.

The scattering efficiency of the polar modes was measured in a 40 meV region above the band gap. It was found that the scattering efficiency remained essentially constant throughout this region. A small monotonic decrease in the scattering cross section was noted but no distinctive features appeared.

5.3.2.2 Selection Rules

In GaSe, the E'(LO) phonon has symmetry components xx, yy, xy (Appendix B) and as has been shown the selection rules are well obeyed far from resonance. As resonance is approached, the allowed scattering decreases in observed intensity due to absorption and the "forbidden" diagonal zz scattering becomes predominant. This situation is very similar to that observed in CdS (Martin and Damen, 1971a) for the CdS E'(LO) mode. The E'(LO) mode in GaSe thus represents an example of the type of selection rule breakdown discussed in detail by Martin (1971 a and b)

The A_2'' (LO) phonon is an example of a completely forbidden phonon that becomes active when resonance is approached and q-dependent scattering predominates. Such a selection rule

breakdown has also been predicted by Martin (1971b) and has been observed previously (Anastassakis and Burstein, 1971; Williams and Porto, 1973) in other compounds. In the present case, however, the phonon observed propagates in a direction perpendicular to the scattering plane and thus crystal momentum conservation is also lacking. This facet of the scattering is very puzzling and at present the only plausible explanation known to the author is presented in the following subsection.

As was mentioned earlier the general behaviour of the scattering efficiency of the polar A_2'' (LO) and E'(LO) phonons in GaSe is very similar to that observed in CdS by Martin and Damen (1971a) for the E'(LO) mode. In CdS, however, the near degeneracy of the A-type and E-type vibrations (the wavenumber splitting of these modes is $\Delta\tilde{\nu} \approx 1.8$ cm^{-1} (Damen et al., 1970) makes the study of their individual behaviour difficult. The occurrence in CdS of phenomena similar to those observed here for the A_2'' and E' (LO) phonons cannot be ruled out on the basis of present experimental evidence. In particular, it is possible that near resonance the A phonon in CdS contributes to the observed scattering enhancement at 305 cm^{-1} (Martin and Damen, 1971a). If this were so, a high resolution RRE experiment on CdS would be desirable to see whether the non-conservation of momentum and apparent angular independence of the scattering is peculiar to GaSe alone or is a more general feature of RRS.

5.3.2.3 Direction Dependence

From the results of Section 4.2, in particular equation 4.25, it has been shown that the scattering efficiency for RRS by the Fröhlich interaction should be proportional to $|\vec{q}|^2$. Since $|\vec{q}| = |\vec{k}_i - \vec{k}_s|$, Martin thus predicted that scattering in the forward direction, where $|\vec{k}_i - \vec{k}_s|^2$ is relatively small, should go to zero. This prediction, however, is in clear disagreement with the present experimental observation of a nearly angularly independent scattering efficiency as was depicted in Figure 5.6 . While Figure 5.6 shows a slight enhancement in the backward scattering approximately 30 meV below the exciton, the magnitude of this effect is far smaller than would be predicted by a q-dependent scattering mechanism. One explanation which has been used to explain this deviation in the only other experiment of this type is that the scattering may be impurity induced (Colwell and Klein, 1970; Martin 1971b). This is not a likely cause here, though, since the scattering efficiency clearly peaks at the n = 1 free exciton and in addition the phonon linewidths are only about 3 cm^{-1} even in resonance. Colwell and Klein, on the other hand, observed a severe (25 cm^{-1}) broadening of the one-phonon line due to impurities.

The non-conservation of momentum in the scattering process discussed in the previous section and the lack of any angular dependence could be explained if some momentum breaking mechanism existed that was preferentially directed in the

crystal (Williams and Porto, 1973; Martin, 1974a). Such an extrinsic mechanism does exist in the present GaSe crystals and consists of the many stacking faults that occur along the z-axis of the crystal (Terhell and Lieth, 1972). These stacking faults serve to modify the crystalline periodicity in the z-direction and thus destroy the crystal momentum conservation in the z-direction. If this is the case, the angular dependence of the scattering will then be proportional to $|\vec{k}_i - \vec{k}_s + \Delta\vec{q}_z|^2$ (Martin, 1974a) and if Δq_z is large the scattering efficiency may become independent of angle. Thus, the existence of stacking faults can be used to explain non-conservation of momentum and an angularly independent scattering efficiency.

Unfortunately, while this explanation gives a plausible reason for the non-conservation of momentum in the z-direction, one is left with the rather disconcerting bump at 30 meV below the exciton in the backward-forward scattering ratio. The ostrich approach seems to be another possible alternative solution, for if the bump turned out to be artificial the above explanation predicting no angularly dependent scattering would hold. The fact though that the bump appears in both the A_2'' (LO) and E'(LO) cross-sections at the same energy suggests that the effect is a real one.

While several alternative effects have been examined to explain the bump in the backward-forward scattering ratio, all seem unsatisfactory at the present time. One conclusion

is untenable and that is that if the LO efficiency is solely Fröhlich enhanced and thus an intrinsic process, the scattering is q-dependent. This would require a monotonic increase in this ratio as the exciton is approached which does not experimentally occur. The conclusion which seems most plausible at the present time is that some extrinsic mechanism (such as the stacking faults) is destroying the q-dependent behaviour of the Fröhlich scattering. It is clear that this facet of the RRE in GaSe is still not completely understood and further work is indicated.

5.3.3 Non-Polar Phonons (A_1' 135 cm^{-1}, A_1' 308 cm^{-1}, E'(TO) 215 cm^{-1})

The observed antiresonant behaviour for the 135 cm^{-1} mode is qualitatively similar to that observed for non-polar modes (e.g. $E_2(1)$) in CdS (Ralston et al., 1970; Damen and Scott, 1971). Ralston et al. (1970) suggested that the observed minimum in the scattering cross section arose from the cancellation of resonant and non-resonant terms in the scattering tensor (see equation 2.10). They obtained a phenomenological form for the cross section of

$$\sigma \simeq \pm A \{ (\omega_g - \omega_s)^{\frac{1}{2}} - (\omega_g - \omega_\ell)^{\frac{1}{2}} \} + B \qquad (5.24)$$

where ω_g is the gap frequency, ω_ℓ is the laser frequency, ω_s is the scattered photon frequency and A and B are positive and negative constants.

Their expression for the cross-section was later modified

by Damen and Scott (1971) who neglected the phonon energy and obtained the phenomenological form

$$\sigma \simeq \left| \frac{A\,\omega_g^{\,2}}{(\omega_g - \omega_\ell)^2} + B \right|^2 \qquad (5.25)$$

where ω_g is the gap frequency, ω_ℓ is the laser frequency and A and B are positive or negative constants. Damen and Scott found that this expression gave a qualitative fit to the limited number of data points that were available for the $E_2(1)$ (43 cm^{-1}) mode of CdS. These relations, however, do not yield even qualitative agreement with the present results. The antiresonance in GaSe occurs much closer to the band edge and is much deeper than the antiresonances observed in CdS. As a result the expressions (5.24 and 5.25) give antiresonance minima that are much narrower than the observed dip. It is clear that an alternate mechanism will have to be found to explain the present observations. The A_1' 308 cm^{-1} mode has been observed to exhibit an almost identical behaviour to the 135 cm^{-1} mode and is not shown in the figure.

The behaviour of the cross section of the E'(TO) mode at 215 cm^{-1} is also shown in Figure 5.5. This mode shows a monotonically increasing scattering efficiency below the exciton rising to a peak at the n = 1 exciton level. The scattering here is interpreted as being due to the deformation potential. There is no observed antiresonance in the cross section but the behaviour of the mode at energies lower than approximately 80 meV from the exciton is unknown since the

phonon is not normally allowed in the Y(ZZ)X geometry. This phonon has also been seen to be markedly absent (especially in the γ-GaSe case) in allowed geometries at some frequencies far into the gap which indicates the possibility of deep lying antiresonances as havebeen observed for TO phonons in CdS (Damen and Scott, 1971). The lack of a source at energies less than 1.95 eV prohibits a search for such an antiresonance at the present time.

5.3.4 Second-Order Phonons (2E'(LO) 509 cm^{-1})

The two-LO phonon feature at 509 cm^{-1} can also be clearly observed in Figure 5.3. Detailed measurements of the cross section of this mode shows that the scattered efficiency is nearly identical to the 215 cm^{-1} TO mode and thus has not been displayed. Certain similarities with the CdS case can be noted. This involves the fact that only the 2E'(LO) combination appears and, although the peak is smeared out to a certain extent by anisotropy, the $2A_2''$ (LO) mode is clearly absent (although both modes are second-order allowed in this geometry). The relative intensity of the 2LO peak in GaSe is much weaker than that observed in CdS, and a large number of multiple phonon peaks has not been observed in GaSe (while CdS has had up to nine peaks reported (Leite, Scott and Damen, 1969a)). Without going into this subject in any detail, this supports the observation (Malm and Haering, 1970, 1971) that the number of such peaks observed in the multiple phonon RRE seems to increase not with the strength of the Fröhlich

coupling constant α, which is 0.7 in CdS and 0.54 in GaSe, but with a Franck-Condon coupling parameter S which is 2.3 for CdS and 0.17 for GaSe (Malm and Haering, 1970).

CHAPTER VI

CONCLUSION

6.1 Conclusion

The objective of this thesis was to examine the Resonant Raman effect in detail to ascertain the nature and behaviour of the intermediate electronic states responsible for the scattering process. With the advent of the tunable dye laser such an investigation became quite possible for certain compounds whose band gaps are within the tuning range of these lasers. Gallium selenide is one of these compounds and with the use of a Rhodamine 6G cw tunable dye laser, the Resonant Raman Spectrum of GaSe was obtained.

In order to completely understand the results, however, it was necessary to examine in detail the non-resonant Raman spectra of the gallium layer compounds GaS and GaSe. Spectra were taken on all three possible polytypes, β (as represented by GaS), ε (as represented by the large mixed crystals) and γ (as represented by the needles). It was possible to obtain the frequencies and symmetries of vibration of the Raman active phonons in these compounds, and as a result the behaviour of the phonon modes at the zone centre is believed to be well understood.

Conclusions to be drawn from the non-resonant work include the observation that the large plate crystals grown by the Bridgeman technique are predominantly (at least 95%) ε in character. It was shown that the ε and γ polytypes display

an LO-TO phonon splitting for the E' mode at 215 cm^{-1} thus establishing the polar nature of this compound. Finally, it was shown that the γ-polytype shows dispersive behaviour in the frequencies of the $A_1(2)$ and E(2) phonons, which in the ε-polytype correspond to the modes which turn out to be highly resonant. This angularly dispersive behaviour has been compared to the predictions of Loudon (1964) for anisotropic polar modes and the agreement is excellent.

This work did not find any evidence of "conjugate modes" as has been suggested elsewhere (Wieting and Verble, 1972; Hayek et al., 1973). It is suggested that if these conjugate modes do exist, their splittings from the Raman active modes which correspond to the "even" type of the β-polytype (i.e. the lower row of vibrations of Figures 2.6 and 2.7) are too small to experimentally resolve and in addition their intensities would be expected to be quite small.

The Resonant Raman spectrum of the ε-γ mixed crystals was obtained at 81 ± 1°K. The results are consistent with the observations of the non-resonant spectrum, and in addition the A_2'' (LO) phonon has been positively identified and placed at 247 cm^{-1}, corresponding to the $A_1(2)$ phonon of the γ-polytype. This result confirms the previous infrared measurements (Leung et al., 1966). This identification and observation of the resonant behaviour of the A_2''(LO) and E'(LO) modes of ε-GaSe is a further indication of the polar nature of this compound.

The scattering cross section for the polar longitudinal modes exhibits a definite maximum at the n = 1 free exciton energy level. This clearly identifies the exciton as the intermediate state in the scattering process. The wavelength dependence observed was in satisfactory agreement with the theory of Martin (1971b) provided the ground state of the exciton was treated as the sole intermediate state in the scattering process. The calculated scattering efficiency for intraband Fröhlich scattering then gave better agreement with the experimental data than with the inclusion of higher excited states and the continuum contribution.

In contradiction to the above theory, however, was the observation that the scattering for the polar phonons was independent of scattering angle for most of the region studied and that momentum conservation did not hold for the A_2'' (LO) phonon. The breakdown of momentum conservation and the angular independence were attributed to an extrinsic mechanism, thus providing no significant disagreement with the theory which applies, of course, to the intrinsic effect. The extrinsic mechanism which seems most plausible is the existence of stacking faults along the c-axis of the crystal (Terhell and Lieth, 1972) which will break the crystalline symmetry in the z-direction. A slight bump in the scattering cross section ratio for backward and forward scattering was observed for which no satisfactory explanation has been reached.

The non-polar A_1' Raman active phonons were observed to undergo a well defined antiresonance, analogous to that observed in CdS (Ralston et al., 1970; Damen and Scott, 1971). The present experimental wavelength dependence could not be reproduced by the empirical model (Ralston et al., 1970; Damen and Scott, 1971) used previously. Further work on antiresonance behaviour in polar semiconductors is indicated. Further work on second (and higher) order modes in these semiconductors is also necessary to fully understand the nature of the scattering and distinguish the RRE from resonant fluorescence (or "hot excitonic luminescence").

6.2 Suggestions for Further Work

It seems apparent at this time that this work has raised nearly as many new questions as it originally set out to answer. This is not unusual since there are many aspects of the Resonant Raman effect which continue to be poorly understood. There are several non-trivial experiments on the RRE in GaSe yet to be performed. GaSe fails in its promise to give clean cut answers to some of the crucial aspects of the theory of Martin, such as the q-dependence of the scattering, because, it appears, of an extrinsic mechanism, the stacking faults. These faults, however, only occur in ε-γ mixed crystals and if the resonant backward-forward scattering experiment could be performed on γ-needles, one would have a more conclusive test of the intrinsic mechanism. This however will be very difficult because of the usually triangular cross section of the needles thus inhibiting forward scattering in the necessary x or y directions ($\hat{\epsilon}_i$ must be parallel to the c-axis). Perhaps some needles could be obtained with a rectangular cross section in order to do this experiment.

The question of the antiresonant behaviour of the A_1' symmetry phonons has no positive theoretical explanation. If an antiresonant effect is occurring the relative magnitudes and signs of all the terms in equation 2.10 must be considered. This is not a problem solely isolated in GaSe but should be examined for the general first order RRE theory.

The treatment of the second (and higher order) modes visible in the Raman spectrum was ignored in this work. The cause of such multiple phonon scattering is currently open to speculation and it was felt that such an experimental study might lead somewhat far afield. The study of the symmetries, intensities, efficiencies and possible frequency deviations of these modes in polar semiconductors should be however a subject for a considerable amount of experimental work.

Further Resonant Raman work on pure and, more importantly, easily oriented compounds is needed to check the theory. Obvious candidates for further study with a widely tunable dye laser now under construction are CdS (pure crystals), ZnO, $BaTiO_3$, and the zinc-blende compounds such as ZnS and ZnSe. ZnO is a very appealing compound since the energy separation between the A(LO) and E(LO) modes is larger than in GaSe and as a crystal to study for anisotropic effects, the splitting between the A symmetry and E symmetry modes is easily resolvable. This would be an interesting crystal to compare with CdS and GaSe.

Finally, a more remote possibility is the practical application of the Resonant Raman effect to excite Raman spectra at medium energy (1 to 4 eV) higher excited states of semimetals or semiconductors with narrow band gaps. In these compounds absorption (and/or high surface reflection) often makes recording of the normal one-phonon Raman spectrum difficult. The use of light which is resonant with electronic

transitions of the crystal might provide a way of obtaining phonon frequencies which would otherwise be difficult or impossible to obtain.

APPENDIX A
GROUP THEORY FOR LAYER COMPOUNDS

The number and symmetry of the normal modes of vibration of a crystal are easily found from the group theoretical knowledge of the space group of the crystal. In this appendix, the correlation method (Fateley et al., 1971) will be used to derive the symmetry properties of the crystal at the zone centre, Γ. In Section 2.4, it was stated that the symmetry of the zone at this point is just the point group of the space group. In the following three sections results will be derived for the β, ε, and γ polytypes.

A.1 β-polytype, D_{6h}^4 (P6/mmm) (Gallium Sulphide)

The notation of this Appendix will follow that of Fateley (1971) and thus some definitions are necessary. First, it is necessary to know the number of molecules per Bravais space cell, Z^B, which is equal to the number of molecules in the crystallographic unit cell, Z, divided by the number of lattice points in the unit cell, LP:

$$Z^B = Z/LP \qquad (A.1)$$

Since not all atoms lie on the same symmetry sites in the lattice, one must know (or figure out) the site group species, ν. Each species will have zero, one, two, or three

degrees of translational freedom, t^ν , and zero, one, two, or three degrees of rotational freedom, R^ν . In crystals only the degrees of translational freedom need be considered and thus for each site species one has the number of degrees of translational freedom of:

$$f^\nu = t^\nu \cdot n \qquad (A.2)$$

where n is the number of atoms in an equivalent set in the Bravais cell.

C^ξ is defined as the degeneracy of the species ξ of the factor group (which may not be the same as the site group). This is the dimensionality of the representation of the vibration, which is one for species of symmetry A or B, two for species E and three for species F.

The irreducible representation of the crystal vibrations is the sum of the irreducible representations of each equivalent set of constituent atoms:

$$\Gamma_{crystal} = \sum_\nu \Gamma_\nu \qquad (A.3)$$

where

$$\Gamma_\nu = \sum_\xi a_\xi \cdot \xi \qquad (A.4)$$

and a_ξ is the number of lattice vibrations of the symmetry ξ of the factor group.

It is easier to show how the method works by example. For β-GaS (D_{6h}^4 space group), one needs to know the site symmetry of the Ga and S atoms. From Wykoff (1965) and the International Tables of X-Ray Crystallography (1969), the site symmetries are identified as C_{3v}(3m) with atoms at:

$$u = \{\tfrac{1}{3},\tfrac{2}{3},z;\ \tfrac{2}{3},\tfrac{1}{3},\bar{z};\ \tfrac{2}{3},\tfrac{1}{3},\tfrac{1}{2}+z;\ \tfrac{1}{3},\tfrac{2}{3},\tfrac{1}{2}-z\} \qquad (A.5)$$

where z = 0.17 for the Ga atoms and 0.60 for the S atoms (Wykoff, 1965). Thus, C_{3v} is the site group for both the Gallium and Sulphur atoms. One has:

$$Z = 4 \text{ molecules} \qquad LP = 1 \qquad z^B = 4 \qquad (A.6)$$

and since there are four molecules per equivalent set:

$$f^\nu = 4 \cdot t^\nu = a_\nu \sum_\xi {}^\nu C_\xi \qquad (A.7)$$

where a_ν is the number of vibrations of the site group species ν and ${}^\nu C_\xi$ is the degeneracy of the species ξ of the factor group which correlates (i.e. is compatible) with the site species ν.

The groups C_{3v} and D_{6h} have their elements listed in Table A.1. The site group C_{3v} has symmetry characters A_1, A_2, and E with:

ν	t	t^ν	f^ν
A_1	T_z	1	4
A_2	-	0	0
E	T_x, T_y	2	8

(A.8)

From the correlation tables of Wilson, Decius and Cross (1955), one finds that the symmetries of these vibrations of C_{3v} are compatible with the symmetries of the D_{6h} factor group as follows:

f^{ν}	ν	$C_{3v} \rightarrow D_{6h}$	ξ	C_ξ	a_ξ	=	a_A	+	a_E
4	A_1	→	A_{1g}	1	1	=	1	+	0
		→	B_{2g}	1	1	=	1	+	0
		→	A_{2u}	1	1	=	1	+	0
		→	B_{1u}	1	1	=	1	+	0
8	E	→	E_{1g}	2	1	=	0	+	1
		→	E_{2g}	2	1	=	0	+	1
		→	E_{1u}	2	1	=	0	+	1
		→	E_{2u}	2	1	=	0	+	1

(A.9)

Thus,

$$\Gamma_{Ga} = A_{1g} \oplus B_{2g} \oplus A_{2u} \oplus B_{1u} \oplus E_{1g} \oplus E_{2g} \oplus E_{1u} \oplus E_{2u} \qquad \text{(A.10)}$$

Since the sulphur atoms lie on the same symmetry sites, the crystal representation is just this doubled:

$$\Gamma_{crystal} = 2A_{1g} \oplus 2B_{2g} \oplus 2A_{2u} \oplus 2B_{1u} \oplus 2E_{1g} \oplus 2E_{2g} \oplus 2E_{1u} \oplus 2E_{2u} \qquad \text{(A.11)}$$

This gives 24 normal modes of vibration (remember that E is a doubly degenerate representation). Of these modes, the point group has A_{2u} and E_{1u} as translational symmetry representations and thus,

$$\Gamma_{acoustic} = 1A_{2u} \oplus 1E_{1u} \qquad \text{(A.12)}$$

The representations below have bilinear basis functions (Tinkham, 1964) and since the polarizability tensor transforms as these basis functions, they give the normally Raman active phonons:

species	basis functions
A_{1g}	$x^2 + y^2, z^2$
E_{1g}	xz, yz
E_{2g}	$x^2 - y^2, xy$

(A.13)

There are six Raman active modes in the β-polytype with the above symmetry elements. In infrared absorption one should see two modes corresponding to $1A_{2u} \oplus 1E_{1u}$.

A.2 ε-polytype, D_{3h}^1 ($P\bar{6}m2$) (ε-GaSe)

Now that the method has been shown the calculation is only sketched below. The crystal structure of the ε-polytype was identified as a D_{3h}^1 space group (Schubert et al., 1955) with the two Ga atoms on (g) sites (C_{3v} or 3m site group) with:

$$u_{Ga} = \{ 0,0,z; 0,0,\bar{z} \} \qquad \text{(A.14a)}$$

and the two Se atoms on (i) sites of the convention of the International Tables (1969) (again a C_{3v} site group symmetry), with:

$$u_{Se} = \{ \tfrac{2}{3},\tfrac{1}{3},z; \tfrac{2}{3},\tfrac{1}{3},\bar{z} \} \qquad \text{(A.14b)}$$

where for the Ga atoms z = 0.075 and for the Se atoms z = 0.150 (Wykoff, 1965). Thus, again the site symmetries for each species of atoms is a C_{3v}. The site species and degrees of freedom for the site group must correspond to the D_{3h} factor group as follows (Wilson, Decius and Cross, 1955):

f^{ν}	ν $C_{3v} \rightarrow D_{3h}$	ξ	C_ξ	a_ξ	=	a_A	+	a_E
4	A_1	A_1'	1	2	=	2	+	0
		A_2''	1	2	=	2	+	0
8	E	E'	2	2	=	0	+	2
		E''	2	2	=	0	+	2

(A.15)

so that

$$\Gamma_{Ga} = 2A_1' \oplus 2A_2'' \oplus 2E' \oplus 2E'' \qquad (A.16)$$

and since the selenium atoms are on the same symmetry sites, one doubles this to get the crystal representation:

$$\Gamma_{crystal} = 4A_1' \oplus 4A_2'' \oplus 4E' \oplus 4E'' \qquad (A.17)$$

Of these:

$$\Gamma_{acoustic} = 1A_2'' \oplus 1E' \qquad (A.18)$$

The bilinear basis functions are (Tinkham, 1964):

species	basis functions
A_1'	$x^2 + y^2$, z^2
E'	$x^2 - y^2$, xy
E''	xz, yz

(A.19)

Thus, in the ε-polytype eleven distinct modes are Raman active (one E' mode is acoustic and all E modes are two dimensional):

$$\Gamma_{Raman} = 4A_1' \oplus 3E' \oplus 4E'' \qquad (A.20)$$

In the infrared one has $3A_2'' \oplus 3E'$ active and thus the three E' modes are both Raman and IR active, i.e. polar modes.

A.3 γ-polytype, C_{3v}^5 (R3m) (γ-GaSe)

Schubert et al. (1955) identified the γ-polytype as a C_{3v}^5 (R3m) space group with six Ga atoms on 3 (a) sites (C_{3v} site group species) (International Tables, 1969):

$$u = \{ 0,0,z \} \quad (3 \text{ sites}) \tag{A.21a}$$

where $z = \pm 0.050$ and the six Se atoms are on 3 (a) sites (C_{3v} site group species) with:

$$u = \{ 0,0,z \} \quad (3 \text{ sites}) \tag{A.21b}$$

where $z = \frac{2}{3} \pm 0.100$.

Again the site symmetries are C_{3v} and since the site group is isomorphic to the factor group of this polytype, the reduction is simple. There are now six atoms of Ga and six of Se per unit cell. Thus:

ν	f^ν
A_1	6
E	12

(A.22)

and since the correlation table is trivial, one can write down the crystal representation as twice each site representation:

$$\Gamma_{crystal} = 12A_1 \oplus 12E \tag{A.23}$$

Of these one has:

$$\Gamma_{acoustic} = 1A_1 \oplus 1E$$

and the basis functions are:

species	basis functions
A_1	$x^2 + y^2, z^2$
E	$x^2 - y^2, xy, xz, yz$

(A.24)

All twenty-two optical modes are both Raman and IR active.

TABLE A.1
CHARACTER TABLES

C_{3v} (3m)			E	$2C_3$	$3\sigma_v$
$(x^2 + y^2, z^2)$	z	A_1	1	1	1
	R_z	A_2	1	1	-1
$(x^2 - y^2, xy)$ (xz, yz)	(x,y) (R_x,R_y)	E	2	-1	0

D_{3h} ($\bar{6}$m2)			E	σ_h	$2C_3$	$2S_3$	$3C_2'$	$3\sigma_v$
(x^2+y^2,z^2)		A_1'	1	1	1	1	1	1
	R_z	A_2'	1	1	1	1	-1	-1
		A_1''	1	-1	1	-1	1	-1
	z	A_2''	1	-1	1	-1	-1	1
(x^2-y^2,xy)	(x,y)	E'	2	2	-1	-1	0	0
(xz,yz)	(R_x,R_y)	E''	2	-2	-1	1	0	0

TABLE A.1 (CONT.)

D_{6h} (6/mmm)			E	C_2	$2C_3$	$2C_6$	$3C_2'$	$3C_2''$	I	σ_h	$2S_6$	$2S_3$	$3\sigma_v$	$3\sigma_d$
(x^2+y^2, z^2)		A_{1g}	1	1	1	1	1	1	1	1	1	1	1	1
		A_{2g}	1	1	1	1	-1	-1	1	1	1	1	-1	-1
		B_{1g}	1	-1	1	-1	1	-1	1	-1	1	-1	1	-1
		B_{2g}	1	-1	1	-1	-1	1	1	-1	1	-1	-1	1
(xz, yz)		E_{1g}	2	-2	-1	1	0	0	2	-2	-1	1	0	0
(x^2-y^2, xy)		E_{2g}	2	2	-1	-1	0	0	2	2	-1	-1	0	0
		A_{1u}	1	1	1	1	1	1	-1	-1	-1	-1	-1	-1
	R_z, z	A_{2u}	1	1	1	1	-1	-1	-1	-1	-1	-1	1	1
		B_{1u}	1	-1	1	-1	1	-1	-1	1	-1	1	-1	1
		B_{2u}	1	-1	1	-1	-1	1	-1	1	-1	1	1	-1
	(x,y) (R_x, R_y)	E_{1u}	2	-2	-1	1	0	0	-2	2	1	-1	0	0
		E_{2u}	2	2	-1	-1	0	0	-2	-2	1	1	0	0

APPENDIX B
SELECTION RULES FOR RAMAN SCATTERING

In Appendix A, the normal selection rules for non-polar optical phonons in the three polytypes were derived from the inspection of the basis functions of the point groups D_{6h}, D_{3h}, and C_{3v}. It is possible to get this derivation from equation 2.30 as well by using the Raman tensors given by Loudon (1964). This is not necessary to do since for the non-polar phonons the results are identical. It will suffice in this section to derive the selection rules for the polar phonons according to equation 2.31.

B.1 β-polytype (GaS)

There are no polar phonons in the β-polytype since this crystal structure is centrosymmetric. The symmetries of the Raman active phonons are just those derived in Appendix A, that is:

$$\Gamma_{Raman} = 2A_{1g} \oplus 2E_{1g} \oplus 2E_{2g}$$

with

Irred. Rep.	Polarizability Tensor
A_{1g}	$\alpha_{xx} + \alpha_{yy}$, α_{zz}
E_{1g}	α_{yz}, α_{zx}
E_{2g}	$\alpha_{xx} - \alpha_{yy}$, α_{xy}

B.2 ε-polytype (ε-GaSe)

In the ε-polytype only the modes E′ are both Raman and infrared active. The Raman tensors for the phonons are (Loudon, 1964):

A_1'

$$\begin{pmatrix} a & 0 & 0 \\ 0 & a & 0 \\ 0 & 0 & b \end{pmatrix}$$

E″

$$\begin{pmatrix} 0 & 0 & 0 \\ 0 & 0 & c \\ 0 & c & 0 \end{pmatrix}$$

E″

$$\begin{pmatrix} 0 & 0 & -c \\ 0 & 0 & 0 \\ -c & 0 & 0 \end{pmatrix}$$

E′(x)

$$\begin{pmatrix} 0 & d & 0 \\ d & 0 & 0 \\ 0 & 0 & 0 \end{pmatrix}$$

E′(y)

$$\begin{pmatrix} d & 0 & 0 \\ 0 & -d & 0 \\ 0 & 0 & 0 \end{pmatrix}$$

For convenience, in the following equations these tensors will be labelled by the Roman numerals I through V, respectively.

The following nine geometries will be examined for Case I of Loudon's work only (the electrostatic limit):

(1) Backscattering or forward scattering x-face

(2) Backscattering or forward scattering y-face

(3) Backscattering or forward scattering z-face

(4) Right angle scattering X( )Y

(5) Right angle scattering Y( )X

(6) Right angle scattering Y( )Z

(7) Right angle scattering X( )Z

(8) Right angle scattering Z( )Y

(9) Right angle scattering Z( )X

It will be noted that Loudon's Cases I and II (the electro-

static and anisotropic limits) will give different selection rules only when the phonon propagates at an angle with respect to the c-axis of the crystal which is not zero or ninety degrees. This will occur for geometries 6-9 above. In Case I, the phonon is taken to be primarily longitudinal or transverse. For Case II, the phonon polarization will be either parallel or perpendicular to the c-axis. For GaSe, the phonon behaviour near the zone centre more closely obeys Case I as is seen by the relative phonon energy spacings of the polar modes. Thus only Case I will be considered here. The extension to Case II is straightforward.

(1) $X(\ )\bar{X}$

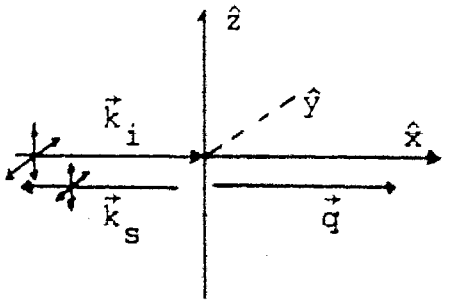

$$e_i^{\sigma} = (0 \; e_y \; e_z)$$

$$e_s^{\rho} = \begin{pmatrix} 0 \\ 1 \\ 0 \end{pmatrix}_{\perp} \text{ or } \begin{pmatrix} 0 \\ 0 \\ 1 \end{pmatrix}_{\parallel}$$

(a) For LO phonon $\hat{\xi}^T = \hat{x} = R^T$

$$S_{\parallel} = \left[(0 \quad e_y \; e_z)(\alpha + \beta) \; \underline{\underline{IV}} \begin{pmatrix} 0 \\ 0 \\ 1 \end{pmatrix} \right]^2 = 0$$

$$S_{\perp} = \left[(0 \quad e_y \; e_z)(\alpha + \beta) \; \underline{\underline{IV}} \begin{pmatrix} 0 \\ 1 \\ 0 \end{pmatrix} \right]^2 = 0$$

(b) For TO extraordinary phonon, one has $\hat{\xi}^T = \hat{z}$ and this must give zero contribution since A_2'' is inactive.

(c) For TO ordinary phonon $\hat{\xi}^T = \hat{y}$; $\beta = 0$ and thus,

$$S_{\parallel} = \left[(0\ e_y\ e_z)\ \alpha\ \underline{\underline{V}} \begin{pmatrix} 0 \\ 0 \\ 1 \end{pmatrix} \right]^2 = 0$$

$$S_{\perp} = \left[(0\ e_y\ e_z)\ \alpha\ \underline{\underline{V}} \begin{pmatrix} 0 \\ 1 \\ 0 \end{pmatrix} \right]^2 = e_y^2 \alpha^2 d^2 \quad X(YY)\overline{X}$$

(2) $Y(\ )\overline{Y}$

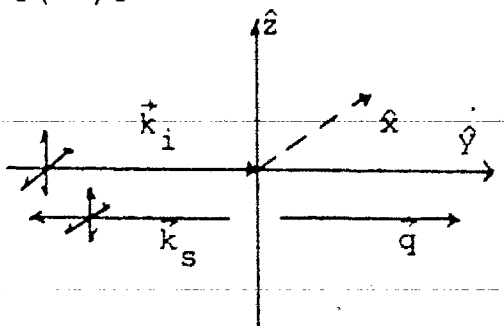

$$e_i^{\sigma} = (e_x\ 0\ e_z)$$

$$e_s^{\rho} = \begin{pmatrix} 1 \\ 0 \\ 0 \end{pmatrix} \text{ or } \begin{pmatrix} 0 \\ 0 \\ 1 \end{pmatrix}_{\parallel}$$

(a) LO phonon $\hat{\xi}^{\tau} = \hat{k}^{\tau} = \hat{y}$

$$S_{\parallel} = \left[(e_x\ 0\ e_z)(\alpha + \beta)\ \underline{\underline{V}} \begin{pmatrix} 0 \\ 0 \\ 1 \end{pmatrix} \right]^2 = 0$$

$$S_{\perp} = \left[(e_x\ 0\ e_z)(\alpha + \beta)\ \underline{\underline{V}} \begin{pmatrix} 1 \\ 0 \\ 0 \end{pmatrix} \right]^2 = e_x^2 (\alpha+\beta)^2 d^2$$
$$Y(XX)\overline{Y}$$

(b) For TO extraordinary phonon $\hat{\xi}^{\tau} = \hat{z}$ which is not allowed.

(c) TO ordinary phonon $\hat{\xi}^{\tau} = \hat{x}$, and

$$S_{\parallel} = \left[(e_x\ 0\ e_z)\ \alpha\ \underline{\underline{IV}} \begin{pmatrix} 0 \\ 0 \\ 1 \end{pmatrix} \right]^2 = 0$$

$$S_{\perp} = \left[(e_x\ 0\ e_z)\ \alpha\ \underline{\underline{IV}} \begin{pmatrix} 1 \\ 0 \\ 0 \end{pmatrix} \right]^2 = 0$$

(3) $Z(\ )\overline{Z}$

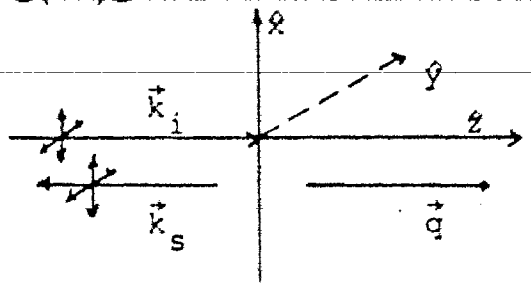

$$e_i^{\sigma} = (e_x\ e_y\ 0)$$

$$e_s^{\rho} = \begin{pmatrix} 1 \\ 0 \\ 0 \end{pmatrix}_{\parallel} \text{or} \begin{pmatrix} 0 \\ 1 \\ 0 \end{pmatrix}_{\perp}$$

(a) LO phonon $\hat{\xi}^T = \hat{k}^T = \hat{z}$, and again since A_2'' is inactive this phonon polarization gives no contribution.

(b) Two ordinary degenerate TO phonons, $\hat{\xi}^T = \hat{x}$ or $\hat{y}$. In this case, the scattered efficiencies are added (Loudon, 1964):

$$S_{\parallel} = \left[(e_x\ e_y\ 0)\ \alpha\ \underline{\underline{IV}} \begin{pmatrix}1\\0\\0\end{pmatrix}\right]^2 + \left[(e_x\ e_y\ 0)\ \alpha\ \underline{\underline{V}} \begin{pmatrix}1\\0\\0\end{pmatrix}\right]^2 = e_y^2\alpha^2d^2 + e_x^2\alpha^2d^2$$

$$Z(YX)\bar{Z},\ Z(XX)\bar{Z}$$

$$S_{\perp} = \left[(e_x\ e_y\ 0)\ \alpha\ \underline{\underline{IV}} \begin{pmatrix}0\\1\\0\end{pmatrix}\right]^2 + \left[(e_x\ e_y\ 0)\ \alpha\ \underline{\underline{V}} \begin{pmatrix}0\\1\\0\end{pmatrix}\right]^2 = e_x^2\alpha^2d^2 + e_y^2\alpha^2d^2$$

$$Z(XY)\bar{Z},\ Z(YY)\bar{Z}$$

(4) X( )Y

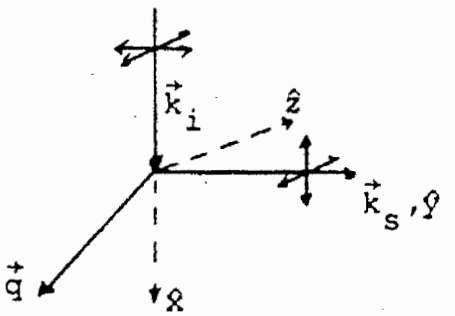

$$e_i^{\sigma} = (0\ e_y\ e_z)$$

$$e_s^{\rho} = \begin{pmatrix}1\\0\\0\end{pmatrix}_{\parallel} \text{ or } \begin{pmatrix}0\\0\\1\end{pmatrix}_{\perp}$$

(a) LO phonon $\hat{\xi}^T = \hat{k}^T = \frac{\sqrt{2}}{2}(\hat{x} - \hat{y})$

$$S_{\parallel} = \tfrac{1}{2}\left[(0\ e_y\ e_z)\ (\alpha + \beta)\ \underline{(IV - V)} \begin{pmatrix}1\\0\\0\end{pmatrix}\right]^2$$

$$= \tfrac{1}{2} e_y^2(\alpha + \beta)^2d^2 \qquad X(YX)Y$$

$$S_{\perp} = \tfrac{1}{2}\left[(0\ e_y\ e_z)\ (\alpha + \beta)\ \underline{(IV - V)} \begin{pmatrix}0\\0\\1\end{pmatrix}\right]^2 = 0$$

(b) TO extraordinary phonon $\hat{\xi}^{\tau} = \hat{z}$ and is not allowed.

(c) TO ordinary phonon $\hat{\xi}^{\tau} = \frac{\sqrt{2}}{2}(\hat{x} + \hat{y})$

$$S_{\parallel} = \tfrac{1}{2}\left[(0\ e_y\ e_z)\alpha\ \underline{(IV + V)}\begin{pmatrix}1\\0\\0\end{pmatrix}\right]^2$$

$$= \tfrac{1}{2}\, e_y^{\,2}\alpha^2 d^2 \qquad X(YX)Y$$

$$S_{\perp} = 0 \quad \text{(see 4(a) above)}$$

(5) Y( )X

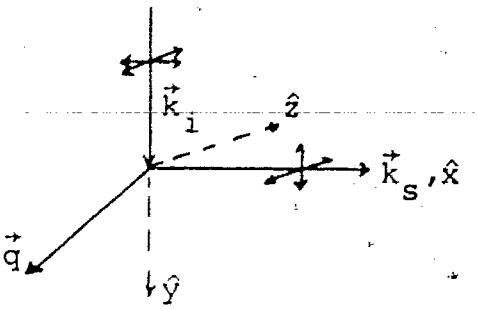

$$e_i^{\sigma} = (e_x\ 0\ e_z)$$

$$e_s^{\rho} = \begin{pmatrix}0\\1\\0\end{pmatrix}_{\parallel} \text{ or } \begin{pmatrix}0\\0\\1\end{pmatrix}_{\perp}$$

(a) LO phonon $\hat{\xi}^{\tau} = \hat{k}^{\tau} = \frac{\sqrt{2}}{2}(\hat{y} - \hat{x})$

$$S_{\parallel} = \tfrac{1}{2}\left[(e_x\ 0\ e_z)(\alpha + \beta)\underline{(V - IV)}\begin{pmatrix}0\\1\\0\end{pmatrix}\right]^2$$

$$= \tfrac{1}{2}(\alpha + \beta)^2 d^2 e_x^{\,2} \qquad Y(XY)X$$

$$S_{\perp} = \tfrac{1}{2}\left[(e_x\ 0\ e_z)(\alpha + \beta)\underline{(V - IV)}\begin{pmatrix}0\\0\\1\end{pmatrix}\right]^2 = 0$$

(b) TO extraordinary phonon $\hat{\xi}^{\tau} = \hat{z}$ and is not allowed.

(c) TO ordinary phonon $\hat{\xi}^{\tau} = \frac{\sqrt{2}}{2}(\hat{x} + \hat{y})$

$$S_{\parallel} = \tfrac{1}{2}\left[(e_x\ 0\ e_z)\ \alpha\underline{(IV + V)}\begin{pmatrix}0\\1\\0\end{pmatrix}\right]^2 = \tfrac{1}{2}\, e_x^{\,2}\alpha^2 d^2$$

$Y(XY)X$

$$S_{\perp} = 0 \quad \text{(see 5(a) above)}$$

(6) Y( )Z

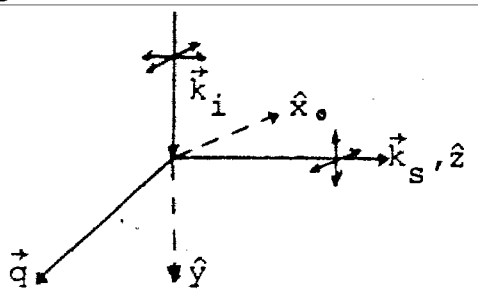

$$e_i^{\sigma} = (e_x\ 0\ e_z)$$

$$e_s^{\rho} = \begin{pmatrix}1\\0\\0\end{pmatrix}_{\perp} \text{ or } \begin{pmatrix}0\\1\\0\end{pmatrix}_{\parallel}$$

(a) LO phonon $\hat{\xi}^{\tau} = \hat{k}^{\tau} = \frac{\sqrt{2}}{2}(\hat{y} - \hat{z})$. Now in this geometry and those to follow, the z component of the phonon polarization can be neglected since the A_2'' phonon is inactive, thus,

$$S_{\parallel} = \tfrac{1}{2}\left[(e_x\ 0\ e_z)(\alpha + \beta)\ \underline{\underline{V}}\begin{pmatrix}0\\1\\0\end{pmatrix}\right]^2 = 0$$

$$S_{\perp} = \tfrac{1}{2}\left[(e_x\ 0\ e_z)(\alpha + \beta)\ \underline{\underline{V}}\begin{pmatrix}1\\0\\0\end{pmatrix}\right]^2 = \tfrac{1}{2}\, e_x^2(\alpha+\beta)^2 d^2 \qquad Y(XX)Z$$

(b) TO extraordinary phonon $\hat{\xi}^{\tau} = \frac{\sqrt{2}}{2}(\hat{y} + \hat{z})$. As can be easily verified the selection rules are the same as for the LO phonon, that is $S_{\parallel} = 0$; $S_{\perp} = \tfrac{1}{2}\, e_x^2\alpha^2 d^2$ (Y(XX)Z).

(c) TO ordinary phonon $\hat{\xi}^{\tau} = \hat{x}$ and

$$S_{\parallel} = \left[(e_x\ 0\ e_z)\ \alpha\ \underline{\underline{IV}}\begin{pmatrix}0\\1\\0\end{pmatrix}\right]^2 = e_x^2\alpha^2 d^2 \qquad Y(XY)Z$$

$$S_{\perp} = \left[(e_x\ 0\ e_z)\ \alpha\ \underline{\underline{IV}}\begin{pmatrix}1\\0\\0\end{pmatrix}\right]^2 = 0$$

(7) X( )Z

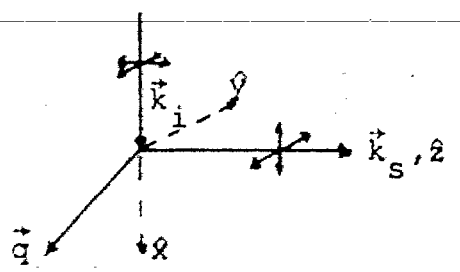

$$e_i^{\sigma} = (0\ e_y\ e_z)$$

$$e_s^{\rho} = \begin{pmatrix}1\\0\\0\end{pmatrix}_{\parallel} \text{ or } \begin{pmatrix}0\\1\\0\end{pmatrix}_{\perp}$$

(a) LO phonon $\hat{\xi}^\tau = \hat{k}^\tau = \frac{\sqrt{2}}{2}(\hat{x} - \hat{z})$

$$S_{\parallel} = \tfrac{1}{2}\left[(0\ e_y\ e_z)(\alpha+\beta)\ \underline{\underline{IV}}\begin{pmatrix}1\\0\\0\end{pmatrix}\right]^2 = \tfrac{1}{2}\,e_y^{\,2}(\alpha+\beta)^2d^2 \qquad X(YX)Z$$

$$S_{\perp} = \tfrac{1}{2}\left[(0\ e_y\ e_z)(\alpha+\beta)\ \underline{\underline{IV}}\begin{pmatrix}0\\1\\0\end{pmatrix}\right]^2 = 0$$

(b) TO extraordinary phonon $\hat{\xi}^\tau = \frac{\sqrt{2}}{2}(\hat{x} + \hat{z})$ which gives the same result as that for the LO phonon except $S_{\parallel} = \tfrac{1}{2}e_y^{\,2}\alpha^2d^2$ (X(YX)Z).

(c) TO ordinary phonon $\hat{\xi}^\tau = \hat{y}$

$$S_{\parallel} = \left[(0\ e_y\ e_z)\ \alpha\ \underline{\underline{V}}\begin{pmatrix}1\\0\\0\end{pmatrix}\right]^2 = 0$$

$$S_{\perp} = \left[(0\ e_y\ e_z)\ \alpha\ \underline{\underline{V}}\begin{pmatrix}0\\1\\0\end{pmatrix}\right]^2 = e_y^{\,2}\alpha^2d^2 \qquad X(YY)Z$$

(8) Z( )Y

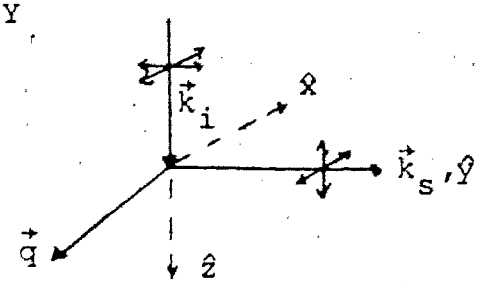

$$e_i^{\sigma} = (e_x\ e_y\ 0)$$

$$e_s^{\rho} = \begin{pmatrix}0\\0\\1\end{pmatrix}_{\parallel} \text{ or } \begin{pmatrix}1\\0\\0\end{pmatrix}_{\perp}$$

(a) LO phonon $\hat{\xi}^\tau = \hat{k}^\tau = \frac{\sqrt{2}}{2}(\hat{z} - \hat{y})$

$$S_{\parallel} = \tfrac{1}{2}\left[(e_x\ e_y\ 0)(\alpha+\beta)\ \underline{\underline{V}}\begin{pmatrix}0\\0\\1\end{pmatrix}\right]^2 = 0$$

$$S_{\perp} = \tfrac{1}{2}\left[(e_x\ e_y\ 0)(\alpha+\beta)\ \underline{\underline{V}}\begin{pmatrix}1\\0\\0\end{pmatrix}\right]^2 = \tfrac{1}{2}\,e_x^{\,2}(\alpha+\beta)^2d^2 \qquad Z(XX)Y$$

(b) TO extraordinary phonon $\hat{\xi}^\tau = \frac{\sqrt{2}}{2}(\hat{z} + \hat{y})$ which gives the same result as (a) except $S_{\perp} = \tfrac{1}{2}\,e_x^{\,2}\alpha^2d^2$ (Z(XX)Y).

(c) TO ordinary phonon $\hat{\xi}^{\tau} = \hat{x}$ and

$$S_{\parallel} = \left[(e_x \; e_y \; 0) \; \alpha \; \underline{\underline{IV}} \begin{pmatrix} 0 \\ 0 \\ 1 \end{pmatrix} \right]^2 = 0$$

$$S_{\perp} = \left[(e_x \; e_y \; 0) \; \alpha \; \underline{\underline{IV}} \begin{pmatrix} 1 \\ 0 \\ 0 \end{pmatrix} \right]^2 = e_y^{\,2} \alpha^2 d^2 \quad Z(YX)Y$$

(9) Z( )X

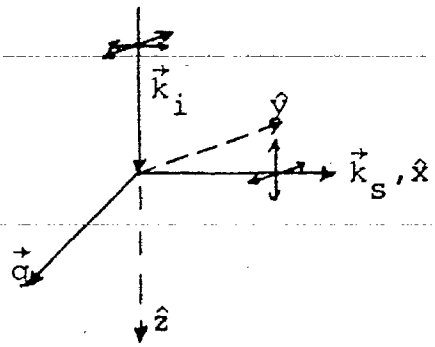

$$e_i^{\sigma} = (e_x \; e_y \; 0)$$

$$e_s^{\rho} = \begin{pmatrix} 0 \\ 0 \\ 1 \end{pmatrix}_{\parallel} \text{ or } \begin{pmatrix} 0 \\ 1 \\ 0 \end{pmatrix}_{\perp}$$

(a) LO phonon $\hat{\xi}^{\tau} = \hat{k} = \frac{\sqrt{2}}{2} (\hat{z} - \hat{x})$

$$S_{\parallel} = \tfrac{1}{2} \left[(e_x \; e_y \; 0)(\alpha + \beta) \; \underline{\underline{IV}} \begin{pmatrix} 0 \\ 0 \\ 1 \end{pmatrix} \right]^2 = 0$$

$$S_{\perp} = \tfrac{1}{2} \left[(e_x \; e_y \; 0)(\alpha + \beta) \; \underline{\underline{IV}} \begin{pmatrix} 0 \\ 1 \\ 0 \end{pmatrix} \right]^2 = \tfrac{1}{2} \, e_x^{\,2} (\alpha+\beta)^2 d^2$$

(b) TO extraordinary phonon $\hat{\xi}^{\tau} = \frac{\sqrt{2}}{2} (\hat{z} + \hat{x})$ which gives the same result as (a) except $S_{\perp} = \tfrac{1}{2} \, e_x^{\,2} \alpha^2 d^2$ $\overset{Z(XY)X}{(Z(XY)X)}$.

(c) TO ordinary phonon $\hat{\xi}^{\tau} = \hat{y}$ and

$$S_{\parallel} = \left[(e_x \; e_y \; 0) \; \alpha \; \underline{\underline{V}} \begin{pmatrix} 0 \\ 0 \\ 1 \end{pmatrix} \right]^2 = 0$$

$$S_{\perp} = \left[(e_x \; e_y \; 0) \; \alpha \; \underline{\underline{V}} \begin{pmatrix} 0 \\ 1 \\ 0 \end{pmatrix} \right]^2 = e_y^{\,2} \alpha^2 d^2 \quad Z(YY)X$$

All of the above result for the ε-polytype are summarized in Table 2.2.

B.3 γ-polytype (γ-GaSe)

In the γ-polytype both the A_1 and E modes are both Raman and infrared active, and thus all modes must be considered to be polar. The Raman tensors for the C_{3v} point group are (Loudon, 1964):

$$\underline{\underline{R}}^{\tau}_{\sigma\rho} = \underset{A_1(z)}{\underset{\underline{\underline{I}}}{\begin{pmatrix} a & 0 & 0 \\ 0 & a & 0 \\ 0 & 0 & b \end{pmatrix}}} \quad \underset{E(y)}{\underset{\underline{\underline{II}}}{\begin{pmatrix} c & 0 & 0 \\ 0 & -c & d \\ 0 & d & 0 \end{pmatrix}}} \quad \underset{E(-x)}{\underset{\underline{\underline{III}}}{\begin{pmatrix} 0 & -c & -d \\ -c & 0 & 0 \\ -d & 0 & 0 \end{pmatrix}}}$$

The same nine geometries will be considered for this polytype and the reader should refer to the previous section for the geometries.

(1) $X(\ )\bar{X}$

(a) LO phonon $\hat{\xi}^{\tau} = \hat{k}^{\tau} = \hat{x}$

$$S_{\parallel} = \left[(0\ e_y\ e_z)(\alpha + \beta)\ \underline{\underline{III}} \begin{pmatrix} 0 \\ 0 \\ 1 \end{pmatrix}\right]^2 = 0$$

$$S_{\perp} = \left[(0\ e_y\ e_z)(\alpha \not{+} \beta)\ \underline{\underline{III}} \begin{pmatrix} 0 \\ 1 \\ 0 \end{pmatrix}\right]^2 = 0$$

(b) TO extraordinary phonon $\hat{\xi}^{\tau} = \hat{z}$

$$S_{\parallel} = \left[(0\ e_y\ e_z)\ \alpha\ \underline{\underline{I}} \begin{pmatrix} 0 \\ 0 \\ 1 \end{pmatrix}\right]^2 = e_z^2\alpha^2b^2 \qquad X(ZZ)\bar{X}$$

$$S_{\perp} = \left[(0\ e_y\ e_z)\ \alpha\ \underline{\underline{I}} \begin{pmatrix} 0 \\ 1 \\ 0 \end{pmatrix}\right]^2 = e_y^2\alpha^2a^2 \qquad X(YY)\bar{X}$$

(c) TO ordinary phonon $\hat{\xi}^{\tau} = \hat{y}$

$$S_{\parallel} = \left[(0\ e_y\ e_z)\ \alpha\ \underline{\underline{II}} \begin{pmatrix}0\\0\\1\end{pmatrix}\right]^2 = e_y^2\alpha^2d^2 \quad X(YZ)\overline{X}$$

$$S_{\perp} = \left[(0\ e_y\ e_z)\ \alpha\ \underline{\underline{II}} \begin{pmatrix}0\\1\\0\end{pmatrix}\right]^2 = (-e_y\alpha c + e_z\alpha d)^2$$
$$X(YY)\overline{X},\ X(ZY)\overline{X}$$

(2) $Y(\ )\overline{Y}$

(a) LO phonon $\hat{\xi}^T = \hat{k}^T = \hat{y}$

$$S_{\parallel} = \left[(e_x\ 0\ e_z)(\alpha + \beta)\ \underline{\underline{II}} \begin{pmatrix}0\\0\\1\end{pmatrix}\right]^2 = 0$$

$$S_{\perp} = \left[(e_x\ 0\ e_z)(\alpha + \beta)\ \underline{\underline{II}} \begin{pmatrix}1\\0\\0\end{pmatrix}\right]^2 = e_x^2(\alpha+\beta)^2c^2$$
$$Y(XX)\overline{Y}$$

(b) TO extraordinary phonon $\hat{\xi}^T = \hat{z}$

$$S_{\parallel} = \left[(e_x\ 0\ e_z)\ \alpha\ \underline{\underline{I}} \begin{pmatrix}0\\0\\1\end{pmatrix}\right]^2 = e_z^2\alpha^2b^2 \quad Y(ZZ)\overline{Y}$$

$$S_{\perp} = \left[(e_x\ 0\ e_z)\ \alpha\ \underline{\underline{I}} \begin{pmatrix}1\\0\\0\end{pmatrix}\right]^2 = e_x^2\alpha^2a^2 \quad Y(XX)\overline{Y}$$

(c) TO ordinary phonon $\hat{\xi}^T = \hat{x}$

$$S_{\parallel} = \left[(e_x\ 0\ e_z)\ \alpha\ \underline{\underline{III}} \begin{pmatrix}0\\0\\1\end{pmatrix}\right]^2 = e_x^2\alpha^2d^2 \quad Y(XZ)\overline{Y}$$

$$S_{\perp} = \left[(e_x\ 0\ e_z)\ \alpha\ \underline{\underline{III}} \begin{pmatrix}1\\0\\0\end{pmatrix}\right]^2 = e_z^2\alpha^2d^2 \quad Y(ZX)\overline{Y}$$

(3) $Z(\ )\overline{Z}$

(a) LO phonon $\hat{\xi}^T = \hat{k}^T = \hat{z}$

$$S_{\parallel} = \left[(e_x\ e_y\ 0)(\alpha + \beta)\ \underline{\underline{I}} \begin{pmatrix}1\\0\\0\end{pmatrix}\right]^2 = e_x^2(\alpha+\beta)^2a^2$$
$$Z(XX)\overline{Z}$$

$$S_{\perp} = \left[(e_x\ e_y\ 0)(\alpha + \beta)\ \underline{\underline{I}} \begin{pmatrix}0\\1\\0\end{pmatrix}\right]^2 = e_y^2(\alpha+\beta)^2a^2$$
$$Z(YY)\overline{Z}$$

(b) TO ordinary phonons (two-fold degenerate) $\hat{\xi}^T = \hat{x}$ or $\hat{y}$

$$S_{\parallel} = \left[(e_x\ e_y\ 0)\alpha\ \underline{\underline{II}} \begin{pmatrix}1\\0\\0\end{pmatrix}\right]^2 + \left[(e_x\ e_y\ 0)\ \alpha\ \underline{\underline{III}} \begin{pmatrix}1\\0\\0\end{pmatrix}\right]^2$$
$$= e_x^2\alpha^2c^2 + e_y^2\alpha^2c^2 \qquad Z(XX)\overline{Z},\ Z(YX)\overline{Z}$$

$$S_{\perp} = \left[(e_x\ e_y\ 0)\alpha\ \underline{\underline{II}} \begin{pmatrix}0\\1\\0\end{pmatrix}\right]^2 + \left[(e_x\ e_y\ 0)\ \alpha\ \underline{\underline{III}} \begin{pmatrix}0\\1\\0\end{pmatrix}\right]^2$$
$$= e_y^2\alpha^2c^2 + e_x^2\alpha^2c^2 \qquad Z(YY)\overline{Z},\ Z(XY)\overline{Z}$$

(4) X( )Y

(a) LO phonon $\hat{\xi}^T = \hat{k}^T = \frac{\sqrt{2}}{2}(\hat{x} - \hat{y})$

$$S_{\parallel} = \tfrac{1}{2}\left[(0\ e_y\ e_z)(\alpha + \beta)\underline{(III - II)}\begin{pmatrix}1\\0\\0\end{pmatrix}\right]^2$$
$$= \tfrac{1}{2}(e_yc + e_zd)^2(\alpha + \beta)^2 \qquad X(YX)Y,\ X(ZX)Y$$

$$S_{\perp} = \tfrac{1}{2}\left[(0\ e_y\ e_z)(\alpha + \beta)\underline{(III - II)}\begin{pmatrix}0\\0\\1\end{pmatrix}\right]^2$$
$$= \tfrac{1}{2}e_y^2(\alpha + \beta)^2d^2 \qquad X(YZ)Y$$

(b) TO ordinary phonon $\hat{\xi}^T = \frac{\sqrt{2}}{2}(\hat{x} + \hat{y})$. This will be the same as for (a) above except:

$$S_{\parallel} = \tfrac{1}{2}(e_yc + e_zd)\ \alpha^2d^2 \qquad X(YX)Y,\ X(ZX)Y$$

and $$S_{\perp} = \tfrac{1}{2}e_y^2\alpha^2d^2 \qquad X(YZ)Y$$

(c) TO extraordinary phonon $\hat{\xi}^T = \hat{z}$

$$S_{\parallel} = \left[(0\ e_y\ e_z)\ \alpha\ \underline{\underline{I}}\begin{pmatrix}1\\0\\0\end{pmatrix}\right]^2 = 0$$

$$S_{\perp} = \left[(0\ e_y\ e_z)\ \alpha\ \underline{\underline{I}} \begin{pmatrix} 0 \\ 0 \\ 1 \end{pmatrix} \right]^2 = e_z^2 \alpha^2 b^2 \quad X(ZZ)Y$$

(5) Y( )X

(a) LO phonon $\hat{\xi}^{\tau} = \hat{k}^{\tau} = \frac{\sqrt{2}}{2} (\hat{y} - \hat{x})$

$$S_{\parallel} = \tfrac{1}{2} \left[(e_x\ 0\ e_z)(\alpha + \beta)\underline{(II - III)} \begin{pmatrix} 0 \\ 1 \\ 0 \end{pmatrix} \right]^2$$

$$= \tfrac{1}{2}(-e_x c + e_z d)^2 (\alpha + \beta)^2 \quad Y(XY)X,\ Y(ZY)X$$

$$S_{\perp} = \tfrac{1}{2} \left[(e_x\ 0\ e_z)(\alpha + \beta)\underline{(II - III)} \begin{pmatrix} 0 \\ 0 \\ 1 \end{pmatrix} \right]^2$$

$$= \tfrac{1}{2} e_x^2 (\alpha + \beta)^2 d^2 \quad Y(XZ)X$$

(b) TO extraordinary phonon $\hat{\xi}^{\tau} = \hat{z}$

$$S_{\parallel} = \left[(e_x\ 0\ e_z)\ \alpha\ \underline{\underline{I}} \begin{pmatrix} 0 \\ 1 \\ 0 \end{pmatrix} \right]^2 = 0$$

$$S_{\perp} = \left[(e_x\ 0\ e_z)\ \alpha\ \underline{\underline{I}} \begin{pmatrix} 0 \\ 0 \\ 1 \end{pmatrix} \right]^2 = e_z^2 \alpha^2 b^2 \quad Y(ZZ)X$$

(c) TO ordinary phonon $\hat{\xi}^{\tau} = \frac{\sqrt{2}}{2} (\hat{y} + \hat{x})$. The selection rules will be the same as for (a) above except:

$$S_{\parallel} = \tfrac{1}{2} (e_x c + e_z d)^2 \alpha^2 \quad Y(XY)X,\ Y(ZY)X$$

$$S_{\perp} = \tfrac{1}{2} e_x^2 \alpha^2 d^2 \quad Y(XZ)X$$

(6) Y( )Z

(a) LO phonon $\hat{\xi}^{\tau} = \hat{k}^{\tau} = \frac{\sqrt{2}}{2} (\hat{y} - \hat{z})$

$$S_{\parallel} = \tfrac{1}{2} \left[(e_x\ 0\ e_z)(\alpha + \beta)\underline{(II - I)} \begin{pmatrix} 0 \\ 1 \\ 0 \end{pmatrix} \right]^2$$

$$= \tfrac{1}{2} e_z^2 (\alpha + \beta)^2 d^2 \quad Y(ZY)Z$$

$$S_{\perp} = \tfrac{1}{2}\left[(e_x\ 0\ e_z)(\alpha+\beta)\underline{\underline{(II - I)}}\begin{pmatrix}1\\0\\0\end{pmatrix}\right]^2$$

$$= \tfrac{1}{2} e_x^2 (c-a)^2(\alpha+\beta)^2 \qquad Y(XX)Z$$

(b) TO extraordinary phonon $\hat{\xi}^{\tau}=\frac{\sqrt{2}}{2}(\hat{y}+\hat{z})$. The selection rules will be the same as (a) above except:

$$S_{\parallel} = \tfrac{1}{2} e_z^2 \alpha^2 d^2 \qquad Y(ZY)Z$$

and $$S_{\perp} = \tfrac{1}{2} e_x^2 (c+a)^2 \alpha^2 \qquad Y(XX)Z$$

(c) TO ordinary phonon $\hat{\xi}^{\tau} = \hat{x}$

$$S_{\parallel} = \left[(e_x\ 0\ e_z)\ \alpha\ \underline{\underline{III}}\begin{pmatrix}0\\1\\0\end{pmatrix}\right]^2 = e_x^2\alpha^2c^2 \qquad Y(XY)Z$$

$$S_{\perp} = \left[(e_x\ 0\ e_z)\ \alpha\ \underline{\underline{III}}\begin{pmatrix}1\\0\\0\end{pmatrix}\right]^2 = e_z^2 d^2\alpha^2 \qquad Y(ZX)Z$$

(7) X( )Z

(a) LO phonon $\hat{\xi}^{\tau} = \hat{k}^{\tau} = \frac{\sqrt{2}}{2}(\hat{x}-\hat{z})$

$$S_{\parallel} = \tfrac{1}{2}\left[(0\ e_y\ e_z)(\alpha+\beta)\underline{\underline{(III - I)}}\begin{pmatrix}1\\0\\0\end{pmatrix}\right]^2$$

$$= \tfrac{1}{2}(e_y c + e_z d)^2(\alpha+\beta)^2 \qquad X(YX)Z,\ X(ZX)Z$$

$$S_{\perp} = \tfrac{1}{2}\left[(0\ e_y\ e_z)(\alpha+\beta)\underline{\underline{(III - I)}}\begin{pmatrix}0\\1\\0\end{pmatrix}\right]^2$$

$$= \tfrac{1}{2} e_y^2(\alpha+\beta)^2 a^2 \qquad X(YY)Z$$

(b) TO extraordinary phonon $\hat{\xi}^{\tau} = \frac{\sqrt{2}}{2}(\hat{x}+\hat{z})$. The selection rules are the same as for (a) above except:

$$S_{\parallel} = \tfrac{1}{2}(e_y c + e_z d)^2\alpha^2 \qquad X(YX)Z,\ X(ZX)Z$$

and $$S_{\perp} = \tfrac{1}{2} e_y^2\alpha^2 a^2 \qquad X(YY)Z$$

(c) TO ordinary phonon $\hat{\xi}^{\tau} = \hat{y}$

$$S_{\parallel} = \left[(0\ e_y\ e_z)\ \alpha\ \underline{\underline{II}} \begin{pmatrix}1\\0\\0\end{pmatrix}\right]^2 = 0$$

$$S_{\perp} = \left[(0\ e_y\ e_z)\ \alpha\ \underline{\underline{II}} \begin{pmatrix}0\\1\\0\end{pmatrix}\right]^2 = (e_z d - e_y c)^2 \alpha^2 \qquad X(YY)Z,\ X(ZY)Z$$

(8) Z( )Y

(a) LO phonon $\hat{\xi}^{\tau} = \hat{k}^{\tau} = \frac{\sqrt{2}}{2}(\hat{z} - \hat{y})$

$$S_{\parallel} = \tfrac{1}{2}\left[(e_x\ e_y\ 0)(\alpha + \beta)\underline{\underline{(I - II)}} \begin{pmatrix}0\\0\\1\end{pmatrix}\right]^2$$

$$= \tfrac{1}{2} e_y^2 (\alpha + \beta)^2 d^2 \qquad Z(YZ)Y$$

$$S_{\perp} = \tfrac{1}{2}\left[(e_x\ e_y\ 0)(\alpha + \beta)\underline{\underline{(I - II)}} \begin{pmatrix}1\\0\\0\end{pmatrix}\right]^2$$

$$= \tfrac{1}{2} e_x^2 (\alpha + \beta)(a - c)^2 \qquad Z(XX)Y$$

(b) TO extraordinary phonon $\hat{\xi}^{\tau} = \frac{\sqrt{2}}{2}(\hat{z} + \hat{y})$. The selection rules will be the same as (a) above except:

$$S_{\parallel} = \tfrac{1}{2} e_y^2 \alpha^2 d^2 \qquad Z(\bar{Y}Z)Y$$

$$S_{\perp} = \tfrac{1}{2} e_x^2 \alpha^2 (a + c)^2 \qquad Z(XX)Y$$

(c) TO ordinary phonon $\hat{\xi}^{\tau} = \hat{x}$

$$S_{\parallel} = \left[(e_x\ e_y\ 0)\ \alpha\ \underline{\underline{III}} \begin{pmatrix}0\\0\\1\end{pmatrix}\right]^2 = e_x^2 \alpha^2 d^2 \qquad Z(XZ)Y$$

$$S_{\perp} = \left[(e_x\ e_y\ 0)\ \alpha\ \underline{\underline{III}} \begin{pmatrix}1\\0\\0\end{pmatrix}\right]^2 = e_y^2 \alpha^2 c^2 \qquad Z(YX)Y$$

(9) Z( )X

(a) LO phonon $\hat{\xi}^{\tau} = \hat{k}^{\tau} = \frac{\sqrt{2}}{2}(\hat{z} - \hat{x})$

$$S_{\parallel} = \tfrac{1}{2}\left[(e_x\ e_y\ 0)(\alpha+\beta)\underline{(I-III)}\begin{pmatrix}0\\0\\1\end{pmatrix}\right]^2$$

$$= \tfrac{1}{2}\, e_x^2(\alpha+\beta)^2 d^2 \qquad Z(XZ)X$$

$$S_{\perp} = \tfrac{1}{2}\left[(e_x\ e_y\ 0)(\alpha+\beta)\underline{(I-III)}\begin{pmatrix}0\\1\\0\end{pmatrix}\right]^2$$

$$= \tfrac{1}{2}\,(e_x c + e_y a)^2(\alpha+\beta)^2 \qquad Z(XY)X,\ Z(YY)X$$

(b) TO extraordinary phonon $\hat{\xi}^{\tau} = \frac{\sqrt{2}}{2}(\hat{z}+\hat{x})$. As (a), except:

$$S_{\parallel} = \tfrac{1}{2}\, e_x^2\alpha^2 d^2 \qquad Z(XZ)X$$

$$S_{\perp} = \tfrac{1}{2}\,(e_y a - e_x c)^2\alpha^2 \qquad Z(XY)X,\ Z(YY)X$$

(c) TO ordinary phonon $\hat{\xi}^{\tau} = \hat{y}$

$$S_{\parallel} = \left[(e_x\ e_y\ 0)\ \alpha\ \underline{II}\begin{pmatrix}0\\0\\1\end{pmatrix}\right]^2 = e_y^2\alpha^2 d^2 \qquad Z(YZ)X$$

$$S_{\perp} = \left[(e_x\ e_y\ 0)\ \alpha\ \underline{II}\begin{pmatrix}0\\1\\0\end{pmatrix}\right]^2 = e_y^2\alpha^2 c^2 \qquad Z(YY)X$$

All of the above results for the γ-polytype are summarized in Table 2.2.

LIST OF REFERENCES

Akhundov, G.A., Gasanova, N.A. and Nizametdinova, M.A., 1966. Phys. Status Sol. 15, K109.

Anastassakis, E. and Burstein, E., 1971. "Resonant Raman Scattering by Raman-Inactive F_{1u}-Type Phonons in II-VI Semiconductors" in Proc. of Second Int. Conf. on Light Scattering in Solids, ed. M. Balkanski, Flammarion Sciences.

Basinski, Z.S., Dove, D.B. and Mooser, E., 1961. Helv. Phys. Acta 34, 373.

Beck, A. and Mooser, E., 1961. Helv. Phys. Acta 34, 370.

Bendow, B. and Birman, J.L., 1970. Phys. Rev. B1, 1678. 1971. Phys. Rev. B4, 569.

Bir, G.L. and Picus, G.E., 1961. Sov. Phys. Solid State 2, 2039.

Born, M. and Bradburn, M., 1947. Proc. Roy. Soc. A 188, 161.

Born, M. and Huang, K., 1954. Dynamical Theory of Crystal Lattices, Clarendon Press.

Bourdon, A. and Khelladi, F., 1971. Solid State Commun. 9, 1715.

Brebner, J.L., Jandl, S. and Powell, B.M., 1973. Solid State Commun. 13, 1555.

Burstein, E. and Pinczuk, A., 1971. "Light Scattering by Collective Excitations in Dielectrics and Semiconductors", in The Physics of Opto-Electronic Materials, ed. Walter A. Albers, Jr., Plenum Press.

Callender, R.H., Sussman, S.S., Selders, M. and Chang, R.K., 1973. Phys. Rev. B7, 3788.

Cochran, W. and Cowley, R.A., 1962. J. Phys. Chem. Solids 23, 447.

Colwell, P.A. and Klein, M.V., 1970. Solid State Commun. 8, 2095.

Compaan, A. and Cummins, H.Z., 1973. Phys. Rev. Letts. 31, 41.

Chemical Rubber Co. Handbook, 1964. Ed. R. C. Weast, 47th ed., The Chemical Rubber Co., Cleveland, U.S.A.

Damen, T.C. and Scott, J.F., 1971. Solid State Commun. 9, 383.

Damen, T.C., Leite, R.C.C., and Shah, J., 1970. Proc. X Int. Conf. on Physics of Semiconductors, Cambridge, Mass. p. 735.

Dean, P.J. and Thomas, D.G., 1966. Phys. Rev. 150, 690.

Devlin, G.E., Davis, J.L., Chase, L. and Geschwind, S., 1971. Appl. Phys. Letts. 19, 138.

Elliott, R.J., 1957. Phys. Rev. 108, 1384.

Fateley, W.G., McDevitt, N.T. and Bentley, F.F., 1971. Appl. Spect. 25, 155.

Fischer, G., 1963. Helv. Phys. Acta 36, 317.

Fröhlich, H., 1954. Adv. in Phys. 3, 325.

Ganguly, A.K. and Birman, J.L., 1967. Phys. Rev. 162, 806.

Grechko, L.G. and Ovander, L.N., 1962. Sov. Phys. Solid State 4, 112.

Hamilton, D.C., 1969. Phys. Rev. 188, 1221.

Hayek, M., Brafman, O. and Lieth, R.M.A., 1973. Phys. Rev. B8, 2772.

Hodgins, C.G., 1974. Ph.D. Thesis, Simon Fraser University (unpublished).

Hoff, R.M. and Irwin, J.C., 1974. Phys. Rev. B (in press).

Hostler, L. and Pratt, R.H., 1963. Phys. Rev. Letts. 10, 469.

International Tables of X-ray Crystallography, 1969. Ed. N.F.M. Henry and K. Lonsdale, Kynock Press, Birmingham, U.K.

Irwin, J.C., Hoff, R.M., Clayman, B.P. and Bromley, R.A., 1973. Solid State Commun. 13, 1531.

Jellinek, F. and Hahn, H., 1961. Naturforsch. 16b, 713.

Kamimura, H., Nakao, K. and Nishina, Y., 1969. Phys. Rev. Letts. 22, 1379.

Knox, R.S., 1963. Theory of Excitons, Supp. 5 of Solid State Physics, Academic Publishers, New York.

Kurik, M.V., Savchuk, A.I., and Rarenko, I.M., 1968. Optics and Spect. 24, 536.

Kuroda, N., Nishina, Y., and Fukorai, T., 1968. J. Phys. Soc. Japan 24, 214. 1970. Jour. Phys. Soc. Japan 28, 981.

Leite, R.C.C. and Porto, S.P.S., 1966. Phys. Rev. Letts. 17, 10.

Leite, R.C.C., Scott, J.F. and Damen, T.C., 1969a. Phys. Rev. Letts. 22, 780.

Leite, R.C.C. and Scott, J.F., 1969b. Phys Rev. Letts. 22, 130.

Leite, R.C.C., Damen, T.C., and Scott, J.F., 1969c. "Resonant Raman Effect in CdS and ZnSe" in Proc. of Int. Conf. on Light Scattering Spectra in Solids, N.Y.U. 1968. Springer-Verlag, New York.

Leung, P.C., Anderman, G., Spitzer, W.G. and Mead, C.A., 1966. J. Phys. Chem. Solids 27, 849.

Loudon, R.A., 1963. Proc. Roy. Soc. A 275, 218.

Loudon, R.A., 1964. Adv. in Phys. 13, 423.

Loudon, R.A., 1965. J. de Physique 26, 677.

Malm, H.L. and Haering, R.R., 1971. Can. J. Phys. 49, 1823 and 2970.

Martin, R.M. and Damen, T.C., 1971a. Phys. Rev. Letts. 26, 86.

Martin, R.M., 1971b. Phys. Rev. B4, 3676.

Martin, R.M., 1973. Unpublished preprint.

Martin, R.M., 1974a. Private Communication.

Martin, R.M., 1974b. Preprint.

Mercier, A., Mooser, E. and Voitchovsky, J.P., 1973. J. Lumin. 7, 241.

Mercier, A. and Voitchovsky , J. P., 1974. Solid State Commun. 14, 757.

Mills, D.L. and Burstein, E., 1969. Phys. Rev. 188, 1465.

Nye, J.F., 1957. Physical Properties of Crystals, Clarendon Press, Oxford.

Ottaviani, G., Canali, C., Nava, F., Schmid, Ph., Mooser,E. Minder, R. and Zschokke, I., 1974. Solid State Commun. 14, 933.

Ovander, L.N., 1962a. Optics and Spect. 9, 302. 1962b. Opticsand Spect. 12, 405.

Pinczuk, A. and Burstein, E., 1968. Phys. Rev. Letts. 21, 1073.

Ralston, J.M., Wadsack, R.L., and Chang, R.K., 1970. Phys. Rev. Letts. 25, 814

Salaev, E. Yu., Solovyev, L.E. and Khalilov, V. Kh., 1972. Optics and Spect. 32, 183.

Sapre, V.B. and Mande, C., 1973. J. Phys. Chem. Solids 34, 1351.

Schiff, L.I., 1955. Quantum Mechanics, McGraw-Hill Co.

Schlueter, M., 1972. Helv. Phys. Acta 45, 73.

Schubert, K., Dörre, E. and Kluge, M., 1955. Z. Metallk. 46, 216.

Scott, J.F., Damen, T.C., Leite, R.C.C. and Silfvast, W.T. 1969. Solid State Commun. 7, 953.

Scott, J.F., Damen, T.C., Silfvast, W.T., Leite, R.C.C., and Cheesman, L.E., 1970. Optics Commun. 1, 397.

Terhell, J.C.J.M. and Lieth, R.M.A., 1972a. J. Crys. Growth 16, 54. 1972b. Phys. Status Solidi, a10, 529.

Tinkham, M., 1964. Group Theory and Quantum Mechanics, McGraw-Hill Co.

Toyazawa, Y., 1958. Prog. Theor. Phys. 20, 53.

Van der Ziel, J.P., Meixner, A.E. and Kasper, H.M., 1973. Solid State Commun. 12, 1213.

Wasscher, J.D. and Dieleman, 1972. J. Phys. Letts. 39a, 279.

Whittaker, F.T. and Watson, C.N., 1963. A Course in Modern Analysis, Cambridge Univ. Press, London.

Wieting, T.J. and Verble, J.L., 1972. Phys. Rev. B5, 1473.

Wieting, T.J., 1973. Solid State Commun. 12, 937.

Williams, P.F. and Porto, S.P.S., 1973. Phys. Rev. B8, 1782.

Wilson, E.B., Decius, J.C. and Cross, P.C., 1955. Molecular Vibrations, McGraw-Hill Co., New York.

Wright, G.B. and Mooradian, A., 1966. Bull. Am. Phys. Soc. 11, 812.

Wykoff, R.W.G., 1965. Crystal Structure, Vol. 1, Second Ed., Interscience Publ., New York.

Yoshida, H., Nakashima, S. and Mitsuishi, A., 1973. Phys. Status Solidi b59, 655

Yu, P.Y., Shen, Y.R., Petroff, Y., and Falicov, L.M., 1973. Phys. Rev. Letts. 30, 283.

Yu, P.Y. and Shen, Y.R., 1972. Phys. Rev. Letts. 29, 468.

Ziman, J.M., 1960. Electrons and Phonons, Clarendon Press, Oxford.